

**UNIVERSITA'**  
**Degli Studi di Napoli "Federico II"**



**SCUOLA POLITECNICA E DELLE SCIENZE DI BASE**  
**DIPARTIMENTO DI INGEGNERIA CHIMICA, DEI MATERIALI**  
**E DELLA PRODUZIONE INDUSTRIALE (DICMaPI)**

**Thermodynamics of Thermoplastic Polymers and their**  
**Solutions**

***TUTOR***

*Ch.mo Prof. Giuseppe Mensitieri*

***CO-TUTOR***

*Dott. Ing. Giuseppe Scherillo*

***PhD Student***

*Ing. Valerio Loianno*

## **Abstract**

Glassy organic polymers are technologically important across the gamut of materials applications from structural (hyperbaric windows) to electronic (ionic conductors, surface coatings for printed circuit boards) to environmental (membranes for industrial gas separation). A formal description and understanding of the glass transition temperature is necessary in order to determine the configurational state and hence physical properties of the glass. Moreover, the non-equilibrium glassy state appears to be unstable: volume-relaxation studies of glassy materials have revealed that they undergo slow processes, which attempt to establish equilibrium. These types of retardation/relaxation phenomena are called physical ageing. As well as pressure and temperature, sorption of a plasticizer may affect in several ways the membrane physical properties. Generally speaking structural rearrangement of the chains is enhanced and, consequently, the glass transition temperature decreases, physical ageing is usually speed up, the membrane is affected by swelling and/or plasticization and even crystallization can be activated.

The research work focuses on the investigation of industrial polymers' glassy – rubbery behaviour due to thermodynamic state variables change (e.g. temperature  $T$ , mechanical pressure  $P$  and solvent content  $\Omega$ ) within the polymer matrix. The goal is to obtain a fundamental insight of the sorption process on both macroscopic and microscopic levels. As a result several polymer—penetrant systems have been studied. Different techniques have been implemented to achieve this goal: dilatometry, MTDSC, gravimetry, manometry and *in situ* FTIR. The instruments used are: a PVT apparatus from GNOMIX<sup>®</sup>; a MDSC from TA Instruments<sup>®</sup>; four different handmade systems consisting of a CAHN microbalance from Thermo Fisher Scientific<sup>®</sup>, a QSM from RUSKA Co.<sup>®</sup>, a pressure decay system from MKS<sup>®</sup> and finally a FTIR from Perkin-Elmer<sup>®</sup>. All data have been modelled with statistical thermodynamic theories and empirical approaches .

The study is divided as follows: the first chapter introduces the research goal and fields of application along with the theoretical background for membrane science; the second chapter reports the study conducted on the system PEI—CO<sub>2</sub>; the third chapter describes the results obtained on the PS—Toluene system; finally in the fourth chapter the results for the PPO—benzene system are given. The order in which these systems are presented is related to the increase of structural modifications as a result of polymer—penetrant interactions.

# Contents

<b>List of Figures</b>	v
------------------------	---

<b>List of Tables</b>	viii
-----------------------	------

<b>1 Thermodynamics of Thermoplastic Polymers and their Solutions</b>	1
1.1 Motivations . . . . .	1
1.2 Applications: State of the art . . . . .	2
1.3 Crystallization vs Vitrification . . . . .	5
1.4 Vitrification of Thermoplastic Polymers: Dilatometry and Calorimetry . . . . .	7
1.5 Vitrification Theories . . . . .	16
1.6 Thermoplastic Polymer Solutions: Theory and Practice . . . . .	20
1.6.1 Flory's Statistical lattice fluid model . . . . .	23
1.6.2 Sanchez and Lacombe Statistical lattice fluid model . . . . .	26
1.6.3 NRHB Statistical lattice fluid model . . . . .	30
1.6.4 The glassy state: NELF-SL and NETGP-NRHB frameworks . . . . .	36
1.6.5 $T_g$ depression: a II order phase transition approach . . . . .	39
1.7 Empirical theories . . . . .	47
<b>2 PEI—CO<sub>2</sub> System</b>	50
2.1 Materials . . . . .	51
2.2 Apparatuses and Methods . . . . .	51
2.3 Results and Discussion . . . . .	55
<b>3 PS—Toluene System</b>	67
3.1 Materials . . . . .	68
3.2 Apparatuses and Methods . . . . .	69
3.2.1 Pressure Decay . . . . .	69
3.2.2 Dynamic Gravimetry . . . . .	71
3.3 Results and Discussion . . . . .	73
3.3.1 MDSC experiments on A-PS . . . . .	74

3.3.2	Static sorption tests . . . . .	77
3.3.3	Dynamic Experiments . . . . .	83
3.4	Theoretical interpretation . . . . .	94
<b>4</b>	<b>PPO—Benzene System</b>	<b>100</b>
4.1	Materials . . . . .	101
4.2	Apparatuses and Methods . . . . .	102
4.3	Results and Discussion . . . . .	103
	<b>Conclusions</b>	<b>115</b>
	<b>Future Directions</b>	<b>117</b>
	<b>References</b>	<b>118</b>
	<b>Appendices</b>	<b>124</b>
	<b>A</b>	<b>125</b>

# List of Figures

1.1	Crystallization vs relaxation characteristic times . . . . .	7
1.2	Dilatometric experiments showing the glass transition in pure polymers	9
1.3	Schematic representation of Kovacs dilatometric experiments . . . . .	9
1.4	Kovacs T-Jump dilatometric experiments on PVA . . . . .	10
1.4	Kovacs dilatometric experiments on PVA . . . . .	11
1.4	Kovacs dilatometric experiments on PVA . . . . .	12
1.5	Kovacs T-Jump dilatometric experiments on PMMA . . . . .	13
1.6	MTDSC experiments on PS . . . . .	16
1.7	Comparison between the <i>Kauzmann paradox</i> and the Gibbs/Di Marzio theory . . . . .	19
1.8	Free enthalpy vs. composition plot . . . . .	22
1.9	Types of $T_g$ phase diagram in a generic Polymer-Penetrant system . . . .	46
2.1	PEI Ultem <sup>®</sup> chemical formula . . . . .	51
2.2	QSM sorption apparatus scheme . . . . .	52
2.3	FTIR measurement apparatus scheme . . . . .	54
2.4	CO <sub>2</sub> sorption isotherms in PEI determined gravimetrically at several temperatures . . . . .	55
2.5	Kinetics example of CO <sub>2</sub> sorption in PEI at 35°C . . . . .	56
2.6	Mutual diffusivity of CO <sub>2</sub> in PEI . . . . .	56
2.7	PEI—CO <sub>2</sub> FTIR dynamic frequency spectra example . . . . .	58
2.8	CO <sub>2</sub> main peak curve fitting . . . . .	58
2.9	PEI carbonyl group difference spectra as a function of temperature . . . .	59
2.10	PEI—CO <sub>2</sub> , 2D-COS analysis at 35°C . . . . .	59
2.11	Comparison of gravimetric sorption data for the PEI—H <sub>2</sub> O and PEI—CO <sub>2</sub> systems . . . . .	61
2.12	Dual mode fitting of the PEI-CO <sub>2</sub> mixture . . . . .	62
2.13	PVT data of PEI: (up) SL fitting; (down) NRHB fitting . . . . .	63
2.14	NELF-SL fitting of PEI—CO <sub>2</sub> sorption data . . . . .	64
2.15	NETGP-NRHB fitting of PEI—CO <sub>2</sub> sorption data . . . . .	66

3.1	Toluene and PS unit chain chemical formulas . . . . .	67
3.2	Pressure decay process diagram for <i>static</i> measurements . . . . .	70
3.3	Gravimetric sorption process diagram for <i>dynamic</i> measurements . . . . .	73
3.4	MDSC experiments on A-PS . . . . .	76
3.5	Pressure decay <i>static</i> sorption experiments of Toluene in A-PS at 40°C . . . . .	78
3.6	Pressure decay sorption isotherm of Toluene in A-PS at 40°C . . . . .	79
3.7	Gravimetric <i>static</i> integral sorption tests of Toluene in A-PS at 40°C and 20°C . . . . .	80
3.8	Gravimetric dynamic desorption/sorption cyclic experiment of Toluene in A-PS at 40°C in the rubbery zone . . . . .	81
3.9	Gravimetric dynamic desorption experiments: comparison between specimens of different thickness . . . . .	82
3.10	Gravimetric dynamic desorption/sorption cyclic experiment of Toluene in A-PS in the rubbery/glassy zones . . . . .	83
3.11	Gravimetric dynamic desorption isothermal experiments: effect of depressurization rate on desorption of Toluene from A-PS . . . . .	85
3.12	Evaluation of the glass transition pressure from a gravimetric dynamic isothermal desorption test . . . . .	87
3.13	Gravimetric dynamic isothermal desorption experiments: effect of temperature on desorption of Toluene from A-PS . . . . .	88
3.14	NETGP-NRHB fitting of PS—Toluene sorption isotherms . . . . .	89
3.15	Gravimetric dynamic desorption/sorption isobaric cyclic experiment on the PS—Toluene system . . . . .	91
3.16	Gravimetric dynamic isoactivity sorption experiments of Toluene in A-PS . . . . .	92
3.17	Activity values measured during the 0.3 gravimetric dynamic isoactivity experiment (Peng Robinson EOS) . . . . .	93
3.18	Total set of glass transition points retrieved from the gravimetric dynamic experiments . . . . .	94
3.19	<i>Dynamic</i> desorption or sorption tests scheme: measuring the <i>retrograde vitrification</i> phenomenon . . . . .	96
3.20	GD—NRHB prediction of <i>retrograde vitrification</i> for the PS—Toluene system . . . . .	99
3.21	Dependence of $P_g$ on the depressurization rate: comparison with the GD—NRHB approach . . . . .	99
4.1	Polymerization reaction of PPO . . . . .	101
4.2	FTIR <i>in situ</i> vapour sorption apparatus . . . . .	103
4.3	Gravimetric sorption kinetics of Benzene in aPPO: first and second experiments . . . . .	104
4.4	<i>In situ</i> time resolved FTIR spectra: sorption of Benzene in PPO . . . . .	105
4.5	Gravimetric and FTIR comparison of Benzene in PPO sorption kinetics . . . . .	106

4.6	<i>In situ</i> time resolved FTIR spectra: analysis of the solvent induced crystallisation . . . . .	108
4.7	Evidence of solvent induced crystallisation from WAXS experiments .	109
4.8	Sorption isotherm of Benzene in aPPO at 40°C . . . . .	110
4.9	Fitting of the NRHB model to PPO PVT data . . . . .	111
4.10	Prediction of PPO—Benzene P vs. T phase diagram . . . . .	113
4.11	Prediction of PPO—Benzene Tg depression . . . . .	113
A.1	LabVIEW® user interface to acquire two channels pressure data . . . .	125
A.2	Sanchez and Lacombe lattice fluid model parameters . . . . .	126

# List of Tables

1.1	Hydrogen separation membranes . . . . .	4
1.2	Nitrogen separation membranes . . . . .	4
1.3	US pipeline regulation for NG impurities . . . . .	4
1.4	Membrane materials and selectivities for separation of impurities from natural gas under normal operating conditions . . . . .	5
1.5	$T_g - P_g$ and $T_g - \omega_g$ behaviour predicted . . . . .	46
2.1	Dual Sorption parameters of pure PEI and CO <sub>2</sub> . . . . .	62
2.2	SL parameters of pure PEI and CO <sub>2</sub> . . . . .	64
2.3	NRHB parameters of pure PEI and CO <sub>2</sub> . . . . .	64
2.4	NRHB parameters for the PEI—CO <sub>2</sub> mixture based on the NETGP framework . . . . .	66
3.1	Gravimetric dynamic isothermal experiment at 40°C: $P_g - \Omega_g$ couples as a function of P rate . . . . .	86
3.2	PS—Toluene glass transition triples $T_g - P_g - \Omega_g$ . . . . .	89
3.3	NRHB parameters for the PS—Toluene mixture based on the NETGP framework . . . . .	90
3.4	Isobaric experiment at 36 mbar: $T_g - \Omega_g$ couples as a function of the heating history . . . . .	92
3.5	Isoactivity experiments: $T_g - P_g - \Omega_g$ triples . . . . .	93
3.6	NRHB parameters of pure A-PS and Toluene . . . . .	97
4.1	NRHB parameters of pure PPO and Benzene . . . . .	111

# Chapter 1

## Thermodynamics of Thermoplastic Polymers and their Solutions

A glass can be formed provided the liquid is cooled fast enough to prevent crystallization. The question that arises is not whether a material can vitrify but which conditions enable it to acquire this specific state and what is its behaviour. The first paragraph explains the motivations that encouraged this research program; a picture of the main applications of polymeric glassy membranes for gas separation applications follows. The second part of this chapter focuses on the comparison of the two physical transitions crystallization and vitrification. Next, the basic phenomenology of vitrification of pure polymeric thermoplastic compounds is analysed with both dilatometric and enthalpic experiments: two well-established theories, kinetic and thermodynamic respectively, are presented; last, the thermodynamics of polymeric solutions is treated in detail by outlining the statistical thermodynamic models used to predict the behaviour of the mixtures of interest in this PhD program.

### 1.1 Motivations

Nowadays glassy polymers are used in many applications. The glassy state is metastable and as such its behaviour varies during time (*physical ageing*). Moreover, the transport of low molecular weight compounds within the matrix affects its evolution. Swelling, plasticization, hygrothermal degradation provoke irreversible changes of the material performances during operation. Also, sorption of a gas or vapour can reduce the  $T_g$  and the  $T_m$  of the material. A lack of understanding of the thermodynamics of pure glassy polymers and their mixtures exists; also, transport phenomena of low MW compounds may interact with the matrix and make the problem more difficult. The goal of this PhD research is the study of several thermoplastic polymer—penetrant systems

in order to improve the understanding of thermodynamics of polymer solutions and to control them. This has been done by using several experimental techniques and by applying specific thermodynamic approaches to overcome empirical relations.

## 1.2 Applications: State of the art

Thermoplastic polymers are useful in several applications:

- 1- separation of gases in the Oil&Gas and petrochemical industry;
- 2- maintaining an inert atmosphere during transportation of flammable materials;
- 3- electronic coating [1]
- 4- polymer matrix composites (PMCs)

Moreover, lowering of the melting temperature is desirable in processing of thermally labile polymers without degradation, and lowering of  $T_g$  and expanding the rubbery domain may facilitate polymer impregnation. Lowering of  $T_g$  and  $T_m$  is especially important in foaming with supercritical carbon dioxide as a physical blowing agent. The extent of foaming and the pore morphology that develops depends not only on the extent of sorption and diffusivity of  $CO_2$  in the polymer, but also on the extent to which the polymer transition temperatures are altered. For example, when semi-crystalline polymers are involved, if the crystallization temperature ( $T_c$ ) is significantly lowered, then if the foaming temperature ( $T_f$ ) is relatively high, that is if the ( $T_f - T_c$ ) difference is large, solidification may not be rapidly achieved during decompression, and the  $CO_2$  escape through diffusion may not be prevented, thereby leading to a poor degree of foaming. On the other hand, if the foaming temperature were not be sufficiently high and the modulus of the polymer matrix were to remain high, then  $CO_2$  diffusion may be too slow, leading to restricted bubble growth [2]. Knowledge of  $T_g$  and  $T_m$  and the relative changes in the rigidity of polymers exposed to a highly soluble penetrant is thus crucial in the processing of polymeric materials.

Among the applications and issues listed above, the membrane market for gas separations is here outlined. The application of membranes to gas separation problems has grown rapidly since the installation of the first industrial plants for the separation of Hydrogen (Prism<sup>®</sup>) from ammonia-plant purge-gas streams in the early 1980s by Monsanto [3, 4]. Nowadays, the membrane market can be divided into three areas:

- 1- established processes;
- 2- developing processes;
- 3- unexplored processes.

The first group concerns 80% of the membrane market and it consists in nitrogen and hydrogen recovery, air drying industrial processes, carbon dioxide separation from NG.

Several important improvements have been made since their first introduction so that, today, these technologies are standardized and only small incremental changes in productivity are expected from scientific research. In detail, nitrogen is produced from air as the residue of a membrane stage whereas oxygen is recovered from the permeate side. Of course, the flux of interest depends on the selectivity of the membrane, i.e. on which gas is the most permeable in the mixture to be processed. Hydrogen is a small, noncondensable gas, which is highly permeable compared to all other gases. Indeed it is recovered from the permeate side of a membrane stage. This is particularly true with the glassy polymers primarily used to make hydrogen selective membranes. Table 1.1 shows the state of the art for the hydrogen membrane separation industry. Some relevant examples are the recovery of  $H_2$  from the purge gas in ammonia plants and from hydrotreating processes in the oil industry or from unreacted syngas in the petrochemical industry. In these cases, it is always recycled to improve the productivity. Air is separated into a nitrogen rich residue and an oxygen enriched air permeate. Table 1.2 describes the polymer membrane properties used for this case. The latter is sent to burners or compressors to improve the efficiency of combustion. The former is used for gas blanketing, shipment of food and ultimately for creating inert atmosphere surrounding flammable materials. Carbon dioxide is recovered from NG and is used in EOR (*enhanced oil recovery*) processes. Moreover, the U.S.A regulations dictates the concentration of  $CO_2$  in the US national pipeline grid (table 1.3).

The second group deals with recovery of light hydrocarbons from refinery and petrochemical plant purge gases, separation of  $C_{3+}$  hydrocarbons, hydrogen sulfide, nitrogen, and water from NG, organic vapour separation from air or nitrogen. Researchers are focusing their attention on these applications which are already in use in several facilities because again the regulations dictates low concentration of these compounds in the delivery pipeline to prevent corrosion, limit toxicity and improve quality standards (table 1.3). Important steps forward are being made to create new highly performant membranes. The goal is to improve fluxes, i.e. recoveries, without depleting the selectivity, i.e. the separation capacity. Organic vapour is retrieved from air by using glassy or rubbery polymers as the residue or permeate stream respectively. For instance, as stated by Baker, one of the most successful petrochemical applications is treatment of resin degassing vent gas in polyolefin plants. Typical polymers used to treat NG and their selectivities are given in table 1.4.

Polymer (Developer)	Selectivity			Hydrogen pressure normalized flux ( $10^{-6} \text{cm}^3(\text{STP})/\text{cm}^2 \cdot \text{s} \cdot \text{cmHg}$ )
	$H_2/\text{CO}_2$	$H_2/\text{CH}_4$	$H_2/\text{N}_2$	
Polyaramide (Medal)	100	>200	>200	100
Polysulfone (Permea)	40	80	80	100
Cellulose Acetate (Separex)	30-40	60-80	60-80	200
Polyimide (Ube)	50	100-200	100-200	80-200

**Table 1.1:** Hydrogen separation membranes [3]

Polymer	Oxygen permeability (barrer)	Nitrogen permeability (barrer)	Selectivity $O_2/\text{N}_2$
Poly(1-trimethylsilyl-1-propyne) (PTMSP)	7600	5400	1.4
Teflon AF 2400	1300	760	1.7
Silicone rubber	600	280	2.2
Poly(4-methyl-1-pentene) (TPX)	30	7.1	4.2
Poly(phenylene oxide) PPO	16.8	3.8	4.4
Ethyl cellulose	11.2	3.3	3.4
6FDA-DAF (polyimide)	7.9	1.3	6.2
Polyaramide	3.1	0.46	6.8
Tetrabromobisphenol A polycarbonate	1.4	0.18	7.5
Polysulfone	1.1	0.18	6.2

**Table 1.2:** Nitrogen separation membranes [3]

Component	Concentration Limit
$\text{CO}_2$	<2%
$\text{H}_2\text{O}$	<120 ppm
$\text{H}_2\text{S}$	<4 ppm
$\text{C}_{3+}$	dew point $-20^\circ\text{C}$ 950-1050 BTU/scf
Total Inerts	<4%

**Table 1.3:** US pipeline regulation for NG impurities [3]

Permeating compound	Polymer physical state	Polymeric membrane	Selectivity over Methane
CO <sub>2</sub>	glass	cellulose acetate, polyimide	10-20
H <sub>2</sub> S	rubber	ether-amide block copolymer	20-30
N <sub>2</sub>	glass	polyimide, perfluoro polymers	2-3
N <sub>2</sub>	rubber	silicone rubber	0.35
H <sub>2</sub> O	rubber or glass	Many	>200
Butane	rubber	silicone rubber	7-10

**Table 1.4:** Membrane materials and selectivities for separation of impurities from natural gas under normal operating conditions [3]

Finally, future expansion of gas separation membranes pertains to sequestration of carbon dioxide, production of oxygen enriched air and separation of organic vapours. Governments are starting to rule CO<sub>2</sub> cost emissions in order to limit global warming: carbon dioxide is mainly produced in electrical power plants which are responsible for 35–40% of global emissions. Oxygen enriched air cannot be considered a real market for polymeric membranes if selectivities are not improved by a factor of 5-10. Organic vapours always plasticize the membrane, even at high temperatures when their solubility lowers. The separation efficiency is much reduced because of this phenomenon. Nevertheless, membranes are still attractive because it is still very expensive to separate organic vapours of similar boiling points with distillation processes.

### 1.3 Crystallization vs Vitrification

A material has a crystalline structure when its atoms are located in a repeating or periodic array over large atomic distances. This implies long range atomic order. On the contrary, a glass lacks of crystalline order and the material is said to be amorphous because its structure is similar to that of a liquid. Considering the liquid—solid phase transition, the two solid structures are always in competition; the following theory and phenomenology about supercooled metastable liquids phase are related to low molecular weight compound.

Supercooled liquids are metastable with respect to the crystalline phase [5]. However, crystallization is not the only outcome of supercooling. If a rapid quench is applied, the liquid appears arrested because its structural relaxation time value is comparable (or even higher) to the experimental stimulus time. Indeed, two characteristic times can be defined:

- a)  $\tau_1$ : the crystallization time of a volume fraction  $\phi$

b)  $\tau_2$ : the internal molecular relaxation time

The latter increases the more the temperature is lowered. The former reach a minimum ( $\tau_{1,min}$ ) by lowering the temperature when  $T < T_m$  and it is related to the homogeneous nucleation rate ( $J$ ) and to the constant linear growth velocity of the nucleus ( $u$ ) as follows in isothermal conditions

$$\phi = \pi/3 \cdot J \cdot u^3 \cdot \tau_1$$

where the constant linear velocity is defined as

$$u = \frac{f \cdot k \cdot T}{3\pi \cdot a^2 \cdot \eta} \cdot \{1 - \exp[-\Delta h_m / (kT) \cdot (1 - T_m/T)]\} \quad (1.1)$$

' $\phi$ ' is the crystallized volume liquid fraction; ' $f$ ' represents the fraction of sites on the interface available for the incorporation of molecules; ' $a$ ' is a length of the order of a molecular diameter; ' $\eta$ ' is the viscosity of the liquid; ' $\Delta h_m$ ' is the latent heat of fusion ' $T_m$ ' is the equilibrium melting temperature.  $\tau_{(1,min)}$  and  $T(\tau_{(1,min)})$  define together the maximum cooling rate capable of inducing crystallization of the liquid. Otherwise, by lowering the temperature, vitrification is triggered, provided the characteristic time for molecular rearrangement becomes comparable to the experimental time scale. As pointed out by Debenedetti, structural arrest is a meaningless concept without reference to the time scale being investigated. The increased sluggishness in the exploration of configurations that characterizes vitrification is manifested macroscopically by a sharp viscosity increase. As a consequence, the lower the  $T_m$  the more favoured is vitrification. Figure 1.1(left) compares  $\tau_1$  with  $\tau_2$  as a function of temperature: if the  $\tau_1$  and  $\tau_2$  curves were actually to intersect each other, then the system would be prevented from crystallizing down to a temperature at which the characteristic time for molecular rearrangement becomes comparable to the experimental time scale; this behaviour is expected not to occur and the two curves should always be separated. Thus, crystallization is arrested provided  $\tau_{(1,min)}$  is sufficiently increased. To the right, it is described a way to stabilize the glass: the addition of a solute causes the depression of the crystallization temperature at lower  $T$ , thus increasing  $\tau_{(1,min)}$ . The formation of a solution can also increase the mixture viscosity, thus shifting the  $\tau_2$  curve to the right.

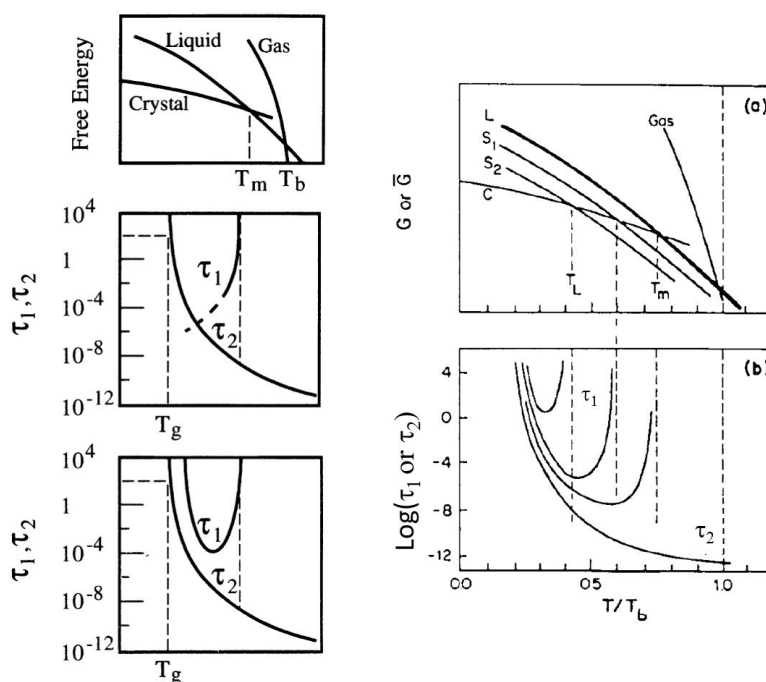


**Figure 1.1:** Crystallization vs relaxation characteristic times: (left) free energy change due to supercooling, unreal (middle) and real (bottom) comparison between  $\tau_1$  and  $\tau_2$ ; (right) free energy change due to the addition of a second compound,  $T_m$  depression and stabilization of the glassy structure [5, 6].

## 1.4 Vitrification of Thermoplastic Polymers: Dilatometry and Calorimetry

The glass transition in pure polymers is observed essentially by monitoring the rather sharp bend that the specific volume or the enthalpy experiences during cooling in a temperature range of  $\sim 10^\circ\text{C}$  around a specific value of  $T$  called the glass transition temperature or  $T_g$  (figure 1.2a). Far from it, the rate of change of these properties is constant and, particularly, higher for the liquid state. Indeed, the thermal expansion coefficient and the specific heat capacity undergo a step change at the  $T_g$ . Figure 1.2a shows the experiments conducted on A-PS by Simon *et al.* and describes this behaviour [7]. The transition observed is called  $\alpha$ -transition because other types of transitions are usually observed when  $T \ll T_g$ . If the rubbery polymer can partly crystallize, then during cooling crystallization precedes vitrification, at a melting temperature ( $T_m$ ) usually 1.5 times  $T_g$  (figure 1.2c). This process is a thermodynamic first order phase transition, characterized for instance by a step change of the specimen specific volume. On the contrary, vitrification is a continuous process: no sudden change of the volume or enthalpy is observed at  $T_g$  (i.e. no heat is involved in the transition) and it always

occurs because of the amorphous polymer content, which cannot crystallize. Three temperature regions are usually identified (figure 1.2a): *rubbery* region (A) well above  $T_g$ ; *glass transition* region (B) close to  $T_g$  ( $\pm 15$ — $20^\circ\text{C}$ ); *glassy* region (C) well below  $T_g$ .

Vitrification is also a non-equilibrium history dependent state because the characteristic time of the applied stimulus affects the physical properties of the material. The lower the stimulus time, the lower the temperature range at which the  $\alpha$ -transition occurs (1.2a). Moreover, a hysteresis is observed when the material is re-heated (figure 1.2b). This response again results from a compromise between the stimulus history applied and the relaxation time the material structure needs to attain the equilibrium glassy structure. Indeed, the state of the system must be described by a variety of order parameters in addition to the thermodynamic site variables. For each of them a characteristic relaxation time can be defined. Another way of describing this phenomenon is to define a landscape of energy minima for the liquid and the glassy structure: then the number of configurational states on an energy landscape is greatly reduced in the glassy state as compared to the liquid state due to freezing of large-scale cooperative rearrangements ( $\alpha$ -transition). The crossing from one configurational state (or energy minimum) to another is dependent on the nature of the energy landscape, which of course depends on the history of the stimulus applied. Multiple aspects affect the state such as the MW distribution, the chain lengths, the chain structure (i.e. side chain length, specific functional groups, number of chain ends) or, generally, the chain mobility. The relaxation towards equilibrium below  $T_g$  usually goes under the name of physical ageing. Several authors have been studying the previous phenomena with dielectric, mechanical and dilatometric measurements [9, 10, 11, 12, 13, 14]. Particularly, Kovacs performed comprehensive volume measurements on PVA and glucose in the range B of figure 1.2a, i.e. close to  $T_g$ . The goal was the investigation of the glassy polymers behaviour such as physical ageing, hysteresis and memory effects (figure 1.3). The experiments were conducted as follows:

- 1- Isobaric T-Jumps around  $T_g$ , the system being always at equilibrium at the beginning of the experiment (figures 1.3a and 1.3b):
  - 1.1- the initial temperature is fixed ( $T_0$ ) and different final temperatures (T) are attained (cases **1a** and **2a**);
  - 1.2- the final temperature is fixed ( $T_0$ ) and different initial temperatures (T) are chosen (cases **1b** and **2b**);
  - 1.3- the final temperature is fixed and alike whether a heating or a cooling T-jump is performed (case **c**).
- 2- Isobaric double consecutive T-Jumps around  $T_g$  starting from  $T > T_g$ . Again, the system is always at equilibrium at the beginning of the experiment (figure 1.3d) and, in addition, physical ageing of fixed  $\Delta V$  is applied between the two T-Jumps.

Figure 1.4 shows several sets of dilatometric data obtained from the previous scheme by Kovacs.

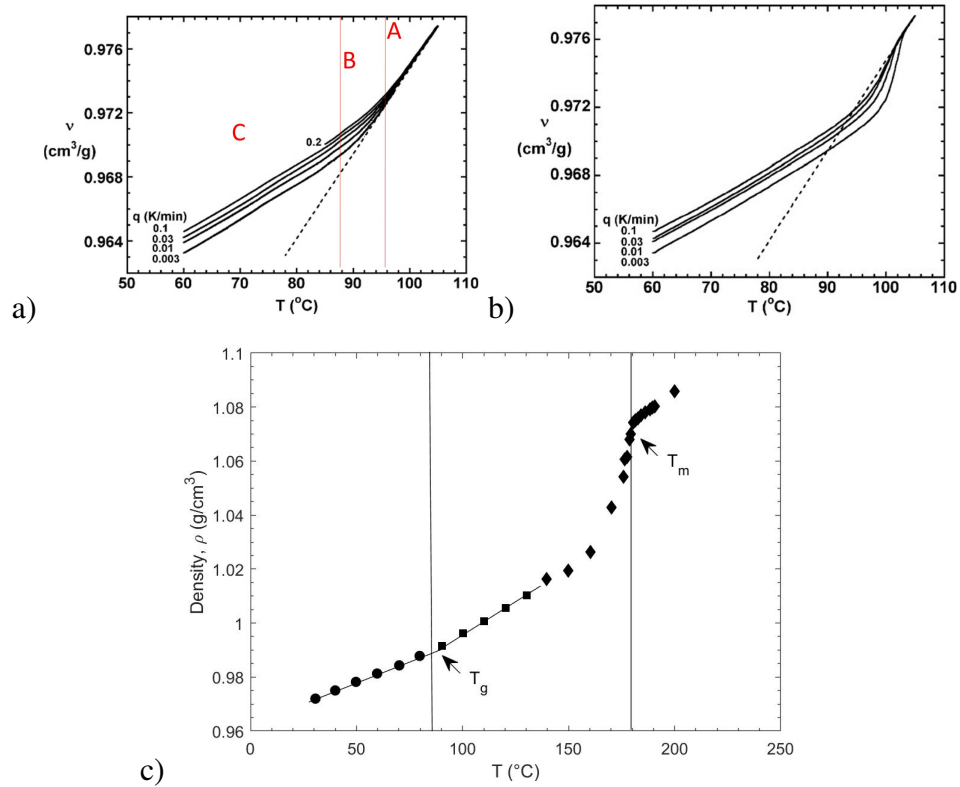


**Figure 1.2:** (a) glass transition of A-PS during cooling at different rates ' $q$ '; (b) glass transition of A-PS during heating at 0.2 K/min after cooling at different rates ' $q$ '; (c) dilatometric step-heating experiments on semicrystalline poly-(N,N'-sebacoylpiperazine) [7, 8]

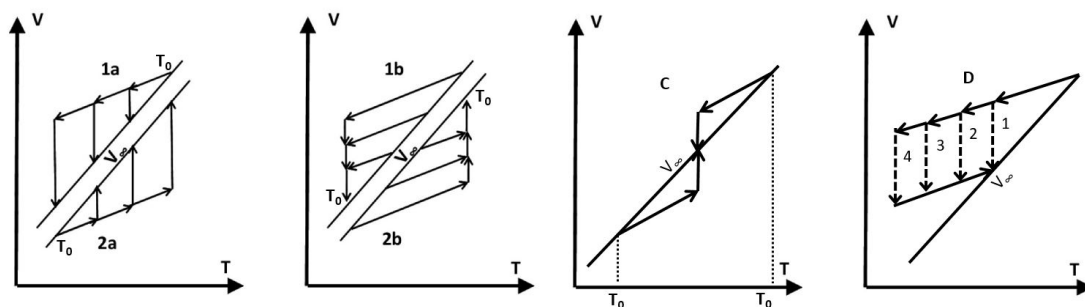


**Figure 1.3:** Schematic representation of Kovacs dilatometric experiments [9]

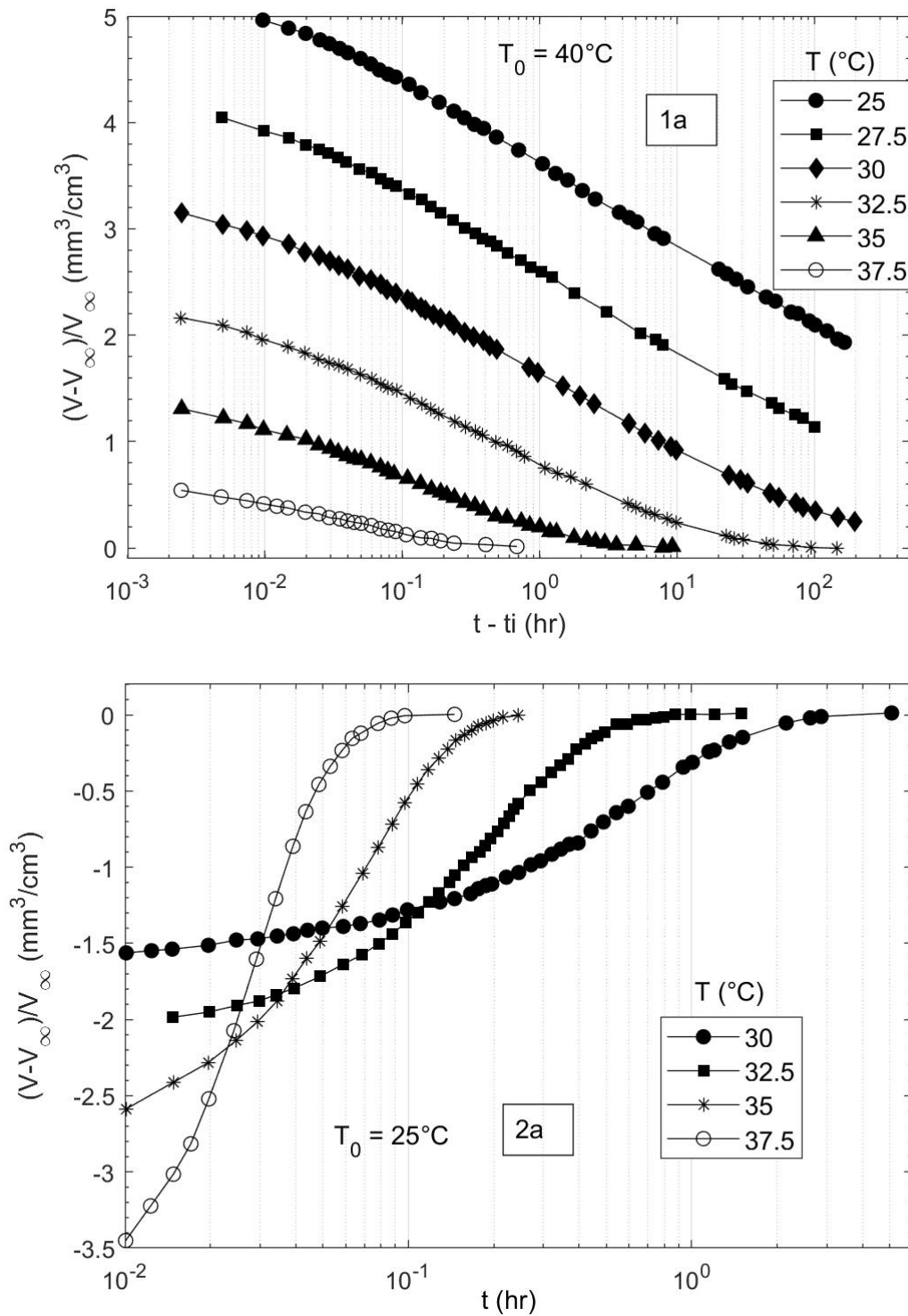


**Figure 1.4:** Kovacs dilatometric experiments on PVA [9].  $t_i = 0.01$  hr is the characteristic time of attainment of temperature equilibrium after quenching

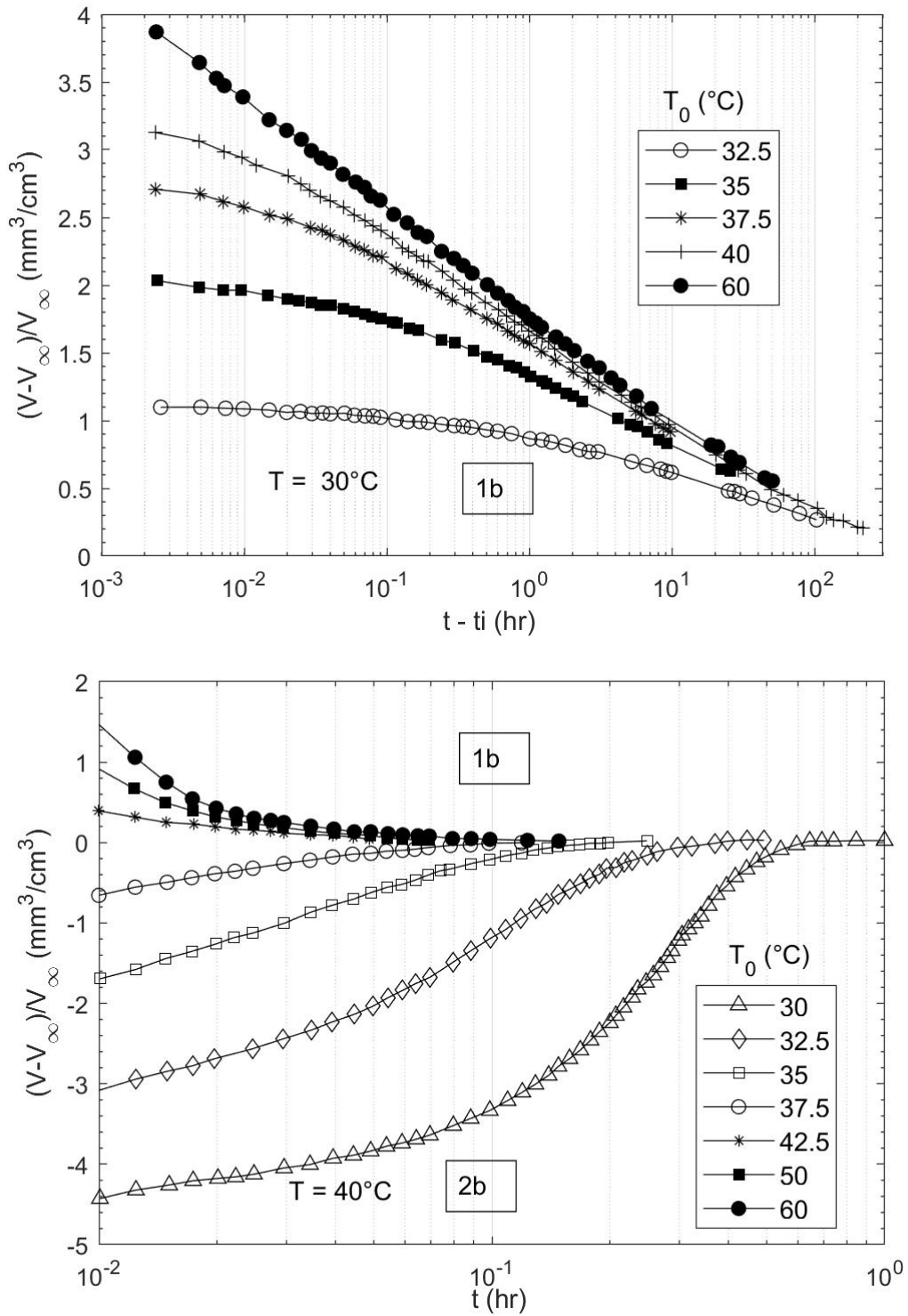


Figure 1.4: (continued)

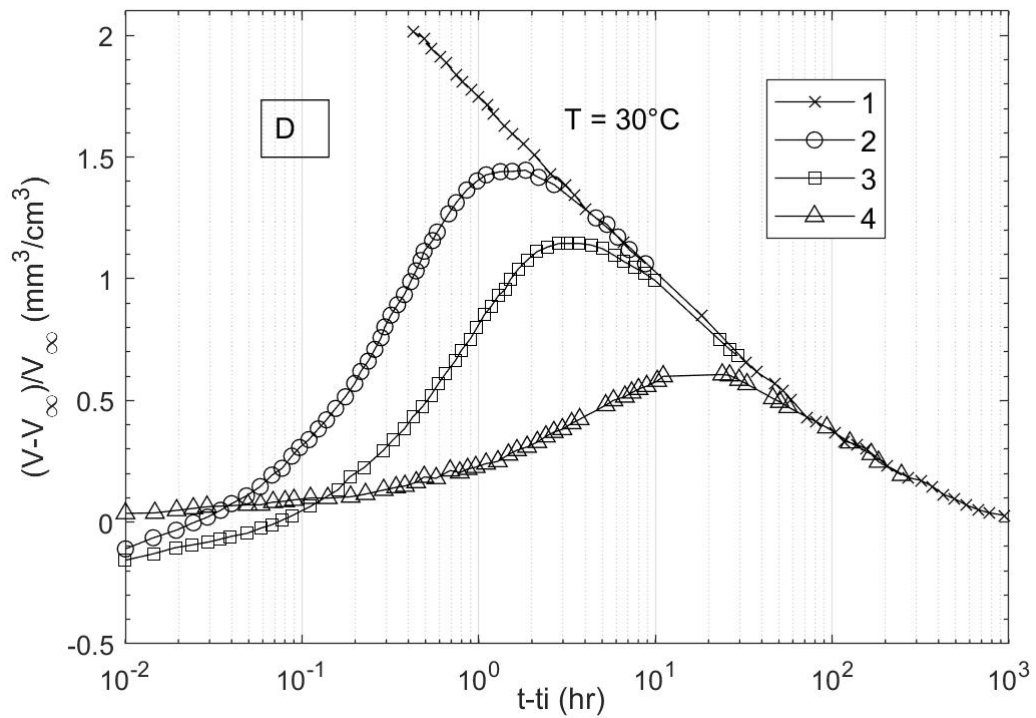
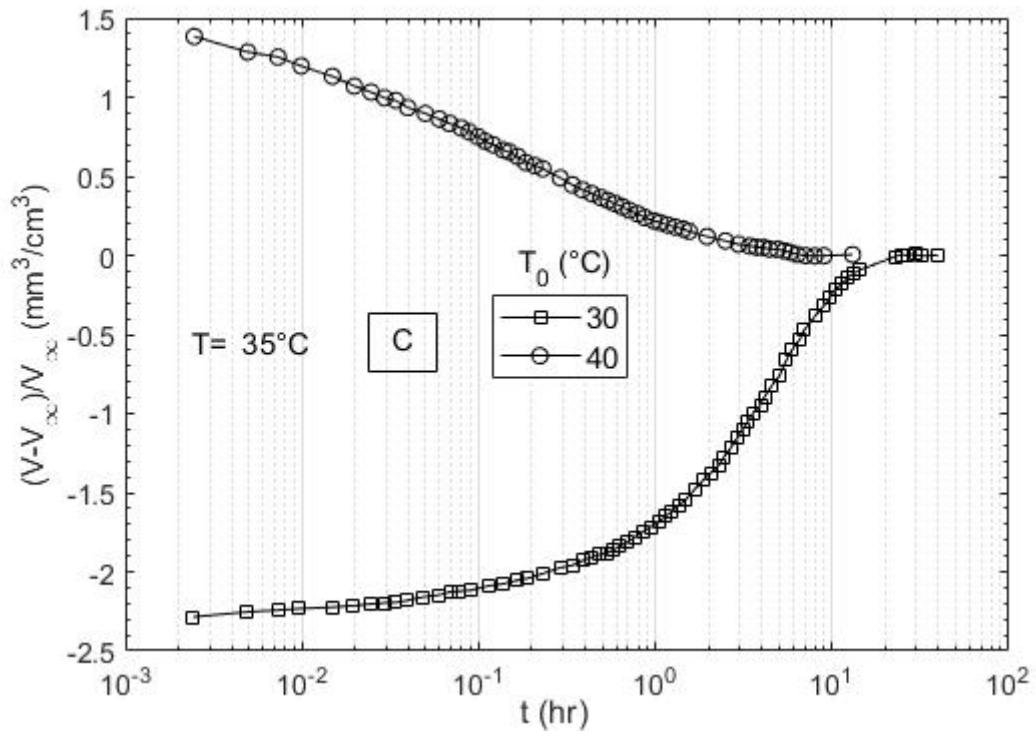


Figure 1.4: (continued)



When  $T \ll T_g$  the glassy structure relaxes very slowly so that, rarely, dilatometric measurements have been performed in the literature (figure 1.5a). Transitions different from the  $\alpha$ -transition mentioned above have been identified: they always appears at lower temperatures and represents a typical feature of the glassy state in the C region (figure 1.2a). In figure 1.5b a variety of molecular mechanisms, that are probably not arrested, are highlighted and, possibly, lead the structure to the glass equilibrium. In the literature, more attention has been focused on mechanical, dielectric and calorimetric measurements aimed to understand the differences between the  $\alpha$  and  $\beta$  transitions. Saito *et al.* performed dielectric and conductive experiments on several polymers (PVC, PVA, PET and PCTFE) by varying the frequency at fixed temperatures and pressures [16]. The  $\beta$ -relaxation peak is well separated and it is attributed to the local motion of the frozen main chain. The relaxation characteristic times in the glassy state follows the arrhenius equation and, as a consequence, this phenomenon is thought to be an activated process. On the contrary,  $\alpha$ -relaxation characteristic times are thought to be associated with the micro-Brownian motion of the main chain. Muzeau *et al.* studied physical ageing of PMMA samples through differential scanning calorimetry (DSC) and dynamic mechanical analysis (DMA) by heating the samples from  $T \ll T_g$  to  $T \gg T_g$  after annealing at  $T \ll T_g$  during a specific time [17, 18]. They found the higher the ageing temperature the higher the enthalpy loss and the enthalpy recovery temperature; the same was true for the shear modulus and the loss spectra measured on the same material. The authors believe physical ageing affects  $\alpha$ -relaxation only. It is possible that the temperature spectrum of the  $\alpha$ -transition is superposed on the  $\beta$ -transition T-spectrum and, as a result, the latter is partly hidden. Moreover, at fixed frequency and pressure, physical ageing does not affect the temperature at which the  $\beta$  peak is observed. As pointed out by Johari, the mechanisms affecting the  $\beta$ -relaxation process have not been still understood. Particularly, it is unknown whether all molecules or just a few confined to certain sites of loose packing (resulting from frozen-in density fluctuations) are involved in the reorientational motions [17].

Calorimetry is a powerful technique to study vitrification although a direct measurement of the material heat capacity, the quantity of interest, is not possible. By choosing a temperature ramp scan, the DSC experiment returns the heat flux associated with the sample by measuring the temperature difference between the sample and an Al empty pan whose properties are well known [19, 20, 21]. Then, by numerical integration, the heat capacity of the sample is derived. A new approach to calorimetric measurements has been introduced in the last few decades: it consists in the addition of a modulated temperature signal to the basic temperature ramp scan of a DSC. This technique called MTDSC allows the user to separate the thermal signal in:

- 1- an average signal (called ‘Total signal’)
  - 2- a ‘reversing’ and a ‘non-reversing’ signals whose sum returns the average signal.
- MTDSC is based on simultaneously measuring the heat capacity of the sample using

both methods and comparing them. When the sample is inert and there are no significant temperature gradients between the sample temperature sensor and the centre of the sample, both methods should give the same value. Assuming the temperature program is as follows:  $T = T_0 + \beta * t + B \cdot \sin(\omega t)$ , two heat capacity measurements are carried out with a MTDSC experiment [21]:

$$C_p^{tot} = \frac{\dot{Q}}{\beta}$$

$$C_p^{rev} = \frac{A_{HF}}{A_{HR}} \quad (1.2)$$

Then  $C_p^{nonrev} = C_p^{tot} - C_p^{rev}$

where  $\dot{Q}$  is the *Total Heat flow* signal, i.e. the heat flow necessary to apply the temperature ramp scan;  $\beta$  is the rate of temperature change chosen for the ramp;  $A_{HF}$  is the amplitude of the *Heat Flow Modulation* signal, i.e. the amplitude of the heat flow needed to yield the desired modulated temperature;  $A_{HR}$  is equal to  $\omega B$  and is called amplitude of modulation in heating rate. In order to understand better the practical meaning of the reversing and non-reversing signals, MTDSC experiments conducted on A-PS are reported in figure 1.6. It is shown that, at low degrees of annealing, the non-reversing signal returns the enthalpy loss on annealing (figure 1.6a). In this sense, it is non-reversing in the same way as a chemical reaction or crystallization event. However, at higher ageing times, this is no more true because the reversing signal changes too and becomes sharper (figure 1.6b). Moreover, the two signals are frequency dependent, i.e. the lower the frequency the lower the  $T_g$  because the time scale of the measurement becomes longer (figure 1.6c); and it is highlighted in figure 1.6d that the rate of cooling inevitably affects the reversing signal. Hourston *et al.* observed that MTDSC can be used to study  $\beta$ -transitions in PS [22]. Annealing at toom temperature for several days causes the appearance of a secondary endothermic peak at a temperature ( $\sim 60^\circ\text{C}$ ) lower than the  $\alpha$ - $T_g$  ( $\sim 80^\circ\text{C}$ ). The PS sample had a  $M_n$  of 9.3E04 and  $M_w$  of 2.1E05.

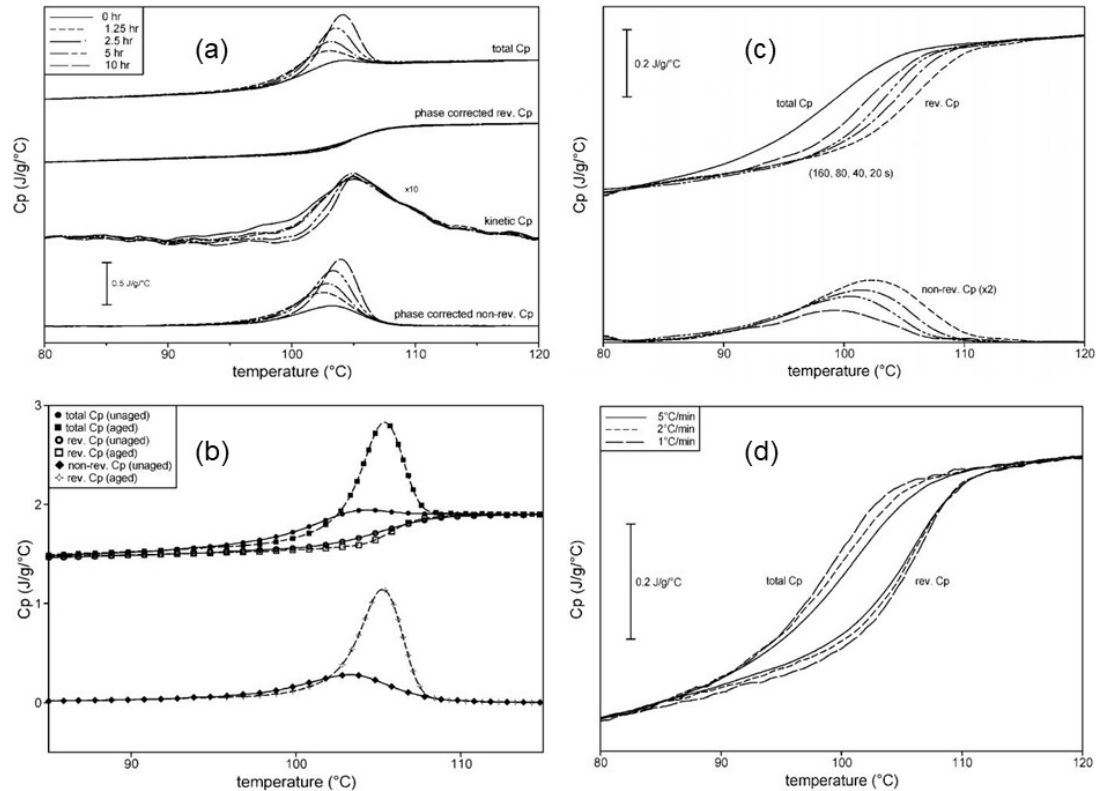


**Figure 1.6:** MTDSC experiments on PS: a) heating after low annealing times; b) heating after high annealing times; c) cooling with different modulation frequencies; d) cooling with different cooling rates [21]

## 1.5 Vitrification Theories

Several theories have been built up in order to explain the glass transition; here, two of them are presented: one kinetic and the other thermodynamic [23]. The former is known as the *free volume* theory: Cohen and Turnbull associated this concept with the translational diffusion coefficient of hard spheres [24, 25]. According to them, vitrification occurs when the volume available for translational molecular motion falls below a critical value. The total volume of a molecule in a glassy state can be divided into two types of volume:  $v_0$  is the volume per molecule excluded to all other molecule (or the *Van der Waals volume*); the excess volume (given by the difference between the total occupied volume,  $v$ , and  $v_0$ ). At low temperatures the excess volume of a glass is uniformly distributed because favoured energetically by packing constraints. The molecules are assumed to vibrate anharmonically around fixed positions and entropy

changes slightly with increasing temperature because randomization of molecular motion is not encouraged. With this picture in mind, a critical value of excess volume exists such that any additional volume can be redistributed at random without energy cost: this is the definition of free volume,  $v_f$ . The thermal expansion coefficient changes consequently from crystal-like to liquid-like and, when  $v_f$  nullifies, the ideal glass transition occurs. The relationship between translational diffusion coefficient and free volume is

$$D = ga^* u \exp\left(-\frac{\gamma v^*}{v_f}\right) \quad (1.3)$$

where  $g$  is a geometric factor usually taken to be  $\frac{1}{6}$ ,  $v^*$  is the minimum free volume capable of accomodating another molecule after the original displacement in the cage,  $a^*$  is of the order of the molecular diameter,  $\gamma$  is a geometric factor accounting for overlapping of free volumes (usually 0.5—1),  $u$  is the gas kinetic velocity. The diffusivity expression has the same form of the viscosity relationship for liquid hydrocarbons proposed by Doolittle *et al.*

$$\eta^{-1} = A \cdot \exp\left(-\frac{bv_0}{v_f}\right) \quad (1.4)$$

where  $A$  and  $b$  are parameters ( $b$  being of order unity),  $v_0$  has the same meaning previously given,  $v_f$  the free volume and  $\tilde{v}$  the specific volume such that

$$v_f = \tilde{v} - v_0 \quad (1.5)$$

The implied inverse relationship between the diffusion and the viscosity is given by the Stokes-Einstein equation. Based on the *kinetic* theory, the WLF equation for the relaxation time spectrum above the glass transition temperature can be explained, i.e. the WLF constants are derived from the free volume concept [25]:

$$\log(a_T) = \log\left(\frac{\tau(T)}{\tau(T_0)}\right) = -\frac{C2(T - T_0)}{C1 + T - T_0} = -\frac{[f^{-1}(T_0)](T - T_0)}{[f(T_0)/\alpha_f] + T - T_0}$$

$T_0$  is the temperature defining the relaxation time scale reference,  $f$  is the fractional free volume ( $v_f/v$ ),  $C1$  and  $C2$  are the WLF constants,  $\alpha_f$  is the thermal expansion coefficient above  $T_g$  ( $\sim 1E - 04$ ). To extend the relaxation time dependence on temperature below  $T_g$  it is necessary to define empirical relations as suggested by Kovacs [26]. The free volume theory was also extended to polymer solutions by Vrentas *et al.* and Fujita [27, 28]. The starting point was respectively the Cohen/Turnbull and the Doolittle theories but the same approximation given by relationship 1.5 was made. The former theory is capable of predicting the composition dependence of the mobilities of the jumping units by estimating the parameters from the pure components properties. The latter is

less predictive but gives the temperature and composition dependence of  $v/v_f$  in actual polymer solutions from appropriate mobility data.

The second thermodynamic approach was derived by Gibbs and Di Marzio during the 50's [29, 30]. The authors combined a statistical lattice model with the theory of second order phase transitions to predict the glass transition of polymers. It is useful to define first the concept of first order phase transition. By assuming a unary closed system whose state is defined by pressure and temperature, the thermodynamic conditions which enable the system to be heterogeneous and at equilibrium are:

$$\begin{cases} P^\alpha = P^\beta \\ T^\alpha = T^\beta \\ \mu^\alpha(P, T) = \mu^\beta(P, T) \end{cases} \quad (1.6)$$

where  $\alpha$  and  $\beta$  refer to the two phases in equilibrium,  $\mu$  is the chemical potential of the compound in each phase (equal to the molar Gibbs free energy). The last relation implies that a space curve exists where all the equilibrium conditions are met and it is defined by the interception of the two surfaces  $\mu$ . At each point of the space equilibrium curve, a step change of the first derivative of the molar Gibbs free energy must be observed, i.e. of both the entropy and the specific volume between the two phases. Briefly, the theory from Gibbs and Di Marzio states that the formation of an ideal glass is a true second order phase transition in the Erhenfest sense, i.e. characterized by continuity of the first derivatives of the Gibbs energy ( $S$  and  $V$ ) and discontinuity of the second derivatives ( $C_p$  and thermal expansion coefficient) [5, 31]. The key of this new approach is the definition of a thermodynamic  $T_g$  (called  $T_2$ ) at which the configurational entropy ( $S_c$ ) of the system nullifies. This idea was capable of both overcoming the Kauzmann paradox (figure 1.7 left) and fixing the difference between the experimental and the theoretical  $T_g$  when a sample is cooled from above it. By extrapolating stable and metastable behaviours below  $T_g$ , Kauzmann assumed the existence of a temperature ( $T_k$ ) at which the entropy difference between the supercooled liquid and crystal phases vanishes. This could happen provided the liquid is cooled sufficiently slowly so that it would not fall out of equilibrium, yet without crystallising. Experimentally, it is not possible to observe this phenomenon because vitrification intervenes. But if this was confirmed, then the entropy of the metastable phase would be lower than the entropy of the crystal at  $T < T_k$  (unusual but not impossible) and, at  $T = 0K$  (when the crystal entropy vanishes), the entropy of the metastable liquid would be negative. The latter is not possible in thermodynamics and it is defined as the Kauzmann paradox [5]. Gibbs and Di Marzio ideal glass transition temperature ( $T_g$ ) is the Kauzmann temperature  $T_2$  (figure 1.7).

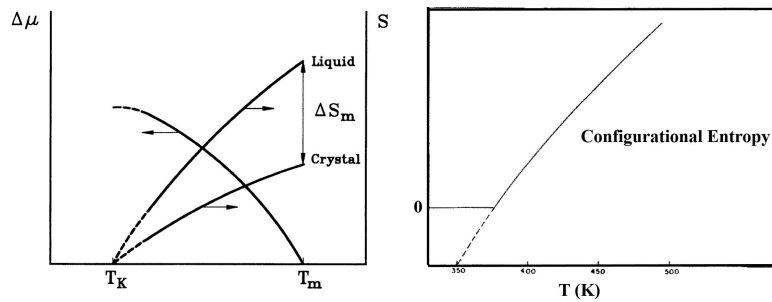


**Figure 1.7:** (left) *Kauzmann paradox*, at  $T_2$  the entropy difference vanishes; (right) Gibbs/Di Marzio theory states the vanishing of the configurational entropy at  $T_g$  [5, 29]

The authors assumed that the entropy of a deeply supercooled polymer liquid can be separated into configurational and vibrational contributions. Furthermore, the latter is equal in the perfectly ordered solid and in the highly supercooled liquid, i.e. the molecules in a deeply supercooled liquid execute vibrations about their local equilibrium positions most of the time, and the slight anharmonicity in the liquid phase vibrations is all that distinguishes fluid and solid phase vibrational entropies. The configurational entropy is then simply the difference between the entropies of the supercooled liquid and the ordered crystal. In the Gibbs and Di Marzio theory this entropy vanishes at a non-zero temperature  $T_2$ . The main parameter accounted for in this model is the *flexibility* ( $\delta$ ) of the linear chain, which is expressed as a *flex* energy ( $u = \varepsilon_2 - \varepsilon_1$ ), i.e. the increase in the intramolecular energy accompanying the “flexing” of a bond in the chain molecule. The thermodynamic theory of Gibbs and Di Marzio works well when cooling experiments from the rubbery equilibrium phase are performed: however, it is not capable of dealing with the hysteresis encountered during heating experiments (figure 1.2a).

The following list summarize several aspects of a II order phase transition [32]:

- a- the state of the body changes continuously (V, T, P, S);
- b- the transition from *order* (lower symmetry) to *disorder* (higher symmetry) is discontinuous (atoms or property positions);
- c- an order parameter ( $\eta$ ) describes the process. It is zero in the disordered phase and non-zero in the ordered phase; the Gibbs free energy reaches a minimum at the transition as a function of  $\eta$ .
- d- usually, the disordered phase corresponds to higher temperatures and viceversa;
- e- it is not accompanied by evolution or absorption of heat;
- f- superheating and supercooling effects are impossible.

To conclude this section, it is worthnoting to report the statement from Landau who asserts ‘*as the transition point is approached, the minimum of the Gibbs free energy as a function of  $\eta$  becomes steadily flatter...the equilibrium value of  $\eta$  becomes steadily*

weaker, so that the relaxation time for the establishment of equilibrium with respect to the order parameter increases without limit' [32]. Also, the Prigogine-Defay ratio is not satisfied [31]. No definitive proof exists that a thermodynamic II order transition is taking place when an organic rubbery polymer vitrifies and viceversa. Moreover, the  $T_g$  measurement is always affected by the applied stimulus rate. Summarizing, thermodynamics and kinetics are to be taken into account both to understand the transition.

## 1.6 Thermoplastic Polymer Solutions: Theory and Practice

The thermodynamics of polymeric solutions is treated theoretically with the approach of rational thermodynamics [31]. Lower case letters identify constitutive functions of the upper case thermodynamic quantities. Equilibrium values are identified by the superscript \*. Starting from a one component—one phase reacting system whose state is defined by:

$$\sigma = \{V, T, x\}$$

where  $V$  and  $T$  are the external site variables and  $x$  the internal state variable, the second law of thermodynamics based on the Helmholtz free energy states that (equation 1.7):

$$[\partial a/\partial V + P]\dot{V} + [\partial a/\partial T + S]\dot{T} + (\partial a/\partial x)\dot{x} \leq 0 \quad (1.7)$$

and must hold true for every conceivable transformation, i.e. whatever the values of  $V$ ,  $T$ ,  $\dot{V}$  and  $\dot{T}$  are chosen at any one instant of time. 'x' cannot be imposed from outside by nature so that a relationship for 'x' is needed: i.e. 'x' is a function of state  $\dot{x} = f(V, T, x)$  and at equilibrium the value  $x = x^*$  is derived from the relationship  $\dot{x} = f(V, T, x^*) = 0$ . As a consequence, the relationships 1.8 are obtained:

$$P = - \partial a/\partial V \quad (1.8a)$$

$$S = - \partial a/\partial T \quad (1.8b)$$

$$Z = - (\partial a/\partial x)\dot{x} \geq 0 \quad (1.8c)$$

The quantity  $\partial a/\partial x$  is called the affinity  $\theta$  of the system and at equilibrium must vanish as well as  $\dot{x}$ . Onwards, a closed two components—two phases non reacting system will be treated with the same approach. The two phases will be identified with superscripts  $\alpha$  and  $\beta$  whereas the component of interest with subscripts 1 and 2. Extensive properties will be identified with an apostrophe (') whereas intensive properties will have no additional symbol. Bold letters identify the vector of their respective variables and whose components are related to each component of the system under investigation. The rate

of change of  $A'$  and  $S'$  for the whole system is given by

$$\begin{aligned}\dot{A}' &= \dot{A}'^\alpha + \dot{A}'^\beta \\ \dot{S}' &= \dot{S}'^\alpha + \dot{S}'^\beta\end{aligned}\quad (1.9)$$

and the second law reduces to (equation 1.9):

$$[\partial A'/\partial V' + P]\dot{V}' + [\partial A'/\partial T + S']\dot{T} + \boldsymbol{\mu}^\alpha \cdot \dot{\mathbf{n}}^\alpha + \boldsymbol{\mu}^\beta \cdot \dot{\mathbf{n}}^\beta \leq 0 \quad (1.10)$$

A balance of matter between the two phases states:

$$\dot{\mathbf{n}}^\alpha = -\dot{\mathbf{n}}^\beta$$

and the same arguments applied above implies:

$$(\boldsymbol{\mu}^\alpha - \boldsymbol{\mu}^\beta) \cdot \dot{\mathbf{n}}^\alpha \leq 0 \quad (1.11)$$

The last inequality is compared with equation 1.8c and the affinity  $\theta$  of the system is derived:

$$\theta = \boldsymbol{\mu}^\alpha - \boldsymbol{\mu}^\beta$$

At equilibrium  $\theta = 0$  implies

$$\boldsymbol{\mu}^{*\alpha} = \boldsymbol{\mu}^{*\beta} \quad (1.12)$$

The inequality 1.11 also implies that, of all two-phase states corresponding to assigned temperature and pressure, the equilibrium state has the lowest total free enthalpy (equation 1.13)

$$\begin{aligned}\boldsymbol{\mu}^\alpha \cdot \dot{\mathbf{n}}^\alpha + \boldsymbol{\mu}^\beta \cdot \dot{\mathbf{n}}^\beta &= \left( \frac{\partial A'^\alpha}{\partial \mathbf{n}^\alpha} \right)_{V,T} \cdot \dot{\mathbf{n}}^\alpha + \left( \frac{\partial A'^\beta}{\partial \mathbf{n}^\beta} \right)_{V,T} \cdot \dot{\mathbf{n}}^\beta \\ &= \left( \frac{\partial G'^\alpha}{\partial \mathbf{n}^\alpha} \right)_{P,T} \cdot \dot{\mathbf{n}}^\alpha + \left( \frac{\partial G'^\beta}{\partial \mathbf{n}^\beta} \right)_{P,T} \cdot \dot{\mathbf{n}}^\beta \\ &= \dot{G}'^\alpha + \dot{G}'^\beta \\ &= \dot{G}' \leq 0\end{aligned}\quad (1.13)$$

Figure 1.8 shows the behaviour of the free enthalpy  $G$  against the composition of component #1 for a two components system exhibiting a miscibility gap. The *spinodal region* is the locus of unstable states whereas the region between points {F, H} and the spinodal region is the locus of metastable states and it is called *binodal region*. No detailed analysis of the diagram is given here. It is only stated that, at point F and H,  $G$  is a minimum (equilibrium points) and, therefore, at the  $T$  and  $P$  of the mixture equation 1.12 is satisfied. To verify that the  $G$  function must have the behaviour highlighted in the figure, a second relation must be fulfilled when the mixture unmixes (equation

1.14c):

$$\text{if} \quad dG' = \left( \left( \frac{\partial G'}{\partial n_1} \right)_{P,T} - \left( \frac{\partial G'}{\partial n_2} \right)_{P,T} \right) dn_1 \quad (1.14a)$$

$$\text{dividing by 'n'} \quad dG = (\mu_1 - \mu_2) dy_1 \quad (1.14b)$$

$$\text{i.e.} \quad \left( \frac{\partial G}{\partial y_1} \right)_{P,T} = \mu_1 - \mu_2 \quad (1.14c)$$

where  $n_1, n_2$  are the moles of component #1, #2 in the mixture and  $n$  is their sum;  $y_1$  is the mole fraction of component #1 in the whole system;  $\mu_i$  is the chemical potential of component 'i' in the mixture. Indeed, the slope of  $G$  is alike at both F and H composition. Equation 1.14c is valid for several pairs  $\{y_1^\alpha; y_1^\beta\}$  in figure 1.8 but {F, H} is the unique pair satisfying also the equilibrium conditions (1.11).

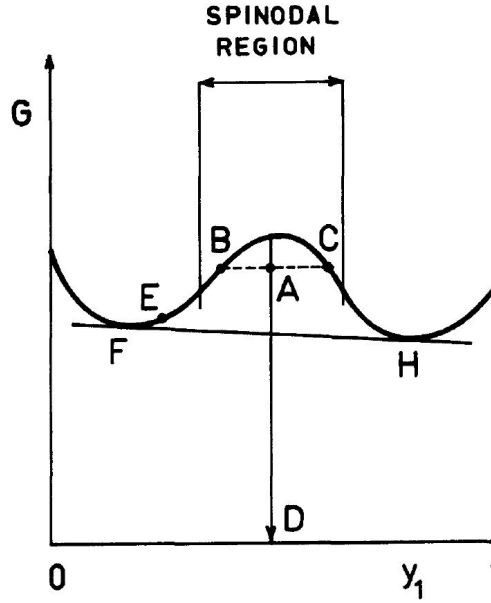


**Figure 1.8:** Free enthalpy vs. composition plot for a two-component mixture exhibiting a miscibility gap. [31]

Finally, in order to study the miscibility gap, it is possible to resort to the chemical potential diagram of a specific component ( $\mu_i$ ) in the mixture and to mathematical relations identifying the spinodal region: e.g., with respect to component #1 (equations 1.15) the following are derived.

$$\begin{aligned} (\partial\mu_1/\partial y_1)_{P,T} &= -(\partial\mu_1/\partial y_2)_{P,T} = 0 \\ (\partial^2\mu_1/\partial y_1^2)_{P,T} &= (\partial^2\mu_1/\partial y_2^2)_{P,T} = 0 \end{aligned} \quad (1.15)$$

The equilibrium thermodynamic theory presented above works very well for thermoplastic polymer solutions in the rubbery state. In fact, the system is fast enough to unmix and to accomplish phase equilibria. Indeed, constitutive equations are needed to express the chemical potentials and predict all the thermodynamic properties of the solution. Generally, ideal solution behaviour of  $c$  components non reacting systems over extended ranges in both composition and temperature requires that the relation 1.16 for the entropy of mixing is fulfilled:

$$\Delta S_{mix} = -R \sum_{k=1}^c n_k \ln n_k \quad (1.16)$$

where  $n_k$  are the moles of component  $k$ . The relation is obtained by stating that the behaviour of the solution is analogous to an ideal gas mixture for which the following constitutive equation holds:

$$PV = nRT$$

The following properties are derived:

- 1- the solution is athermic, i.e.  $\Delta H_{mix} = \Delta U_{mix} = 0$
- 2- the volumes are additive, i.e.  $\Delta V_{mix} = 0$ .

### 1.6.1 Flory's Statistical lattice fluid model

Experimentally, it was observed that the activity of benzene in solution with rubber as a function of the volume fraction of rubber does not follow the ideal behaviour [33]. Flory reports that  $\Delta V_{mix}$  is probably not zero and, therefore, he derived a new expression for the entropy of mixing of a binary liquid mixture based on the following hypotheses:

- a) solvent molecules are identical in size, spatial configuration, external force field and are assumed spherical; the chain polymer is assumed to consist of ' $x$ ' chain segments, each of which is equal in size to a solvent molecule.
- b) molecules may be arranged in a lattice with enough regularity because only the first coordination sphere (' $z$ ') is of importance, i.e. the lattice coordination number or the number of cells which are first neighbours to a given cell;
- c) the same lattice may be used to describe the configurations of both pure components and their solutions;
- d) the polymer solution is diluted;
- e) randomness of mixing is accounted for;

The lattice fluid model based on the previous hypotheses has been the first statistical thermodynamic approach applied to polymer diluted solutions. The goal was the

derivation of the configurational entropy of mixing, i.e. the expression for the entropy as defined by the Boltzmann relation

$$\Delta S_{mix} = k \ln \Omega$$

where  $\Omega$  is the number of ways of arranging the polymer and solvent molecules within the lattice. Equation 1.17 is obtained from Flory's theory.

$$\Delta S_{mix} = -R\{n_1 \ln[n_1/(n_1 + xn_2)] + n_2 \ln[n_2/(n_1 + xn_2)] - n_2(x-1) \ln[(z-1)/e]\} \quad (1.17)$$

The formation of the solution is conceived to occur in two steps: disorientation of the polymer molecules ( $\Delta S_{dis}$ ) and mixing of them with the solvent ( $\Delta S_{mix}^*$ )

$$\Delta S_{mix} = \Delta S_{dis} + \Delta S_{mix}^*$$

. These two contributions are reported in equations 1.18.

$$\Delta S_{dis} = \Delta S_{mix}(n_1 = 0) = -Rn_2\{\ln x + (x-1) \ln(z-1)/e\} \quad (1.18a)$$

$$\Delta S_{mix}^* = \Delta S_{mix} - \Delta S_{dis} = -R(n_1 \ln v_1 + n_2 \ln v_2) \quad (1.18b)$$

where  $v_1$  and  $v_2$  are the volume fractions of solvent and solute or

$$\begin{aligned} v_1 &= n_1/(n_1 + xn_2) \\ v_2 &= xn_2/(n_1 + xn_2) \end{aligned} \quad (1.19)$$

The asterisk indicates that the entropy of mixing is computed by considering the external arrangement of the molecules and their segments without considering energetic contributions between near neighbours. The comparison of equations 1.16 and 1.18b shows that mole fractions occurring in the ideal expression are replaced by volume fractions occurring in the formula for mixing of molecules with different size. Flory's statistical theory also enables the evaluation of the heat and volume of mixing the pure solvent and the pure liquid polymer. Interactions between first near neighbours must now be taken into account whereas long distance interactions give no contribution. Following the *quasichemical* theory of solutions, the interaction between two molecules of different species is represented as follows:

$$[1,1] + [2,2] = 2[1,2]$$

The energy difference involved in this reaction is

$$\Delta w_{12} = 2w_{12} - (w_{11} + w_{22})$$

The total heat of mixing is given by considering all the pairs of unlike molecules and by applying Flory's approximation to the number of neighbours of a single polymer chain:

$$Q = (x-2)(z-2) + 2(z-1) \simeq xz$$

Relation 1.20 shows the final result for the heat of mixing. By generalising it to the case of polymer blends (i.e. the solvent is a polymer of  $x_l$  segments), the number of unlike pairs is related to the total number of possible interactions for the solvent (species #1) molecules ( $zx_l n_l$ ) averaged over the volume fraction of the polymeric (species #2) molecules ( $v_2$ ).

$$\Delta H_{mix} = z\Delta w_{12}x_l n_l v_2 = RT\chi_1 n_l v_2 \quad (1.20)$$

where  $\chi_1 RT$  is the difference in energy of a solvent molecule immersed in the pure polymer ( $v_2 \simeq 1$ ) compared with one surrounded by molecules of its own kind. This parameter indicates whether heat is involved in the mixing process and particularly:

$$\begin{aligned} \chi_1 = 0 &\rightarrow \text{athermic mixing} \\ \chi_1 > 0 &\rightarrow \text{endothermic mixing} \\ \chi_1 < 0 &\rightarrow \text{exothermic mixing} \end{aligned} \quad (1.21)$$

The author chooses to approximate the total entropy of mixing only with the configurational entropy contribution and he assumes that neighbouring interactions are just of importance to the enthalpy of mixing. He tries to generalise the theory by adding the missing entropic interaction contribution within  $\Delta w_{12}$ : i.e. an additional part which is entropic by nature is added and, consequently,  $RT\chi_1 n_l v_2$  is not regarded as a standard state enthalpic change anymore but as a standard state free energy change. The free energy of mixing is provided by equation 1.22.

$$\begin{aligned} \Delta G_{mix} &= \Delta H_{mix} - T\Delta S_{mix} \simeq \Delta H_{mix} - T\Delta S_{mix}^* \\ &= RT\{n_1 \ln(v_1) + n_2 \ln(v_2) + \chi_1 n_l v_2\} \end{aligned} \quad (1.22)$$

Equations 1.23 highlights the final and most generalised formulas for the total entropy and enthalpy of mixing.

$$\begin{aligned} \Delta S_{mix} &= -(\partial\Delta G_{mix}/\partial T)_P \\ &= R\{n_1 \ln(v_1) + n_2 \ln(v_2) + [\partial(\chi_1 T)/\partial T]n_l v_2\} \end{aligned} \quad (1.23)$$

$$\begin{aligned} \Delta H_{mix} &= -T^2(\partial(\Delta G_{mix}/T)/\partial T)_P \\ &= -RT^2(\partial\chi_1/\partial T)n_l v_2 \end{aligned}$$

If no entropy contribution is included in  $\chi_1$ , both equations 1.23 simplify to equations 1.18b and 1.20. The chemical potential  $\mu_1$  of the solvent in the solution relative to its chemical potential in the pure liquid is given in equation 1.24.

$$\mu_1 - \mu_1^0 = R(\partial\Delta G_{mix}/\partial n_1)_{T,P} = RT[\ln(1 - v_2) + (1 - 1/x)v_2 + \chi_1 v_2^2] \quad (1.24)$$

The major drawbacks of Flory's theory are:

- a) it describes only upper critical solution temperature diagrams;
- b) it cannot describe volumetric behaviour;
- c) the parameter  $\chi$  is not independent of temperature, pressure and composition

## 1.6.2 Sanchez and Lacombe Statistical lattice fluid model

The Sanchez and Lacombe lattice fluid statistical theory follows the work of J. Paul Flory [34, 35, 36]. The most important hypothesis added to the previous theory is the presence of holes within the lattice. Again, randomness is the main feature describing the mixing process of the  $r_i$ -mers with each other and with the vacant sites. The latter is also called *mean field approximation* which means that, if a single molecule cannot occupy two sites, the probabilities of being occupied or vacant are independent for the two sites. The primary statistical mechanical problem is to determine the number of configurations available to a system of  $N$  molecules of a single species or a mixture (each of which occupies  $r_i$  sites, i.e. an  $r_i$ -mer) and  $N_0$  vacant sites (holes). Consequently, even in the case of a pure liquid compound, the model treats the fluid phase as a binary mixture, being the holes the second species. Moreover, the following features are used to describe the lattice framework:

- a) the total number of lattice sites ( $N_r$ ) of a binary mixture of  $N$   $r$ -mers and  $N_0$  empty sites is

$$N_r = rN + N_0 \quad (1.25)$$

- b) the coordination number of the lattice is  $z$  and each  $r$ -mer is surrounded by  $Q$  nearest nonbonded neighbours where

$$Q = qz = r(z - 2) + 2 \quad (1.26)$$

This time Flory's approximation is not followed. 'q' is then defined by the ratio between the total interacting number of sites for a  $r$ -mer and the interacting number of sites of a single mer, i.e. it is a parameter describing the amount of interacting surface of each  $r$ -mer.

- c) a  $r$ -mer is characterized by a symmetry number  $\sigma$  (this parameter is of no quantitative importance to the SL theory)
- d) a *flexibility* parameter  $\delta$  characterizes the polymer chain and it is equal to the number of ways in which the  $r$ -mer can be arranged on the lattice after one of its mers has been fixed on a lattice site. It is a measure of the internal degree of freedom and it is assumed independent of temperature and pressure.

Contrary to Flory's theory, the polymer chain is not totally free to move. The close packed volume of a single chain is  $rv^*$  and it is independent of temperature and pressure. Three parameters describe a single compound:

- a)  $r$ : the number of segments constituting the chain. Each segment can occupy a unique cell within the lattice.
- b)  $v^*$ : the close packed volume of a single segment (or its lattice cell). Indeed, a hole occupies the same volume.
- c)  $\varepsilon^*$ : the total interaction energy per segment or  $\varepsilon^* = z\varepsilon/2$  where  $\varepsilon$  is the non-bonded mer-mer interaction energy.

The parameters of the Sanchez and Lacombe model have been standardized during the last decades and the notation is summarized in the Appendix (figure A.2). The main result of the SL statistical theory is the derivation of the free energy ( $G$ ) from the classical Boltzmann expression and of an EOS as follows in equations 1.27.

$$\begin{aligned} \tilde{G} = G/(Nr\varepsilon^*) &= -\tilde{\rho} + \tilde{P}\tilde{v} + \tilde{T}[(\tilde{v} - 1)\log(1 - \tilde{\rho}) + \frac{1}{r}\log(\tilde{\rho}/w)] \\ \left(\frac{\partial\tilde{G}}{\partial\tilde{v}}\right)_{\tilde{T},\tilde{P}} &= \tilde{\rho}^2 + \tilde{P} + \tilde{P}[\log(1 - \tilde{\rho}) + (1 - 1/r)\tilde{\rho}] = 0 \end{aligned} \quad (1.27)$$

where the uppersigned variables are defined as follows

$$\tilde{T} = T/T^*; \quad T^* = \varepsilon^*/R \quad (1.28a)$$

$$\tilde{P} = P/P^*; \quad P^* = \varepsilon^*/v^* \quad (1.28b)$$

$$\tilde{v} = 1/\tilde{\rho} = V/V^*; \quad V^* = Nr v^* \quad (1.28c)$$

In the case of a mixture, the flexibility parameter  $\delta_i$  is defined as follows [37]:

$$\delta_i = z \left(\frac{(z-2)}{f_i}\right)^{(r_i-2)f_i} \left(\frac{1}{1-f_i}\right)^{(r_i-2)(1-f_i)} \quad (1.29)$$

$\delta_i$  is the number of internal configurations available to a semiflexible chain molecule of  $r_i$ -mers in free space when  $f_i(r_i - 2)$  bonds in a type  $i$  molecule are in *flexed* or high-energy states and  $(1 - f_i)(r_i - 2)$  bonds are in a low-energy state. In a completely filled lattice,  $\delta_i$  is reduced by a factor of  $\omega_i$  caused by inter- and intramolecular steric hindrance.  $\Delta\varepsilon_i$  identifies the *flex energy* of compound type  $i$ , i.e. the increase in intramolecular energy that accompanies the *flexing* of a bond in a type  $i$  chain molecule. Usually, only two energy states are taken into account:  $z-2$  are at high energy and one is at low energy.  $f_i$  dependence on  $\Delta\varepsilon_i$  follows:

$$f_i = \frac{(z-2)\exp(-\frac{\Delta\varepsilon_i}{kT})}{1 + (z-2)\exp(-\frac{\Delta\varepsilon_i}{kT})} \quad (1.30)$$

Moreover, the combining rules aim to keep the additivity of:

- a) the close packed pure volumes:

$$V^* = \sum_{i=1}^n r_i^0 v_i^* N_i = \sum_{i=1}^n r_i v^* N_i \quad (1.31)$$

b) the pair interactions of the components in their close packed pure states:

$$(z/2)rN = (z/2) \sum_{i=1}^n r_i^0 N_i = (z/2) \sum_{i=1}^n r_i N_i \quad (1.32)$$

c) the characteristic pressures are pairwise additive in the close packed mixtures:

$$P^* = \sum_{i=1}^n \sum_{j=1}^n \phi_i \phi_j P_{ij}^* \quad (1.33)$$

$$P_{ij}^* = \zeta_{ij} (P_i^* P_j^*)^{1/2} = (1 - k_{ij}) (P_i^* P_j^*)^{1/2}$$

where the superscript 0 refers to the pure component parameter,  $v^*$  is the averaged close packed volume of the mixture and  $N = N_1 + N_2$  is the total number of mole of the mixture.  $\zeta$  describes the deviation of  $P_{12}^*$  from the geometric mean. The interaction energy of the mixture  $\varepsilon^*$  is given as follows

$$\varepsilon^* = P^* \cdot v^* = \left( \sum_{i=1}^n \sum_{j=1}^n \phi_i \phi_j P_{ij}^* \right) \left( \sum_{i=1}^n r_i v_i^* N_i \right) \quad (1.34)$$

and, consequently, it is not pairwise additive unless  $v_1^* = v_2^*$ . The other mixing rules are given in equations 1.35.

$$T^* = P^* \sum_{i=1}^n \phi_i^0 T_i^* / P_i^*$$

$$1/r = \sum_{i=1}^n \phi_i^0 / r_i^0 \quad (1.35)$$

$$\phi_i = (\omega_i / \rho_i^*) / \sum_{j=1}^n (\omega_j / \rho_j^*)$$

$$\phi_i^0 = (\phi_i P_i^* / T_i^*) / \sum_{j=1}^n (\phi_j P_j^* / T_j^*)$$

where  $\omega_i$  is the mass fraction of component  $i$  and  $\phi_i$  is the volume fraction of component 'i'. The definition of the reduced variables as well as the EOS are the same for the mixture and the pure fluid respectively. Equations 1.36 show the SL expressions for the

free energy of a binary mixture, the chemical potential of component #1.

$$\begin{aligned} \tilde{G} = & -\tilde{\rho} + \tilde{P}\tilde{v} + \tilde{T}\tilde{v} \left[ (1 - \tilde{\rho}) \log(1 - \tilde{\rho}) + \frac{\tilde{\rho}}{r} \log(\tilde{\rho}) \right] + \\ & \tilde{T} \left[ \frac{\phi_1}{r_1} \log(\phi_1) + \frac{\phi_2}{r_2} \log(\phi_2) \right] \end{aligned} \quad (1.36a)$$

$$\begin{aligned} \mu_1 = & RT \left[ \log(\phi_1) + (1 - r_1/r_2)\phi_2 + r_1^0\tilde{\rho}\Gamma_{12}\phi_2^2 \right] + \\ & r_1^0RT \left\{ -\tilde{\rho}/\tilde{T}_1 + \tilde{P}_1\tilde{v}/\tilde{T}_1 + \tilde{v} \left[ (1 - \tilde{\rho}) \log(1 - \tilde{\rho}) + \frac{\tilde{\rho}}{r_1^0} \log(\tilde{\rho}) \right] \right\} \end{aligned} \quad (1.36b)$$

The volume and enthalpy of mixing are given by relations 1.37

$$\Delta V_{mix}/V_0 = \tilde{v}/(\phi_1\tilde{v}_1 + \phi_2\tilde{v}_2) - 1 \quad (1.37a)$$

$$\Delta H_{mix}/RT = r \{ \tilde{\rho}\phi_1\phi_2\Gamma_{12} + v^*[\phi_1P_1^*(\tilde{\rho}_1 - \tilde{\rho}) + \phi_2P_2^*(\tilde{\rho}_2 - \tilde{\rho})] / RT \} \quad (1.37b)$$

The entropy of mixing is given by relation 1.38.

$$\begin{aligned} \Delta S_{mix,SL} = & -r \left\{ \frac{\phi_1}{r_1} \log(\phi_1) + \frac{\phi_2}{r_2} \log(\phi_2) + \right. \\ & \left. \tilde{v} \left[ (1 - \tilde{\rho}) \log(1 - \tilde{\rho}) + \frac{\tilde{\rho}}{r} \log(\tilde{\rho}) \right] \right\} + \\ & \frac{r}{\phi_1 + \nu\phi_2} \left\{ \phi_1\tilde{v}_1 \left[ (1 - \tilde{\rho}_1) \log(1 - \tilde{\rho}_1) + \frac{\tilde{\rho}_1}{r_1} \log(\tilde{\rho}_1) \right] \right. \\ & \left. \nu\phi_2\tilde{v}_2 \left[ (1 - \tilde{\rho}_2) \log(1 - \tilde{\rho}_2) + \frac{\tilde{\rho}_2}{r_2} \log(\tilde{\rho}_2) \right] \right\} \end{aligned} \quad (1.38)$$

$V_0$  is the ‘ideal volume’ of the mixture assuming additivity.  $\Gamma_{12}$  is related to  $\zeta_{12}$  as follows:

$$\Gamma_{12} = \Delta P^* v_1^* / RT \quad (1.39a)$$

$$\Delta P^* = P_1^* + P_2^* - 2P_{12}^* = P_1^* + P_2^* - 2\zeta_{ij}(P_i^*P_j^*)^{1/2} \quad (1.39b)$$

The entropy of the system was derived in a following contribution and is presented in

equation 1.40 [37].

$$\tilde{S} = \frac{S}{rNR} = - \left\{ (\tilde{v} - 1) \ln(1 - \tilde{\rho}) + \frac{\ln(\tilde{\rho})}{r} + \left( \frac{\phi_1}{r_1} \right) \ln \left( \frac{\phi_1}{r_1} \right) + \right. \\ \left. \left( \frac{\phi_2}{r_2} \right) \ln \left( \frac{\phi_2}{r_2} \right) + 1 + \frac{\ln(2/z) - 1}{r} + \right. \\ \left. \left( \frac{\phi_1}{r_1} \right) (r_1 - 2) \left[ \ln(1 - f_1) - f_1 \frac{\Delta \varepsilon_1}{RT} \right] + \right. \\ \left. \left( \frac{\phi_2}{r_2} \right) (r_2 - 2) \left[ \ln(1 - f_2) - f_2 \frac{\Delta \varepsilon_2}{RT} \right] \right\} \quad (1.40)$$

Sanchez and Lacombe improve Flory's theory and the new model is capable of predicting LCST's and azeotropic behaviour of solutions beyond retrograde condensation. However, the randomness hypothesis also implies that the energies associated with the bonds of like and unlike molecules are all alike

$$\varepsilon_{11} = \varepsilon_{22} = \varepsilon_{12}$$

Consequently, the enthalpy of mixing for a random solution must be zero. This rule does not belong to the previous theories and it is stated that their validity is of course at high temperatures because  $RT \gg \Delta H_{mix}$ .

### 1.6.3 NRHB Statistical lattice fluid model

The last model treated in this PhD thesis is the NRHB approach built up by Panayiotou *et al.* [38, 39, 40, 40]. The acronym stands for *Non-Random Hydrogen Bonding*. Again, holes are used to account for density variation as a result of temperature and pressure changes but the randomness limitation of the SL model is overcome. Moreover Veytsman's statistics is used to take into account specific interactions between different compounds such as hydrogen bonds [41]. The hypotheses on which the NRHB model is based are:

- a) a parameter 's' defines the surface to volume ratio of each compound as follows

$$s = q/r \quad (1.41)$$

and it is obtained by the group contribution calculation scheme of UNIFAC [42]

- b) the lattice has the same geometry used by Sanchez and Lacombe. 'z' is the lattice coordination number and the total number of contact sites in the system is

$$zN_q = zqN + zN_0 \quad (1.42)$$

- c) the distribution of molecules and holes in the system is nonrandom and the number of configurations available to the molecules and the free volume within the lattice are given by

$$\Omega = \Omega_R \Omega_{NR} \Omega_{HB} \quad (1.43)$$

where the first contribution is due to randomness, the second one refers to nonrandomness of contacts and the last one to specific interactions between the molecules.

- d) each compound is described by three parameters:  $\varepsilon_h^*$  and  $\varepsilon_s^*$  which are used for the calculation of the mean interaction energy per molecular segment  $\varepsilon^*$  according to equation 1.44a;  $v_{sp,0}^*$  which determines the close packed density of a segment  $\rho^* = 1/v_{sp}^*$  as described by equation 1.44b

$$\varepsilon^* = \varepsilon_h^* + (T - 298.15)\varepsilon_s^* \quad (1.44a)$$

$$v_{sp}^* = v_{sp,0}^* + (T - 298.15)v_{sp,1}^* \quad (1.44b)$$

$\varepsilon^*$  can be also thought as the energy required to create a vacancy in the pure component.

- e)  $\delta$  and  $\eta$  define the flexibility parameter and the symmetry/size of the polymer chain respectively. They are related by a parameter  $\omega$  as follows:

$$\omega = \delta/\eta \quad (1.45)$$

Usually  $\eta$  is constant and it is neglected.

The hard core volume per segment  $v^*$  is constant and equal to 9.75 cm<sup>3</sup>/mol for all fluids. A hole occupies the same volume. The remaining parameter  $v_{sp,1}^*$  in equation 1.44b is treated as a constant for a given homologous series. The nonrandom  $\Gamma$  factors correlate random ( $N_{ij}^0$ ) and nonrandom contacts ( $N_{ij}$ ) as follows

$$\begin{aligned} N_{rr} &= N_{rr}^0 \Gamma_{rr} \\ N_{00} &= N_{00}^0 \Gamma_{00} \\ N_{r0} &= N_{r0}^0 \Gamma_{r0} \end{aligned} \quad (1.46)$$

and must follow the material balance equations:

$$\begin{aligned} \theta_0 \Gamma_{00} + \theta_r \Gamma_{r0} &= 1 \\ \theta_r \Gamma_{rr} + \theta_0 \Gamma_{r0} &= 1 \end{aligned} \quad (1.47)$$

as well as the minimization conditions at equilibrium:

$$\left( \frac{\partial G}{\partial N_{r0}} \right)_{T,P,N,\bar{\rho}} = 0 \quad (1.48)$$

i.e.

$$\frac{\Gamma_{r0}^2}{4\Gamma_{rr}\Gamma_{00}} = \exp\left(-\frac{2^*\varepsilon^*}{zRT}\right) \quad (1.49)$$

where the superscript ‘0’ means ‘randomly distributed’ and  $\theta_i$ s are the surface contact fractions of a  $r$ -mer or an empty site. Indeed the theory defines nonrandomness of every molecule and empty sites but in the end the changes of temperature and pressure only affect  $\Gamma_{00}$ . Otherwise stated, the model usually confirms that only empty sites contribute to nonrandomness. The nonrandomness concept implies that the composition of the mixture in the proximity of a molecule  $i$  can be different from the bulk composition of the mixture. The reduced thermodynamic variables are defined just like the SL theory. Equations 1.50 and 1.51 give the EoS and the chemical potential of the pure compound derived by the NRHB theory without taking into account hydrogen bonds.

$$\tilde{P} + \tilde{T} \left[ \ln(1 - \tilde{\rho}) - \tilde{\rho} \frac{l}{r} - \frac{z}{2} \ln\left[\tilde{\rho} + \frac{q}{r}\tilde{\rho}\right] + \frac{z}{2} \ln \Gamma_{00} \right] = 0 \quad (1.50)$$

$$\begin{aligned} \frac{\mu}{RT} &= -\log(\omega r) - l + \ln \tilde{\rho} + r(\tilde{v} - 1) \ln(1 - \tilde{\rho}) - \\ &\frac{z}{2} r \left[ \tilde{v} - 1 + \frac{q}{r} \right] \ln\left[1 - \tilde{\rho} + \frac{q}{r}\tilde{\rho}\right] + \\ &\frac{zq}{2} \left[ \ln \Gamma_{rr} + \frac{r}{q}(\tilde{v} - 1) \ln \Gamma_{00} \right] - \frac{q}{\tilde{T}} + r \frac{\tilde{P}\tilde{v}}{\tilde{T}} \end{aligned} \quad (1.51)$$

In the case of self HB interactions between molecules of the same species the previous relations become (equations 1.52 and 1.53):

$$\tilde{P} + \tilde{T} \left[ \ln(1 - \tilde{\rho}) - \tilde{\rho} \left( \frac{l}{r} - \nu_H \right) - \frac{z}{2} \ln\left[\tilde{\rho} + \frac{q}{r}\tilde{\rho}\right] + \frac{z}{2} \ln \Gamma_{00} \right] = 0 \quad (1.52)$$

$$\begin{aligned} \frac{\mu_{tot}}{RT} &= \frac{\mu}{RT} + \frac{\mu_H}{RT} \\ &= \frac{\mu}{RT} + r\nu_H - \sum_{i=1}^m d_i \ln \frac{\nu_d^i}{\nu_{i0}} - \sum_{j=1}^n a_j \ln \frac{\nu_a^j}{\nu_{0j}} \end{aligned} \quad (1.53)$$

Thus, non randomness is related to physical bonding whereas HB contributions is related to chemical bonding. Precisely, the theory considers there are  $m$  types of proton donors and  $n$  types of proton acceptor in the system.  $d_i$  is the number of proton groups of type  $-i$  in each molecule and  $a_j$  is the number of acceptor groups of type  $-j$  in each molecule.  $\nu_H$  is the average per segment number of hydrogen bonds in the system.  $\nu_d^i$  is the average per segment number of donor groups of type  $-i$ .  $\nu_a^j$  is the average per segment number of acceptor groups of type  $-j$ .  $\nu_H$  is defined as follows:

$$\nu_H = \sum_{i=1}^m \sum_{j=1}^n \nu_{ij} = \sum_{i=1}^m \sum_{j=1}^n \tilde{\rho} \nu_{i0} \nu_{j0} \exp\left(\frac{-G_{ij}^H}{RT}\right) \quad (1.54)$$

where  $\nu_{i0}$  is the average per segment number of donor groups of type  $-i$  not bonded and  $\nu_{j0}$  is the average per segment number of acceptor groups of type  $-j$  not bonded. The free enthalpy of formation of a hydrogen bond depends on the energy, volume and entropy changes due to the new configuration. Usually only energy and entropy of formation are accounted for in the application of the model. It is usually observed that the non random factors defined previously are all equal to unity except for  $\Gamma_{00}$  as a function of temperature and pressure. Mixing rules in the case of more than one component are as follows:

$$x_i = N_i/N \quad r = \sum_{i=1}^k x_i r_i \quad q = \sum_{i=1}^k x_i q_i \quad \phi_i = x_i r_i / r \quad (1.55)$$

thus the surface contact fraction is

$$\theta_i = \phi_i s_i / s \quad (1.56)$$

and the balance equations based on the nonrandomness hypothesis are

$$\sum_{i=1}^k \theta_i \Gamma_{ij} = 1 \quad j = 0, 1, \dots, k \quad (1.57)$$

In the case of a fluid mixture, the nonrandom factors are calculated from the following minimisation conditions

$$\left(\frac{\partial G}{\partial N_{ij}}\right)_{T,P,N,\tilde{\rho}} = 0 \quad i = 0, \dots, t \quad j = i + 1, \dots, t \quad (1.58)$$

$$\frac{\Gamma_{ij}^2}{\Gamma_{ii}\Gamma_{jj}} = \exp\left(-\frac{\Delta\varepsilon_{ij}}{RT}\right) \quad (1.59)$$

$$\Delta\varepsilon_{ij} = \varepsilon_i + \varepsilon_j - 2(1 - k_{ij})\sqrt{\varepsilon_i\varepsilon_j} \quad (1.60)$$

The average interaction energy within the lattice structure is :

$$\varepsilon^* = \sum_{i=1}^k \sum_{j=1}^k \theta_i \theta_j \varepsilon_{ij}^* = \sum_{i=1}^k \sum_{j=1}^k \theta_i \theta_j \sqrt{(\varepsilon_i^* \varepsilon_j^*)} \zeta_{ij} \quad (1.61)$$

No further rules or details are given about the theory and for a binary mixture just one additional parameter appears ( $\zeta_{12}$ ): these can be found in the literature. Nevertheless,

the expressions for the EoS of the mixture and the chemical potential of component #1 of a binary mixture are presented in equations 1.62

$$\tilde{P} + \tilde{T} \left[ \ln(1 - \tilde{\rho}) - \tilde{\rho} \sum_{i=1}^k \phi_i \frac{l_i}{r_i} - \frac{z}{2} \ln[\tilde{\rho} + \frac{q}{r} \tilde{\rho}] + \frac{z}{2} \ln \Gamma_{00} \right] = 0 \quad (1.62a)$$

$$\begin{aligned} \frac{\mu_i}{RT} = & \ln\left(\frac{\phi_i}{\omega_i r_i}\right) - r_i \sum_{j=1}^k \frac{\phi_j l_j}{r_j} + \ln \tilde{\rho} + r_i(\tilde{v} - 1) \ln(1 - \tilde{\rho}) - \\ & \frac{z}{2} r_i \left[ \tilde{v} - 1 + \frac{q_i}{r_i} \right] \ln\left[1 - \tilde{\rho} + \frac{q}{r} \tilde{\rho}\right] + \\ & \frac{z q_i}{2} \left[ \ln \Gamma_{ii} + \frac{r_i}{q_i} (\tilde{v} - 1) \ln \Gamma_{00} \right] - \frac{q_i}{\tilde{T}_i} + r_i \frac{\tilde{P} \tilde{v}}{\tilde{T}} \end{aligned} \quad (1.62b)$$

In the case of HB mixtures,  $\nu_H \tilde{T} \tilde{P}$  and  $\mu_H$  must be added to equations 1.62a and 1.62b respectively.

No heat, volume and entropy of mixing are provided by Panayiotou *et al.*. Anyway, the entropy of mixing (total configurational entropy) of a binary mixture was derived by Mensitieri *et al.* and is reported in equation 1.63 [43].

$$S_{tot} = S_r + S_{nr} + S_{HB} \quad (1.63a)$$

$$\begin{aligned} \frac{S_r}{RrN} = & \sum_i \left( \frac{\phi_i}{r_i} \right) \cdot \ln \delta_i + (1 - \tilde{v}) \cdot \ln(1 - \tilde{\rho}) + \frac{[l + \ln(r\tilde{v})]}{r} \\ & - \sum_i x_i \cdot \ln(x_i) + \left( \frac{z}{2} \right) \left( \tilde{v} - 1 + \frac{q}{r} \right) \left( 1 - \tilde{\rho} + \frac{q}{r} \right) \end{aligned} \quad (1.63b)$$

$$\begin{aligned} \frac{S_{nr}}{RrN} = & \left( \frac{z}{2} \right) \cdot \left[ (1 - \tilde{v}) \cdot \ln(\Gamma_{00}) - \left( \frac{q_1}{r_1} \right) \phi_1 \cdot \ln(\Gamma_{11}) \right. \\ & - \left( \frac{q_2}{r_2} \right) \phi_2 \cdot \ln(\Gamma_{22}) + (\tilde{v} - 1)(\theta_1 \theta_r \cdot \ln(A_{01}) \Gamma_{01} \\ & \left. + \theta_2 \theta_r \ln(A_{02}) \Gamma_{02}) + \left( \frac{q_1}{r_1} \right) \phi_1 \theta_2 \theta_r \cdot \ln(A_{12}) \Gamma_{12} \right] \end{aligned} \quad (1.63c)$$

$$\begin{aligned} \frac{S_{HB}}{RrN} = & \sum_{i=1}^m \sum_{j=1}^n v_{ij} - \sum_{i=1}^m v_d^i \cdot \ln \left( \frac{v_{i0}}{v_d^i} \right) \\ & - \sum_{i=1}^m v_a^i \cdot \ln \left( \frac{v_{0j}}{v_a^i} \right) + \frac{\sum_{i=1}^m \sum_{j=1}^n v_{ij} H_{ij}^0}{RT} \end{aligned} \quad (1.63d)$$

The flexibility parameter  $\delta_i$  is given by the following expression [44]:

$$\ln(\delta_i) = \ln(Z_i) + f_i r_i \ln(Z_i - 2) - f_i r_i \ln(f_i) - r_i (1 - f_i) \ln(1 - f_i) - f_i r_i \frac{\Delta \varepsilon_i}{RT} \quad (1.64)$$

where again

$$f_i = \frac{(Z_i - 2) \exp(-\frac{\Delta \varepsilon_i}{kT})}{1 + (Z_i - 2) \exp(-\frac{\Delta \varepsilon_i}{kT})}$$

By combining the two previous relations, equation 1.64 can be rewritten as:

$$\delta_i = Z_i \cdot (1 - f_i)^{-r_i} \quad (1.65)$$

$Z_i$  is the number of discrete conformations available to each bond and it is assumed in this theory equal to four for any compound whose number of *mers* is higher than three [38, 45].  $\Delta \varepsilon_i$  has the same meaning already described for the SL theory. Following the line of thought of Flory, Gibbs and Di Marzio regarding linear chain structures, the equilibrium position of a bond is related to a minimum of energy and, reasonably, two types of minimum exist. The *flex energy* is the difference between these two minimum values and, with respect to the penetrant, they are alike, i.e. the *flex energy* vanishes.  $f_i$  is the equilibrium number of flexed bonds, and its dependence on the *flex energy* is commonly called the *Boltzmann expression*. Given a semiflexible chain of  $r_i$  mers in free space, the theory states that  $f_i r_i$  bonds are in *flexed* or high energy states whereas  $(1 - f_i) r_i$  bonds are in low energy states (e.g. gauche and trans). A limit of this approach is the assumption that the *flex energy* is neither dependent on the temperature nor on the composition of the mixture. This hypothesis is mathematically relevant in the calculation of the chemical potentials from the lattice fluid theory (eq. 1.62b). On the basis of this simplifying assumption, the *flex energy* of each component could be then straightforwardly calculated by zeroing the equilibrium entropy of a pure component polymer at  $T_2$ . In the case of the penetrant,  $\Delta \varepsilon_i$  is equal to zero so that  $f_i = (Z_i - 2)/(Z_i - 1)$  and  $\delta_i = Z_i \cdot (Z_i - 1)^{r_i}$  as it should for a completely flexible chain without excluded volume.

In this PhD research activity, the SL and NRHB model have been used to study polymer—penetrant mixtures and pure fluids. Indeed a thermoplastic polymer is well described by these statistical theories in the rubbery state where the single compound or the mixture is at equilibrium. In the following chapters proof of that is given by applying them to the polymers and penetrant species of interest for this research. The major problem is related to systems where the polymer is in a glassy state: indeed this is a metastable state as pointed out in the previous sections and the kinetics of specific

thermodynamic variables must be taken into account to describe relaxation phenomena. Following the thermodynamics of internal state variables, the problem can be solved provided the right thermodynamic internal state variables and their kinetics are found. The NELF-SL (Non—Equilibrium Lattice Fluid - Sanchez and Lacombe) and NETGP-NRHB (Non—Equilibrium theory of Glassy Polymers-Nonrandom Hydrogen Bonding) theories are two examples of this approach. Here a description of them is reported because both of them have been applied to the polymer—penetrant systems of interest.

### 1.6.4 The glassy state: NELF-SL and NETGP-NRHB frameworks

The NELF-SL model considers the density of the polymer ( $\rho_2$ ) the internal state variable affecting the relaxation of the mixture physical properties [46, 47, 48]. The combination of expression 1.36a with the kinetics of the polymer density describes now the non-equilibrium phenomenon. Generally, the latter is a function of temperature, pressure, mole fraction of penetrant within the mixture and the polymer density itself (equation 1.66).

$$\frac{d\rho_2}{dt} = f(T, P, \omega_1, \rho_2) \quad (1.66)$$

The entropy inequality for a mixture whose thermodynamic state consists of an additional internal state variable is given in equation 1.67.

$$[\partial G/\partial P - V]\dot{P} + [\partial G/\partial T + S]\dot{T} + (\mu^\alpha - \mu^\beta) \cdot \dot{n}^\alpha + (\partial G/\partial \rho_2) \cdot \dot{\rho}_2 \leq 0 \quad (1.67)$$

The same notation of relations 1.36, 1.50 and 1.51 is used but the free enthalpy 'G' is chosen instead of the free energy 'A'.  $\alpha$  refers to the polymer phase whereas  $\beta$  to the gas phase. By assuming that the polymeric compound cannot be transferred to the gas phase, equation 1.67 simplifies as follows

$$[\partial G/\partial P - V]\dot{P} + [\partial G/\partial T + S]\dot{T} + (\mu_1^\alpha - \mu_1^\beta) \cdot \dot{n}_1^\alpha + (\partial G/\partial \rho_2) \cdot \dot{\rho}_2 \leq 0 \quad (1.68)$$

and, provided temperature and pressure do not change during the sorption/desorption process, equation 1.68 becomes

$$(\mu_1^\alpha - \mu_1^\beta) \cdot \dot{n}_1^\alpha + (\partial G/\partial \rho_2) \cdot \dot{\rho}_2 \leq 0 \quad (1.69)$$

Two simultaneous dissipation mechanisms appear: the first is associated with the mass transport; the second one is due to the viscoelastic evolution of the polymer density.

The equilibrium conditions are (equation 1.70):

$$\begin{cases} \mu_1^\alpha(T, P, n_1^{\alpha,*}, \rho_2^*) = \mu_1^\beta(T, P) \\ \left. \frac{\partial G}{\partial \rho_2} \right|_{T,P} = h(T, P, n_1^{\alpha,*}, \rho_2^*) = 0 \end{cases} \quad (1.70)$$

and describe the mass transport in the rubbery mixture. On the other hand, the NELF theory considers the density of the polymer frozen in the glassy state. Its value corresponds to the last glassy state experienced by the material and induces a condition of pseudoequilibrium on the glassy mixture during ageing i.e.

$$\begin{aligned} \rho_{2,\infty} &\neq \rho_{2,eq} \\ \frac{d\rho_2}{dt} &= f(T, P, n_1^\alpha, \rho_{2,\infty}) \approx 0 \end{aligned} \quad (1.71)$$

Relations 1.71 are called the *pseudoequilibrium* conditions and, particularly, equations 1.72 are derived

$$\begin{cases} \mu_1^\alpha(T, P, n_1^\alpha, \rho_{2,\infty}) \neq \mu_1^\beta(T, P) \\ \left. \frac{\partial G}{\partial \rho_2} \right|_{T,P,n_1^\alpha} = h(T, P, n_1^\alpha, \rho_{2,\infty}) \neq 0 \end{cases} \quad (1.72)$$

The mass transport will be arrested whenever

$$\mu_1^\alpha(T, P, n_1^\alpha, \rho_{2,\infty}) = \mu_1^\beta(T, P)$$

this is the phase equilibrium condition which holds true when the hindered polymer mobility freezes the polymer density at the value  $\rho_{2,\infty}$ . The expression for the chemical potential of the penetrant (#1 species) in a polymer-penetrant mixture where the penetrant is a low molecular weight compound is derived from equation 1.36b by assuming  $r_2 \gg r_1$  [49].

$$\frac{\mu_1^\alpha}{RT} = \ln(\tilde{\rho}\phi_1) - \left[ r_1^0 + \frac{r_1 - r_1^0}{\tilde{\rho}} \right] \ln(1 - \tilde{\rho}) - r_1 - \frac{\tilde{\rho}[r_1^0 v_1^*(P_1^* + P^* - \phi_2 \Delta P^*)]}{RT} \quad (1.73)$$

In case of strongly sorbing penetrants gases such as CO<sub>2</sub> at high pressure, swelling of the matrix is observed empirically and can be described by a linear relation as follows:

$$\rho_2(P) = \rho_2^0(1 - k_{sw}P)$$

where  $k_{sw}$  is called the swelling parameter and  $\rho_2^0$  is the polymer dry density. However,  $k_{sw}$  is not capable of describing systems where strong interactions between the two species are relevant even at low pressures. Scherillo *et al.* built up the extension of the NELF theory to the NRHB case. The theory is more general and acquires the new

acronym of NETGP-NRHB. Thermodynamics of internal state variables is used but the order parameters (internal state variables) are now  $\rho_2$ ,  $\mathbf{N}_{ij}^{HB}$  and  $\mathbf{N}^{NR}$ , i.e.

$$G = g(T, P, \rho_2, n_1^\alpha, \mathbf{N}^{HB}, \mathbf{N}^{NR})$$

where  $\mathbf{N}^{HB}$  is the matrix consisting of the number of hydrogen bonds between donor groups ‘-i’ and acceptor groups ‘-j’ and  $\mathbf{N}^{NR}$  is the matrix consisting of the number of nonrandom contacts between mers of kind ‘-r’ and mers of kind ‘-s’. By assuming that the polymeric compound cannot be transferred to the gas phase, equation 1.68 becomes:

$$(\mu_1^\alpha - \mu_1^\beta) \cdot \dot{n}_1^\alpha + (\partial G / \partial \rho_2) \cdot \dot{\rho}_2 + (\partial G / \partial \mathbf{N}^{HB}) \cdot \dot{\mathbf{N}}^{HB} + (\partial G / \partial \mathbf{N}^{NR}) \cdot \dot{\mathbf{N}}^{NR} \leq 0 \quad (1.74)$$

The authors simplify the matter by assuming an *instantaneous evolution* kinetics for the new internal state variables and by considering additionally that the values of  $N_{ij}^{HB}$  and  $N_{rs}^{NR}$  are the ones which the system would exhibit at equilibrium at the current values of polymer density, temperature, pressure and concentration. The latter is called *instantaneous equilibrium* hypothesis and it is indicated by the superscript *IE* in the following relations.

$$\left\{ \begin{array}{l} \frac{\partial G}{\partial N_{ij}^{HB}} \Big|_{T, P, n_1^\alpha, \rho_2, N_{pq \neq ij}^{IE, HB}, N_{rs}^{IE, NR}} = 0, \quad i = 1, \dots, m \quad j = 1, \dots, n \\ \frac{\partial G}{\partial N_{rs}^{NR}} \Big|_{T, P, n_1^\alpha, \rho_2, N_{ij}^{IE, HB}, N_{pq \neq rs}^{IE, NR}} = 0, \quad r, s = 1, \dots, k + 1 \\ G^{IE} = g(T, P, n_1^\alpha, \rho_2, N_{ij}^{IE, HB}(T, P, n_1^\alpha, \rho_2), N_{rs}^{IE, NR}(T, P, n_1^\alpha, \rho_2)) \end{array} \right. \quad (1.75)$$

where  $m$ ,  $n$ ,  $k$  are the number of proton donors, proton acceptors and components in the system respectively. One more  $r, s$  must be added because of the presence of holes. The kinetics of  $\rho_2$  depends as well on the new internal state variables and the hypothesis of *instantaneous equilibrium* returns equation 1.76.

$$\begin{aligned} \frac{\partial \rho_2}{\partial t} &= f(T, P, n_1^\alpha, \rho_2, N_{ij}^{IE, HB}(T, P, n_1^\alpha, \rho_2), N_{rs}^{IE, NR}(T, P, n_1^\alpha, \rho_2)) \\ &= f^{IE}(T, P, n_1^\alpha, \rho_2) \end{aligned} \quad (1.76)$$

and in view of the *pseudoequilibrium* hypothesis for the internal state variable  $\rho_2$

$$\frac{\partial \rho_2}{\partial t} = f^{IE}(T, P, n_1^\alpha, \rho_{2, \infty}) \approx 0 \quad (1.77)$$

So the same constitutive class of classic NELF-SL model is used and the density of the polymer still remains the only internal state variable whose kinetics describes the relaxation phenomena involved in the out of equilibrium glassy state. The chemical

potential of component #1 in the mixture phase is reported in equation 1.78.

$$\begin{aligned}
 \frac{\mu_1^{IE,\alpha}}{RT} &= \frac{\mu_{1,LF}^{IE,\alpha}}{RT} + \frac{\mu_{1,HB}^{IE,\alpha}}{RT} \\
 \frac{\mu_{1,LF}^{IE,\alpha}}{RT} &= \ln\left(\frac{\phi_1}{\delta_1 r_1}\right) - r_1 \sum_{i=1}^2 \frac{\phi_i l_i}{r_i} + \ln \tilde{\rho} \\
 &\quad + r_1 (\tilde{v} - 1) \ln(1 - \tilde{\rho}) - \frac{z}{2} r_1 \left[ \tilde{v} - 1 + \frac{q_1}{r_1} \right] \ln \left[ 1 - \tilde{\rho} + \frac{q}{r} \tilde{\rho} \right] + \\
 &\quad \frac{z q_1}{2} \left[ \ln \Gamma_{11} + \frac{r_1}{q_1} (\tilde{v} - 1) \ln \Gamma_{00} \right] - \frac{q_1}{\tilde{T}_1} + \\
 &\quad \tilde{T} \left[ \ln(1 - \tilde{\rho}) - \tilde{\rho} \sum_{i=1}^2 \frac{\phi_i l_i}{r_i} - \frac{z}{2} \ln\left(1 - \tilde{\rho} + \frac{q}{r} \tilde{\rho}\right) + \right. \\
 &\quad \left. \frac{z}{2} \ln \Gamma_{00} \right] \cdot \frac{r x_2 \cdot (\partial \tilde{v} / \partial x_1) |_{T,P,\rho_2, N_{ij}^{IE,HB}, N_{rs}^{IE,NR}}}{\tilde{T}} \\
 \frac{\mu_H}{RT} &= r_1 \nu_H - \sum_{i=1}^m d_i \ln \frac{\nu_d^i}{\nu_{i0}} - \sum_{j=1}^n a_j \ln \frac{\nu_a^j}{\nu_{0j}} + \nu_H \frac{\partial \ln \tilde{v}}{\partial x_2} \Big|_{T,P,\rho_2, N_{ij}^{IE,HB}, N_{rs}^{IE,NR}}
 \end{aligned} \tag{1.78}$$

The whole mathematical procedure leading to it is omitted here for the sake of brevity. The additional important hypothesis which must be taken into account is that the change of volume  $V_{ij}^0$  associated with the formation of each kind of HB  $ij$  is equal to zero. The NRHB model states that the volume of the mixture is equal to

$$V = V_{LF} + \sum_{i=1}^m \sum_{j=1}^n N_{ij}^{HB} V_{ij}^0$$

so that

$$V = V_{LF}$$

### 1.6.5 $T_g$ depression: a II order phase transition approach

The glass transition temperature ( $T_g$ ) of a polymer is affected by contact with a fluid that can be absorbed within the material. This phenomenon is ruled by the mechanical action of fluid pressure and by thermodynamic affinity between the fluid and the polymer. In fact, a fluid can have counteracting effects, acting both as a pressure-generating medium, thus promoting an increase of  $T_g$  with increasing pressure, and as an effective plasticizer, thus promoting a decrease of  $T_g$ . In particular, the plasticizing action depends in a complex fashion upon the combined effects of fluid pressure and

temperature on fluid sorption within the polymer. Numerous definitions of the term *plasticizer* are in use nowadays [50, 51]:

- a) a low molecular weight material added to polymeric materials such as paints, plastics, or adhesives to improve their flexibility and to lower their glass transition temperature;
- b) plasticizer interacts with the polymer chains on the molecular level as to speed up its viscoelastic response (or increase chain mobility)

Thus, a plasticizer is usually defined in terms of the desired properties of a given polymer-plasticizer system. Several experimental approaches have been adopted in the literature to investigate the effects of sorption of low molecular weight compounds on the glass transition of a polymer, including methods based on in situ measurement of creep compliance, on gravimetric sorption measurement by identifying a discontinuity in the sorption isotherm from the glassy to rubbery-types of behavior, on stepwise temperature- and pressure-scanning thermal analysis, on a minimum foaming temperature approach, on in situ spectroscopic ellipsometry and on detection of sharp increase in mutual diffusion coefficient in the polymer-penetrant system. The thermodynamics of systems endowed with glass transition due to desorption of a penetrant is presented first: theoretical arguments are given to underline the II order phase transition behaviour of the rubber to glass transition; next, the main results obtained by Condo *et al.* are presented to highlight the results of the Gibbs—Di Marzio approach combined with statistical thermodynamics.

The line of reasoning of De Bruyn Ouboter and Beenakker is followed onwards [52]. In their article, it is demonstrated that *'it appears to be a general property that the first order equilibrium curves for liquid binary mixtures show a singularity at the junction with the second order lambda curve as can be seen on the basis of pure thermodynamic consideration'*. In particular, the authors derived mathematical expressions highlighting there is a discontinuity in the slope of the first order equilibrium curve (boiling curve), i.e. in the values of  $(dT/d\Omega_i)_P$  and  $(dP/d\Omega_i)_T$ , where  $\Omega_i$  is the mole fraction of component 'i', at the junction with the second order line. As a preliminary point, at a I order transition, the first derivatives of molar Gibbs energy  $(\frac{\partial g}{\partial T}, \frac{\partial g}{\partial P}, \frac{\partial g}{\partial \omega_1})$  are discontinuous. It implies that the chemical potential is discontinuous too, i.e. the value of  $\mu_1^\alpha$  and  $\mu_1^\beta$  at the same P, T and  $\omega_1$  are different (here superscripts  $\alpha$  and  $\beta$  are referred to the two phases at equilibrium). Since the equilibrium condition implies the equality of chemical potential at the transition, this, in turn, implies that the  $\omega_1^\alpha \neq \omega_1^\beta$ , hence a discontinuity is generally expected in the value of  $\omega_1$  between the two phases in equilibrium. Actually exception to this behavior takes place just in the case of azeotropic first order transitions, at which the chemical potentials are not discontinuous at a given couple {T; P} at a concentration dictated by equilibrium of phase, and consequently the concentration in the two phases is the same (i.e. continuity of concentration occurs at this transition). Conversely, at a second order transition, the values of the chemical

potentials are the same for the same values of T, P and  $\omega$ , hence no discontinuity is expected for the value of  $\omega_1$  at the phase transition.

a) 1st order transition:  $\mu_1^\alpha = \mu_1^\beta$  at T and P but, in general, with  $\omega_1^\alpha \neq \omega_1^\beta$

b) 2nd order transition:  $\mu_1^\alpha = \mu_1^\beta$  at T and P with, necessarily,  $\omega_1^\alpha = \omega_1^\beta$

We consider now the rubbery polymer-penetrant mixture in equilibrium with the penetrant vapour phase, at pressure P and temperature T. If we assume that the polymer is not soluble within the vapour phase we have to deal with the equilibrium between the polymer mixture and a pure vapour phase, which is dictated by the following expression that holds for the penetrant:

$$\mu_1^\gamma(T, P) = \mu_1^\alpha(T, P, \omega_1) \quad \text{i.e.} \quad \omega_1 = \bar{\omega}_1(T, P)$$

All the quantities referred to the rubbery mixture phase are indicated by the superscript  $\alpha$ ;  $\gamma$  refers to the vapour phase;  $\bar{\omega}_1$  is the equilibrium value of the penetrant mass fraction within the polymer phase in contact with the vapour phase and from the previous relation it is a function only of P and T. Next, three different cases are studied: 1) isothermal case, 2) isobaric case and 3) isoactivity case, focusing on the loci of the equilibrium conditions between the two phases. The rubbery polymer-penetrant mixture is always considered as the initial condition in the following. This means a decreasing pressure path is studied in the isothermal case; a decreasing temperature path is studied in the isobaric case; and a decreasing temperature and pressure path in the isoactivity case. In the case of a isothermal experiment, at each value of pressure, while the polymer mixture is still in a rubbery state, the values of the penetrant chemical potential in both phases have to be the same and, as a consequence, since both are only function of pressure P, the following is true for a differential change of pressure:

$$d\mu_1^\gamma(P) = d\mu_1^\alpha(P, \bar{\omega}_1(P)) \quad (1.79)$$

Now, by introducing the expressions of the differentials of the two chemical potentials we have that:

$$\begin{aligned} d\mu_1^\gamma(P) &= v_1^\gamma dP \\ d\mu_1^\alpha(P, \bar{\omega}_1(P)) &= \tilde{v}_1^\alpha dP + \frac{\partial \mu_1^\alpha}{\partial \bar{\omega}_1^\alpha} \frac{d\bar{\omega}_1^\alpha}{dP} dP \end{aligned} \quad (1.80)$$

where  $v_1^\gamma$  is the molar volume of pure penetrant in the vapour phase and  $\tilde{v}_1^\alpha$  is the partial molar volume of penetrant within the rubbery polymer mixture. By equating the two previous expressions, we have that, at equilibrium along the isothermal path:

$$\frac{d\bar{\omega}_1^\alpha}{dP} = \frac{v_1^\gamma - \tilde{v}_1^\alpha}{\frac{\partial \mu_1^\alpha}{\partial \bar{\omega}_1^\alpha}} \quad (1.81)$$

If a II order transition occurs at a specific  $P_g$ , by definition, a discontinuity of the second derivatives of Gibbs energy occurs, the first derivatives being instead continuous. It is hence expected that both  $\tilde{v}_1$  and  $\frac{\partial \mu_1}{\partial \bar{\omega}_1}$ , display a discontinuity at  $P_g$ . Consequently, it is highly reasonable that  $\frac{d\bar{\omega}_1}{dP}$  experiences a step discontinuity too. Below such a pressure, in the framework of a II order thermodynamic transition, the polymer phase is still assumed to be in equilibrium with the vapour phase, although now the expression of the chemical potential as well as the expression for  $\tilde{v}_1$  is different since it refers to a different polymer phase, i.e. in the glassy state in the present context, and we have:

$$\frac{d\bar{\omega}_1^\beta}{dP} = \frac{v_1^\gamma - \tilde{v}_1^\beta}{\frac{\partial \mu_1^\beta}{\partial \bar{\omega}_1^\beta}} \quad (1.82)$$

Here, the superscript  $\beta$  refers indeed to the phase that is formed at the II order transition. In general, this should result in a discontinuity also for the value of  $\frac{d\bar{\omega}_1}{dP}$ .

In the case of a isothermal experiment, at each temperature, the values of the penetrant chemical potential in both phases are prescribed to be the same and, as a consequence, since both are only function of temperature  $T$ , we also have, for a differential change of temperature:

$$d\mu_1^\gamma(T) = d\mu_1^\alpha(T, \bar{\omega}_1(T)) \quad (1.83)$$

Now, by introducing the expressions of the differentials of the two chemical potentials we have that:

$$\begin{aligned} d\mu_1^\gamma(T) &= -s_1^\gamma dT \\ d\mu_1^\alpha(T, \bar{\omega}_1(T)) &= -\tilde{s}_1^\alpha dT + \frac{\partial \mu_1^\alpha}{\partial \bar{\omega}_1^\alpha} \frac{d\bar{\omega}_1^\alpha}{dT} dT \end{aligned} \quad (1.84)$$

Equating the two previous expressions, we have that, at equilibrium:

$$\frac{d\bar{\omega}_1^\alpha}{dT} = \frac{\tilde{s}_1^\alpha - s_1^\gamma}{\frac{\partial \mu_1^\alpha}{\partial \bar{\omega}_1^\alpha}} \quad (1.85)$$

Generally, the sorption of a penetrant lowers the glass transition of the polymer; starting from a temperature sufficiently high so that the the system is rubbery as the temperature decreases, the polymer phase displays a II order thermodynamic transition, at a certain value of temperature,  $T_g$  whenever a discontinuity of both  $\tilde{s}_1$  and  $d\mu_1^\alpha$  occurs (second derivatives of Gibbs energy). The same argument used for the case aof a isobaric path is applied, i.e. it is highly reasonable that  $\frac{d\bar{\omega}_1}{dT}$  experiences a discontinuity too. The polymer phase is still assumed to be in equilibrium with the vapour phase below  $T_g$ , although now the expression of the chemical potential as well as the expression for  $\tilde{s}_1$

is different since it refers to a different polymer phase, i.e. in the glassy state in the present context, and we have that:

$$\frac{d\bar{\omega}_1^\beta}{dT} = \frac{\tilde{s}_1^\beta - s_1^\gamma}{\frac{\partial \mu_1^\beta}{\partial \bar{\omega}_1^\beta}} \quad (1.86)$$

The third kind of experiments that could possibly induce a II order glass transition, starting from rubbery state, by decreasing the temperature at a fixed rate while maintaining a constant value of the ratio of the actual pressure (P) and the toluene vapour pressure ( $P_s$ ). This restriction, then, imposes that during the experiment the pressure is a function of temperature,  $P = P(T)$ . This function is invertible since  $P_s$  is a monotonic function of temperature. At the temperature and pressure conditions at which the experiment is conducted, the ratio  $P/P_s$  is a reasonable estimate of the activity of the toluene in the vapour phase and the experiments can be considered as being conducted at a rather constant activity (isoactivity test). A proof is provided in Chapter III where the system PS—Toluene is treated. As temperature, and pressure accordingly, are modified, assuming an instantaneous equilibrium between the vapour and polymer phases, we have that the penetrant chemical potentials in both phases are only function of temperature T and are equal at each value of T. Therefore, moving along the equilibrium curve between vapour and polymer phases, we have:

$$d\mu_1^\gamma(T) = d\mu_1^\alpha(T, \bar{\omega}_1^\alpha) \quad (1.87)$$

and consequently:

$$-s_1 dT + v_1 \frac{dP}{dT} dT = -\tilde{s}_1^\alpha dT + \tilde{v}_1 \frac{dP}{dT} dT + \frac{\partial \mu_1^\alpha}{\partial \bar{\omega}_1^\alpha} \frac{\partial \bar{\omega}_1^\alpha}{dT} dT + \frac{\partial \mu_1^\alpha}{\partial \bar{\omega}_1^\alpha} \frac{\partial \bar{\omega}_1^\alpha}{dP} \frac{dP}{dT} dT \quad (1.88)$$

From which the following relation is obtained:

$$(s_1 - \tilde{s}_1^\alpha) dT + (\tilde{v}_1^\alpha - v_1) dP + \frac{\partial \mu_1^\alpha}{\partial \bar{\omega}_1^\alpha} \frac{\partial \bar{\omega}_1^\alpha}{dT} dT + \frac{\partial \mu_1^\alpha}{\partial \bar{\omega}_1^\alpha} \frac{\partial \bar{\omega}_1^\alpha}{dP} dP = 0 \quad (1.89)$$

Moreover, the following is true:

$$d\bar{\omega}_1^\alpha = \frac{\partial \bar{\omega}_1^\alpha}{\partial T} dT + \frac{\partial \bar{\omega}_1^\alpha}{\partial P} dP \quad (1.90)$$

$$P = a \cdot P_s(T)$$

Then,

$$d\bar{\omega}_1^\alpha = \frac{\partial \bar{\omega}_1^\alpha}{\partial T} \frac{dT}{dP} dP + \frac{\partial \bar{\omega}_1^\alpha}{\partial P} dP \quad \text{or} \quad \frac{d\bar{\omega}_1^\alpha}{dP} = \frac{\partial \bar{\omega}_1^\alpha}{\partial T} \frac{dT}{dP} + \frac{\partial \bar{\omega}_1^\alpha}{\partial P} \quad (1.91)$$

In the last equation the value of  $\bar{\omega}_1$  is dictated at each equilibrium point by the isoactivity condition. Now, by combining the previous equations, the following relation is derived:

$$(s_1 - \tilde{s}_1^\alpha) \frac{dT}{dP} + (\tilde{v}_1^\alpha - v_1) + \frac{\partial \mu_1^\alpha}{\partial \bar{\omega}_1^\alpha} \frac{d\bar{\omega}_1^\alpha}{dP} = 0 \quad (1.92)$$

From which:

$$\frac{d\bar{\omega}_1^\alpha}{dP} = \frac{(s_1 - \tilde{s}_1^\alpha) \frac{dT}{dP} + (\tilde{v}_1^\alpha - v_1)}{\frac{\partial \mu_1^\alpha}{\partial \bar{\omega}_1^\alpha}} \quad (1.93)$$

An analogous expression is obtained below a II order transition involving the polymer mixture phase:

$$\frac{d\bar{\omega}_1^\beta}{dP} = \frac{(s_1 - \tilde{s}_1^\beta) \frac{dT}{dP} + (\tilde{v}_1^\beta - v_1)}{\frac{\partial \mu_1^\beta}{\partial \bar{\omega}_1^\beta}} \quad (1.94)$$

At the II order transition the terms  $\tilde{s}_1$ ,  $\tilde{v}_1$  and  $\frac{\partial \mu_1}{\partial \bar{\omega}_1}$  being second derivatives of the total Gibbs energy of the mixture, have a discontinuity while the terms  $s_1$ ,  $v_1$  and  $\frac{dT}{dP}$  are continuous. Then also the derivative  $\frac{d\bar{\omega}_1}{dT}$  is expected to display such a discontinuity. An analogous conclusion can be drawn for the case of  $\frac{d\bar{\omega}_1}{dP}$  by dividing the expression for  $\bar{\omega}_1$  by  $dT$  and following a similar procedure. Based on the previous discussion and on the cited literature, it is concluded that, if a junction of a II order transition curve, involving the polymer phase, actually occurs with the first order equilibrium liquid-vapour curve, a discontinuity is expected in the slope of first order equilibrium curves. In particular, a discontinuity is expected for the values of derivatives  $\frac{d\bar{\omega}_1}{dP}$  and  $\frac{d\bar{\omega}_1}{dT}$  in the case of, respectively, isothermal and isobaric equilibrium experiments and of both these two derivatives in the case of isoactivity equilibrium experiments. Proof of this theory is being given in Chapter III where experimental results for the system Ps—Toluene are presented. The theory does not consider the relevant history-dependent effects of a slowly relaxing glass phase which could overly mask the main features of the underlying thermodynamic transition. So it must be applied to a system which is rubbery at the beginning.

The Gibbs—Di Marzio approach is easily extended to polymer—penetrant mixtures. It suffices to define the configurational entropy of the mixture through a specific lattice fluid model and to nullify it. Originally, the authors defined their own lattice fluid theory starting from the Flory's one. The goal was to derive a relation for the configurational entropy of a homogenous mixture of long chain polymers of degree of polymerization  $r_A$  with short chain polymers of degree of polymerization  $r_B$ . The lattice model was missing two important features which are the presence of holes (i.e. fluid compressibility due to free volume) and the non randomness of molecules location due to preferential mean-field intermolecular interactions (equation: 1.95).

$$\begin{aligned}
 \frac{S}{kr_A N_A} = & \frac{z-2}{2(1-v)} \cdot \ln \left[ \frac{(z-2)r_B + 2v}{zr_B} \right] \\
 & + \frac{v}{r_B(1-v)} \cdot \ln \left[ \frac{(z-2)r_B + 2v}{zv} \cdot \frac{z_1 z_2}{2} \right] \\
 & + \frac{v(r_B - 3)}{r_b(1-v)} \cdot \ln \left[ 1 + (z-2) \exp\left(-\frac{\Delta\varepsilon_B}{kT}\right) \right] + \frac{f_B \Delta\varepsilon_B}{kT} \\
 & + \ln \left[ 1 + (z-2) \exp\left(-\frac{\Delta\varepsilon_A}{kT}\right) \right] + \frac{f_A \Delta\varepsilon_A}{kT}
 \end{aligned} \tag{1.95}$$

where  $f_i$  has already been provided in the NRHB section.  $z_1$  and  $z_2$  are respectively the coordination number of the second segment (after the first has been located) and of the third segment (after the first and the second have been located).  $v$  is the volume fraction of plasticizer.  $\Delta\varepsilon_i$  identifies the *flex energy* of compound  $i$ .

Condo *et al.* combined the SL model with the Gibbs and Di Marzio approach: they used equation 1.40 to predict the glass transition depression of a polymer subject to sorption of a penetrant. The authors predicted the relevant features of polymer-penetrant systems in terms i.e. four fundamental types of behavior (i.e. types I, II, III and IV) for the Tg vs. penetrant pressure plot. Worth of mention is the so-called *retrograde vitrification* phenomenon, consisting in a rubbery to glass transition for the polymer-penetrant mixture occurring with increasing temperature. Its name derives from the *retrograde condensation* phenomenon which is well known in the petroleum industry. In brief, it consists first in the decrease in segmental motion occurring as the temperature is reduced at isobaric conditions. Then the vitrification process is overcome by the increase in the diluent concentration due to the increase in solubility. Experimental evidence of *retrograde vitrification* has been currently provided only for a very limited number of systems, including poly(methyl methacrylate) (PMMA) and poly(ethyl methacrylate) (PEMA) in contact with pressurized CO<sub>2</sub>, thin Polystyrene (PS) film-CO<sub>2</sub> systems, the poly(lactic acid) (PLA)-CO<sub>2</sub> system and, more recently, by our group, for the PS—Toluene system. Figure 1.9 reports Condo's *et al.* results. Table 1.5 explains the specific penetrant case for each type of system.

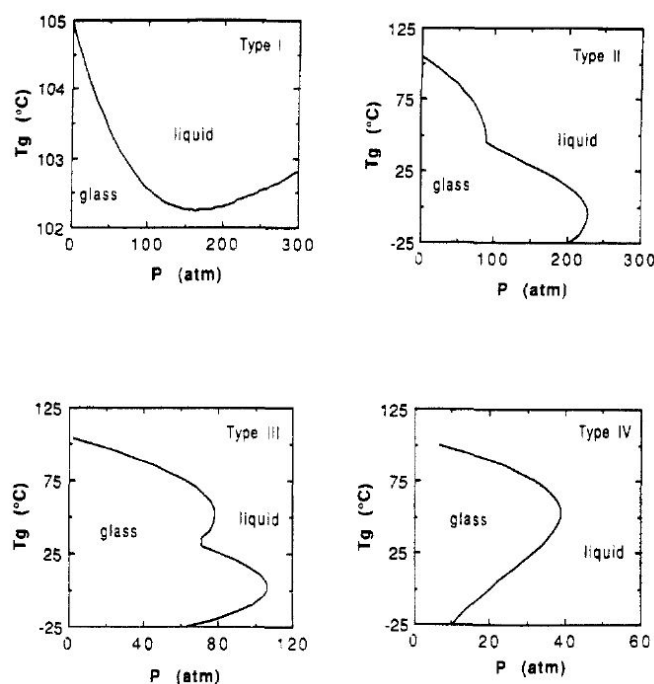


**Figure 1.9:** Types of  $T_g$  phase diagram in a generic Polymer-Penetrant system [37].

Type	$T_g - P_g$ trend	$T_g - \omega_g$ trend	$T_c$ vs. $T_g$
I	$T_g$ minimum	$T_g$ minimum	-
II	$P_g$ maximum	linear	$T < T_c$
III	$P_g$ maximum	linear	$T > T_c$
IV	$P_g$ maximum	linear	$T > T_c$

**Table 1.5:**  $T_g - P_g$  and  $T_g - \omega_g$  behaviour predicted [37]

Type I is typical of low solubility penetrants: the pressure increase trigger the increase of both the hydrostatic pressure and the penetrant solubility. Consequently, the diluent effect of the gas which depresses the  $T_g$  is overcome by the hydrostatic pressure which has the opposite effect by approaching the chains one another. *Retrograde vitrification* is explained by stating the solubility increase counteracts the effect of the temperature decrease in isobaric conditions. From a detailed study of the literature, it seems incorrect the relation  $Z = z = 10$  [29, 30, 37, 45]. Indeed  $Z$  and  $z$  have two different meanings: the former represents the number of conformations of a bond after having fixed two adjacent bonds; the latter corresponds to the lattice coordination number, i.e. the number of cells which are first neighbours to a given cell of the lattice. In the following chapter, this statement is reviewed. In this research work, the NRHB compressible

lattice fluid model is combined with the Gibbs and Di Marzio approach to predict the glass transition of a polymer—penetrant mixture.

## 1.7 Empirical theories

In this section, useful empirical correlations and rules are reported to study the macroscopic behaviour of a polymer—penetrant system. Generally, by performing experiments at fixed temperature ( $T$ ) and pressure ( $P$ ), isotherm sorption/desorption curves are given as a function of pressure or fugacity ( $f$ ). The solubility coefficient ( $S$ ) is defined as the ratio of solubility over the thermodynamic variable which better describes the behaviour of the gas phase in which the sample is immersed (i.e. either  $P$  or  $f$  or  $a$ ). The most applied empirical theory to sorption of a gas within a polymeric glassy matrix is the *dual mode* theory. Particularly, sorption is assumed to take place in two types of voids (free volume): the *Langmuir* contribution is exothermic and it is related to sorption within the excess metastable free volume; the *Henry's* one is endothermic and it derives from the creation of free volume between the polymer chains. The endothermic nature is explained from the energy needed by the penetrant to move the polymeric chains apart.

$$C = K_d \cdot f + \frac{C'_h \cdot b \cdot f}{1 + b \cdot f} \quad (1.96)$$

$K_d$  is the Henry's constant,  $Ch'$  is the maximum concentration available in the Langmuir's sites and  $b$  is the affinity of the penetrant with the polymer in these sites. The theory is extended to the case of mixture of gases. Particularly, the penetrant species are thought to compete only for the *Langmuir's* sites. The new relation between  $C$  and  $f_i$  ( $i=1, \dots, n$ ) is:

$$C_i = K_{d,i} \cdot f_i + \frac{C'_{h,i} \cdot b_i \cdot f_i}{1 + \sum_{j=1}^n b_j \cdot f_j} \quad (1.97)$$

Empirically, it is also observed that sorption is a thermally activated process and the dependence of  $S$  on  $T$  is well described by a van't Hoff equation for gas dissolution:

$$C = S \cdot P \quad (1.98)$$

$$S = S_0 \exp(-\Delta H_s/RT)$$

The enthalpy of sorption  $\Delta H_s$  is thought to be the sum of two contributions i.e. the latent heat involved in the condensation of the penetrant within the matrix and the heat evolved during the mixing of the two compounds. The former is exothermic while the latter is endothermic.

$$\Delta H_s = \lambda + \Delta H_{mix} \quad (1.99)$$

The fugacity of the gas phase is certainly the best variable to estimate its non-ideality and so it must be used to evaluate the enthalpy of sorption. In practice it is more common to show the enthalpy of sorption as a function of pressure. Another way to evaluate the heat involved in the sorption process is to consider its dependence on the penetrant concentration, i.e. at fixed chemical potential of the gas phase. This quantity is called *isosteric heat*. As pointed out by A.L. Myers, this quantity is defined as the penetrant enthalpy difference between the gas state and the condensed/absorbed state in the framework of classical thermodynamics of mixtures where the absorbent is microporous [53]. The concept is applied to dense polymeric membrane in order to have a complete picture whether condensation or mixing is contributing more to the sorption process. Moreover, although the glassy state is metastable, the quasi-equilibrium hypothesis may still be applied when the penetrant neither swells nor plasticizes the matrix and  $T \ll T_g$ . Equation 1.100 shows how to calculate the heat involved at constant concentration of penetrant. Again pressure usually replaces fugacity to make its use immediate.

$$\left( \frac{d \log(f)}{dT^{-1}} \right)_c = \frac{\Delta H_s}{Z \cdot R} \quad (1.100)$$

In order to study non athermic processes, the dual sorption model parameters (the Henry's solubility coefficient  $K_d$  and the Langmuir's affinity parameter  $b$ ) must be function of temperature. Following the idea of sorption as a thermally activated process the following empirical relations are proposed in the literature [54]:

$$\begin{aligned} K_d &= K_{d,0} \cdot \exp\left(\frac{-\Delta H_k}{RT}\right) \\ b &= b_0 \cdot \exp\left(\frac{-\Delta H_b}{RT}\right) \end{aligned} \quad (1.101)$$

Obviously, the sign of the enthalpy difference of the penetrant between the gas state and the condensed state within the Henry's and the Langmuir's regions is positive and negative respectively. This rule follows the idea of endothermic vs exothermic processes respectively. However, specific strong interactions could affect sorption in the dense phase enhancing the exothermicity of the Henry's sorption process.

When dealing with a mixture of a polymer and a light non interacting gas usually  $|\Delta H_m| \ll |\lambda|$  at low pressures (condensability of the penetrant prevails), the logarithm of the solubility coefficient at infinite dilution conditions is well fit to a linear expression as a function of the critical temperature 1.102:

$$\begin{aligned} \Delta H_c &= -\alpha \cdot RT_c \\ \log(S_\infty) &= \log(S_0) + \alpha \cdot T_c/T \end{aligned} \quad (1.102)$$

In the case of highly condensable penetrant (e.g. organic solvents, water etc.),  $|\Delta H_m| < |\Delta H_c|$  and 1.103 holds true empirically.

$$\begin{aligned}\Delta H_c &= -\alpha \cdot RT_c^2 \\ \log(S_\infty) &= \log(S_0) + \alpha \cdot (T_c/T)^2\end{aligned}\tag{1.103}$$

$\alpha$  and  $S_0$  are two fitting parameters while  $S_\infty$  is the infinite dilution solubility coefficient. Many other relations which use physical molecular properties of the penetrant have been used in the literature to correlate sorption data: for instance, the steric hindrance is taken into account by considering its critical volume or the Van Der Waals diameter. None of them however seems to give exhaustive correlations [55].

# Chapter 2

## PEI—CO<sub>2</sub> System

The II chapter focuses on the system PEI—CO<sub>2</sub> and their interactions at low CO<sub>2</sub> pressures. This research work follows the study conducted by De Nicola *et al.* on the system PEI—H<sub>2</sub>O [56, 57]. Several studies have been conducted on the latter because PEI is a high performance polymer of great interest in aeronautics; e.g. it is employed as the organic matrix of carbon fibers reinforced composite materials to improve their thermo-mechanical performances. Water is one of the main ageing factors inducing degradation of the matrix properties. Moreover, PEI is employed in the gas separation industry (figure 2.1). The fundamental study conducted during this PhD program on the system PEI—CO<sub>2</sub> aims to understand better the transport mechanisms involved at low activities. First, the chemistry of polyetherimide will be described; second the work done on the PEI—CO<sub>2</sub> system will be described in detail, showing the differences with the PEI—H<sub>2</sub>O system.

Polyetherimide was first synthesized during the 70's by J.G. Wirth and his research group at General Electric's (GE) Corporate Research and Development Center in Schenectady, New York [58, 59]. To synthesize polyetherimides, the most common procedure consists in performing a cyclization reaction to form the imide rings and a displacement reaction to prepare the ether linkage. First a bisimide monomer is formed by reaction of nitrophthalic anhydride and a diamine; second, a bisphenol dianion is made by treatment of a diphenol with two hydroxyl anions; finally, the polymerization step involves displacement of the nitro groups of the bisimide by the bisphenol dianion to form the ether linkages of the polymer. Polymerization is performed under relatively mild conditions in dipolar solvents or in mixtures of these with toluene. The polymer is typically precipitated by addition to methanol in a blender, then washed with methanol and dried. Figure 2.1 shows Ultem<sup>®</sup> (or Polyetherimide-I) chemical formula, i.e. the most famous compound among the PEI family.

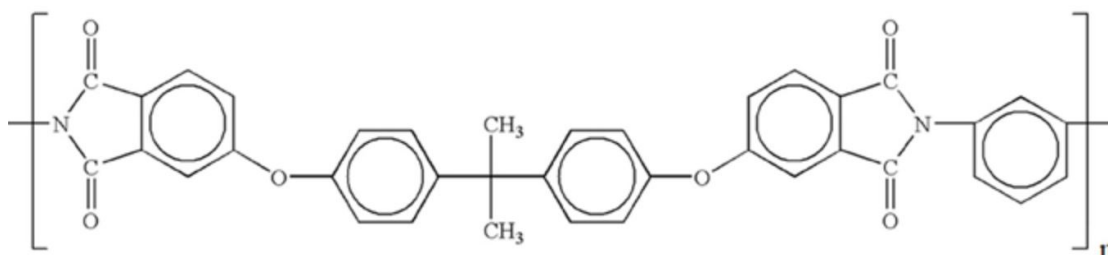


**Figure 2.1:** PEI Ultem<sup>®</sup> chemical formula

The study conducted on the PEI—H<sub>2</sub>O system showed that the interaction between the polymer and the penetrant is twofold: a first layer of water interacts through hydrogen bondings with the carbonyl group of the imide rings while a second layer builds upon the former [56]. This result was obtained by the combination of two experimental techniques: gravimetry and *in-situ* time-resolved FTIR spectroscopy [60, 61]. The same methods are used to study sorption of carbon dioxide. Interestingly, specific interactions are found again between the penetrant and the carbonyl groups. Overall, this is considered a weak mean field type interaction.

## 2.1 Materials

Total amorphous PEI films was a commercial grade product (code E131050) supplied by Goodfellow Co. (PA, USA) in the form of 50  $\mu\text{m}$ . The order of magnitude of the film thickness required for the experiments varied from 1 to 80  $\mu\text{m}$  so that the original product was first dissolved in chloroform (15 % wt/wt concentration) and then cast onto a tempered glass support. The solution was spread by a calibrated Gardner knife, which allows one to control the film thickness. The cast film was dried 1 hr at room temperature and 1 hr at 80°C to allow most of the solvent to evaporate, and at 120°C under vacuum over night. At the end of the drying protocol the film was removed from the glass substrate by immersion in distilled water at 80°C. Chloroform was purchased from Sigma-Aldrich (St. Louis, MO 63178 USA). CO<sub>2</sub> was purchased from Air Liquide Italia S.p.A. (Milan, 20158 Italy). The density of dry PEI is 1.2683 g cm<sup>-3</sup> as estimated previously in the literature [57].

## 2.2 Apparatuses and Methods

A homemade gravimetric apparatus working under vacuum was used to measure the solubility of CO<sub>2</sub> within the PEI matrix (figure 2.2). The instrument consists of a test cell where the quartz spring microbalance displacement along the vertical axis

(RUSKA Co., Houston, TX; maximum elongation 200 mm, maximum weight 100 mg, static sensitivity of  $0.515 \text{ mg mm}^{-1}$ , manually calibrated with a Mitutoyo height gauge having a resolution of 0.01 mm and an accuracy of  $\pm 0.03 \text{ mm}$  and a weight calibration standard) is measured by a couple of CCD cameras (resolution  $\sim 5 \mu\text{m}$ ). The quartz wire and spring are placed in a glass water jacketed compartment kept at the desired temperature. The room is connected by service lines to a flask dead volume, to the penetrant gas or liquid tank and to a combined pumping station incorporating a turbopump and a membrane backing pump (Pfeiffer HiCUBE 80, ultimate pressure  $1\text{E-}07 \text{ mbar}$ , pumping speed  $35 \text{ l s}^{-1}$ ). During the experiment, the pressure within the dead flask is monitored with an absolute capacitance manometer (623F Baratron<sup>®</sup>, full scale 1000 Torr, resolution 0.001% of F.S., accuracy 0.25% of reading from MKS Instruments, Inc. Andover, MA 01810 USA). Vacuum is monitored within the sorption cell with a Pirani vacuumometer Thermovac TM 20 (Leybold GmbH, Colonia 50968 Germany) operating within a pressure range of 0.001—1000 mbar.

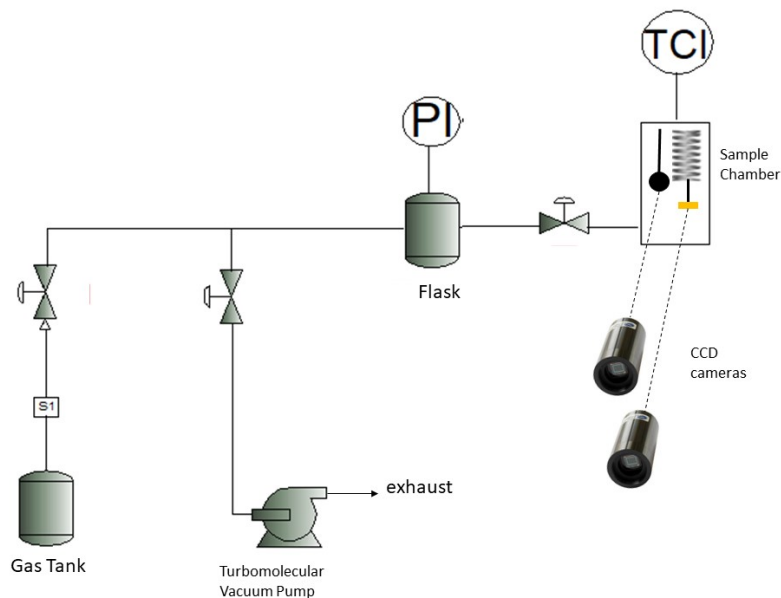


**Figure 2.2:** QSM sorption apparatus scheme

The experimental method consists in stepwise sorption isothermal tests: the sample is always dried at high vacuum before starting the first step. The flask dead volume maintains the pressure constant during each experiment. Sorption kinetics are measured and, from the equilibrium values, sorption isotherms are derived.

The kinetics are modelled by applying Fick's constitutive equation to the diffusion flux of the penetrant in the equation of continuity for the mixture. The specimen geometry is comparable to a plane sheet whose thickness is several order of magnitude

lower than the other dimensions. The specimen thickness error is always lower than 4%. Indeed, the diffusivity is a parameter whose values are found by fitting the model to the experimental kinetic data. The diffusion coefficient is approximately constant when the activity change of the penetrant in the vapour phase is sufficiently low, although its dependence on concentration should be always taken into account. That is, it is always expressed as a function of the average equilibrium solubilities measured for each step experiment. Equation 2.1 represents the PDE problem of interest whose solution is given by equation 2.2.

$$\frac{\partial C}{\partial t} = -\frac{\partial J}{\partial x}, \quad \text{i.c. } C(0, x) = C_0 \quad (2.1)$$

$$J = -D\frac{\partial C}{\partial x}, \quad \text{b.c. } C(t, x = \pm L) = C_\infty$$

$$\frac{C(t)}{C_\infty} = 1 - \sum_{n=0}^{\infty} \frac{8}{(2n+1)^2\pi^2} \exp(-D(2n+1)^2\pi^2t/4L^2) \quad (2.2)$$

where  $J$  is the flux of penetrant into the polymer phase;  $D$  is the mutual diffusion coefficient of CO<sub>2</sub> in PEI; the plane sheet is supposed symmetric and of thickness  $2L$  [62]. A specific Matlab<sup>®</sup> code was implemented to evaluate the best fitting value of  $D$ . The code solves a nonlinear least-squares curve fitting problem by applying the *trust-region-reflective* algorithm.

Time-resolved FTIR spectra were recorded *in situ* using a modified Linkam cell, THMS350V (Surrey, UK), equipped with temperature control (83—623 K) and a vacuum system. The cell was connected through service lines to a mass-flow-controller MKS Type GM50A (Andover, MA) to set the CO<sub>2</sub> flux, while a solenoid valve regulated the downstream pressure. The system was equipped with a Pirani vacuumeter and a MKS Baratron 121 pressure transducer (full scale 1000 Torr, resolution 0.01 Torr, accuracy  $\pm 0.5\%$  of the reading) (Andover, MA). The experimental apparatus is represented in figure 2.3. The diffusion cell was coupled to a Spectrum-100 FTIR spectrometer (Perkin-Elmer, Norwalk, CT, USA), equipped with a beam splitter made of a thin Ge film supported on KBr plates and a wide-band DTGS detector. Instrumental parameters were set as follows: resolution 2 cm<sup>-1</sup>; Optical Path Difference (OPD) velocity 0.20 cm s<sup>-1</sup>; number of coadded scans 16. Full absorbance spectra (i.e., PEI ULTEM<sup>®</sup> + sorbed CO<sub>2</sub>) were obtained using a background collected on the cell containing a plain KBr window, at the test conditions. The spectra representative of CO<sub>2</sub> sorbed at equilibrium were obtained by Difference Spectroscopy (DS) eliminating the interference of the substrate, i.e.:

$$A_d = A_s - A_r \quad (2.3)$$

where  $\{A_d, A_s, A_r\}$  represent, respectively, the difference spectrum (sorbed CO<sub>2</sub>), the

sample spectrum (PEI ULTEM<sup>®</sup> equilibrated at the test pressure) and the reference spectrum (PEI ULTEM<sup>®</sup> after total desorption at the temperature of interest). The data gathered by the instrument were preprocessed (linear baseline correction, offset to zero absorbance) to prevent artefacts due to baseline instabilities. The molar absorptivity of the probe within the polymer is calculated from the Lambert-Beer law:

$$A = abc$$

where  $A$  is the absorbance integrated over the frequency range of interest in the sorption analysis (expressed in  $\text{cm}^{-1}$ ),  $a$  is the *absorptivity* (in  $\text{cm mol}^{-1}$ ),  $b$  is the specimen thickness (in cm) and  $c$  the concentration of the probe within the specimen usually expressed in  $\text{mol cm}^{-3}$ . A Matlab<sup>®</sup> algorithm was implemented to perform a two dimensional correlation spectroscopy (2D-COS) analysis. Moreover, to separate the individual components in the case of unresolved bands, a curve fitting algorithm was applied, based on the Levenberg–Marquardt method. The peak functions used for the sharp peak at higher frequency is a Gaussian profile expressed as:

$$f(x) = H \exp\left(-\left(\frac{(x - x_0)}{w}\right)^2 \ln(2)\right) \quad (2.4)$$

where  $x_0$  is the peak position;  $H$  the peak height;  $w$  the full-width at half height (FWHM).

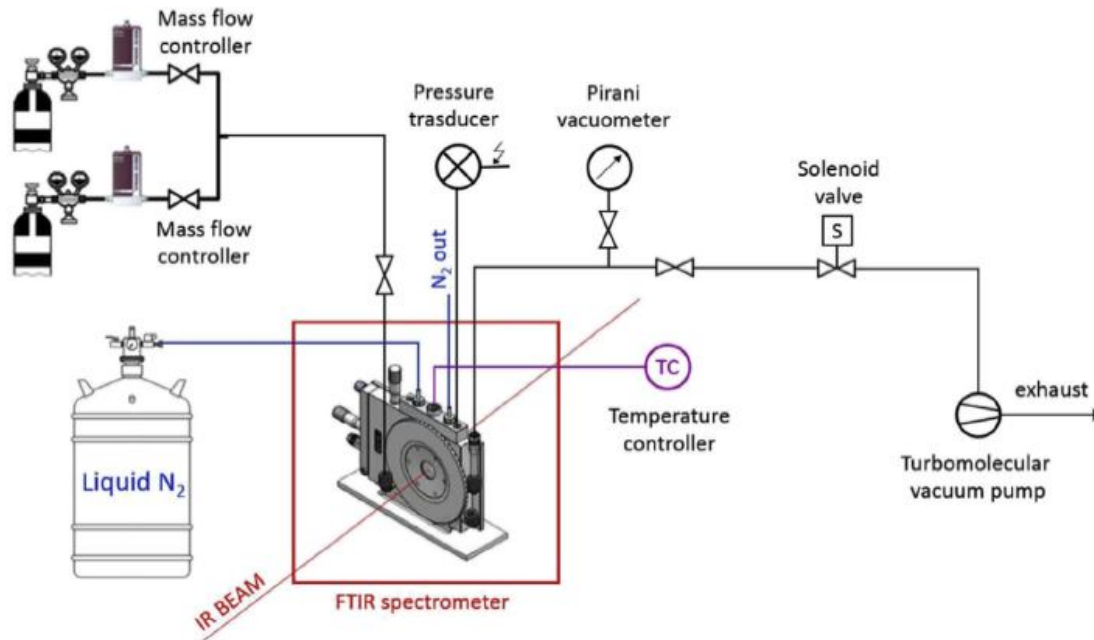


**Figure 2.3:** FTIR measurement apparatus scheme [61]

## 2.3 Results and Discussion

First, the gravimetric sorption experiments are described along with an example of the recorded fickian kinetics. Second, the FTIR measurements are presented along with a fundamental analysis of the sorption process. Last, the dual mode, NELF-SL and NETGP-NRHB frameworks are used to model the solubility data.

CO<sub>2</sub> sorption isotherms in PEI are presented in figure 2.4. The error bars are evaluated from the random error associated with the measurement and takes into account fluctuations of temperature and pressure around their mean values. An example of the recorded kinetics is presented in figure 2.5. Figure 2.6 displays the corresponding Fickian diffusivities of carbon dioxide in PEI as a function of the arithmetic mean concentration. For the sake of simplicity, the reported kinetics has been normalized over the equilibrium concentration. The fickian diffusion based fitting is displayed in red. As expected, the diffusion coefficient trend increases with the temperature but it appears almost invariant with the gas average concentration (figure 2.6). Noteworthy, the mutual diffusion coefficient evaluated from the fickian best fitting of a FTIR *in situ* dynamic experiment (i.e. integral sorption step at 93.33 mbar and 35°C) is coherent with the gravimetric set of data and it is equal to 2.90E-09 cm<sup>2</sup> s<sup>-1</sup>.

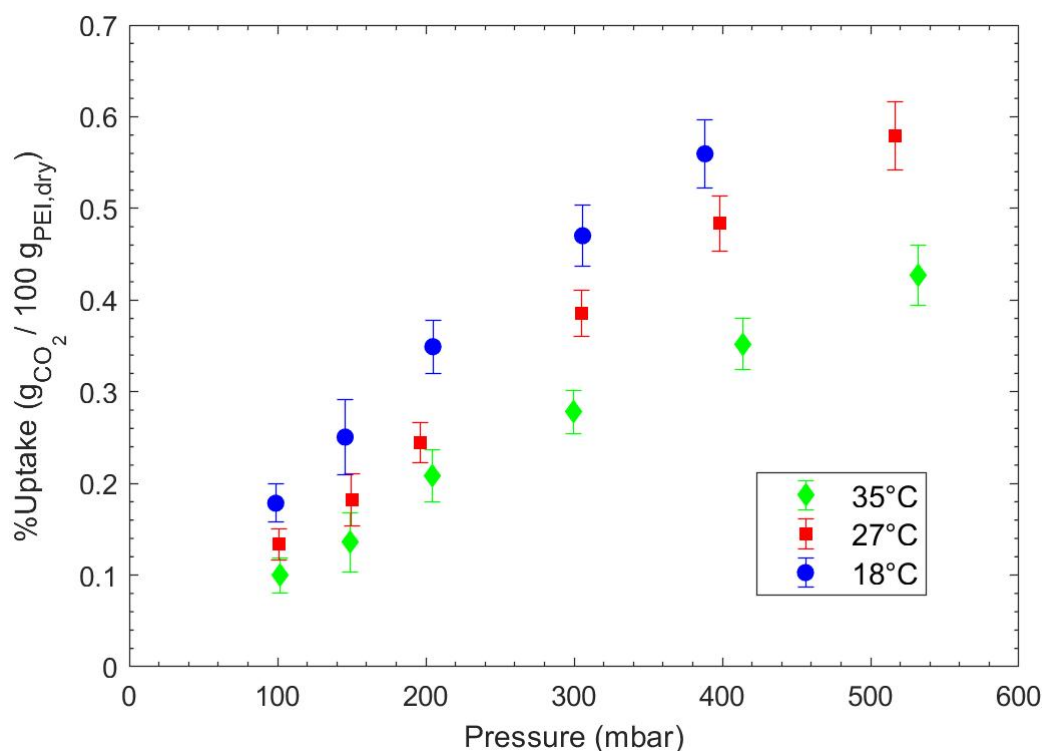


**Figure 2.4:** CO<sub>2</sub> sorption isotherms in PEI determined gravimetrically at several temperatures. Film thickness:  $\sim 70\mu\text{m}$

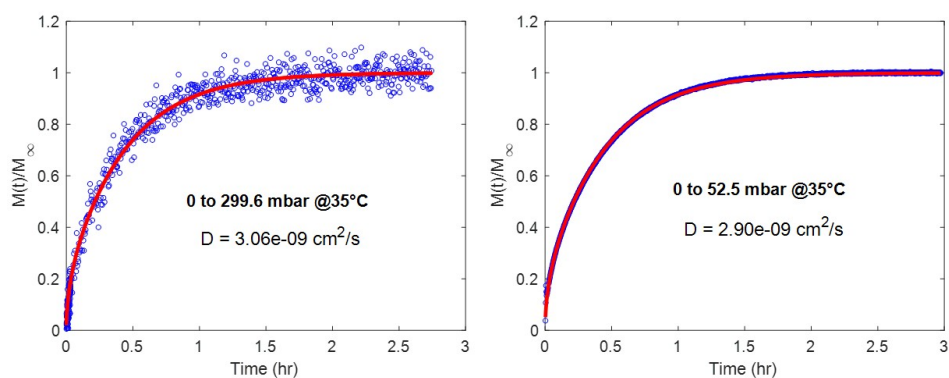


**Figure 2.5:** Kinetics examples of CO<sub>2</sub> sorption in PEI at 35°C: gravimetry (left); *in situ* FTIR (right)

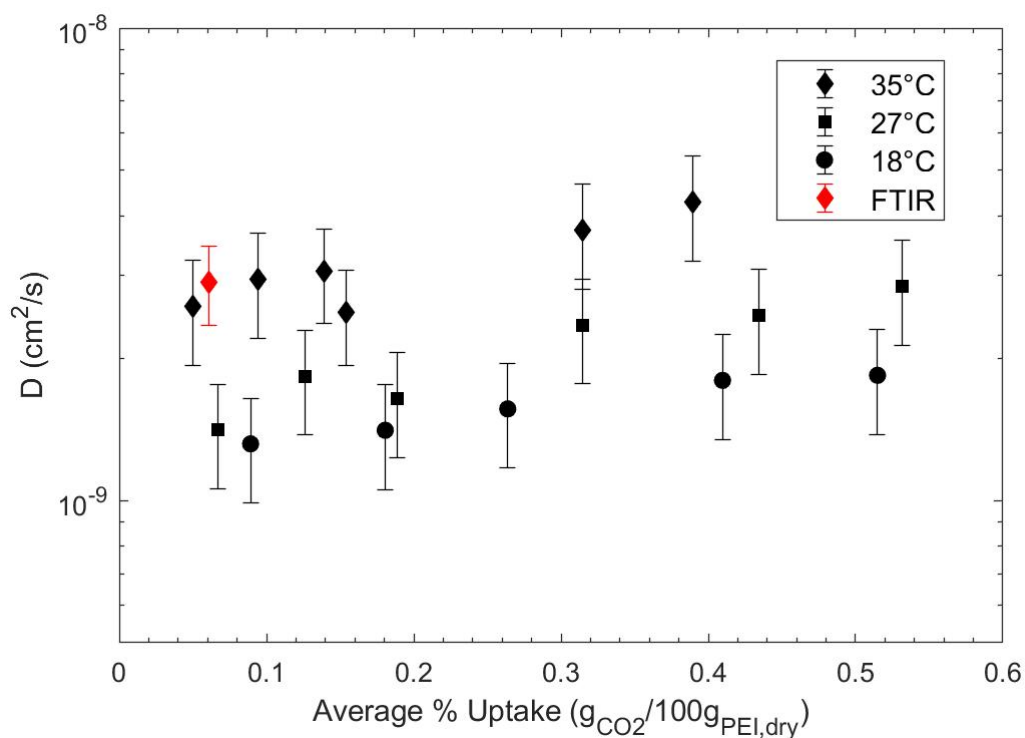


**Figure 2.6:** Mutual diffusivity of CO<sub>2</sub> in PEI based on the Fickian model

FTIR *in situ* spectroscopy gives a microscopic insight of the sorption process thus completing the macroscopic analysis from the gravimetric experiments [63]. *In situ* dynamic frequency spectra are recorded during sorption of CO<sub>2</sub> in PEI. Difference Spectroscopy and two dimensional correlation spectroscopy (2D-COS) are used to analyse them. Isothermal experiments are recorded at {0, 18, 27, 35}°C by testing a specimen of 67.7 μm. The evolution of the CO<sub>2</sub> antisymmetric stretching peak (wavenumber 2336 cm<sup>-1</sup>) integrated over the range of frequency [2300, 2360] cm<sup>-1</sup> is studied. For instance, figure 2.7a shows an example of spectra obtained at the beginning and at the end of a sorption experiment. The red spectrum refers to the neat dry polymer after desorption of all CO<sub>2</sub> at the temperature of interest. The blue spectrum refers to the polymer-penetrant mixture at equilibrium. *Difference Spectroscopy* discards the neat dry polymer signal and returns the sole adsorbate evolution within the polymeric phase. The correlation between the gravimetric isotherm curves and the FTIR spectroscopic results is still ongoing at {0, 18, 27, 35}°C and at the pressures tested from the latter technique. The data processing will return the absorptivity for the PEI—CO<sub>2</sub> system as a function of temperature.

The function proposed in the *Apparatus and methods* section is fit to the spectrum CO<sub>2</sub> within PEI in the frequency range including the peaks at 2336 and 2324 cm<sup>-1</sup>. The same deconvolution is repeated to derive the second couple of peaks outlined in figure 2.8. The two signals at 2336 and 2324 cm<sup>-1</sup> correspond to CO<sub>2</sub> molecules interacting with the carbonyl groups of the imide through a Lewis-acid (CO<sub>2</sub> carbon)/Lewis-base (carbonyl oxygen) interaction. This is demonstrated first by comparing the pure CO<sub>2</sub> IR spectrum with the main peak at 2336 cm<sup>-1</sup>. The antisymmetric stretching peak shifts to lower frequencies and becomes sharper as a consequence of the interaction with the new environment [64]. In addition, independent experiments are performed at low temperatures on a thinner sample (~ 3 μm) to highlight the interacting polymer moiety. Indeed, the lowering of the carbonyl group population prevents the signal from being saturated as shown in figure 2.7. At low temperatures, the new specimen thickness prevents the diffusion time from being too long. These isothermal integral experiments show the shifting of both the in-phase and out of phase carbonyl peaks after sorption. Also the lowering of the temperature has two effects: the bandshape is broader because the population of adsorbate is higher (exothermic sorption process) and, as such, the probability of more interactions is higher; the kinetic energy of the probe is lower and the interaction strength, although weak can overcome it. Difference spectroscopy is used in figure 2.9: the in-phase peak shifts to 1780 cm<sup>-1</sup> and the out of phase peak shifts to 1725 cm<sup>-1</sup>. At 35°C, only noise is registered.

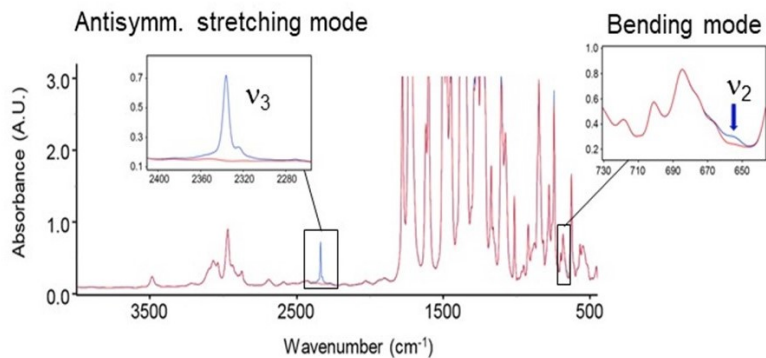


**Figure 2.7:** PEI—CO<sub>2</sub> FTIR dynamic frequency spectra example

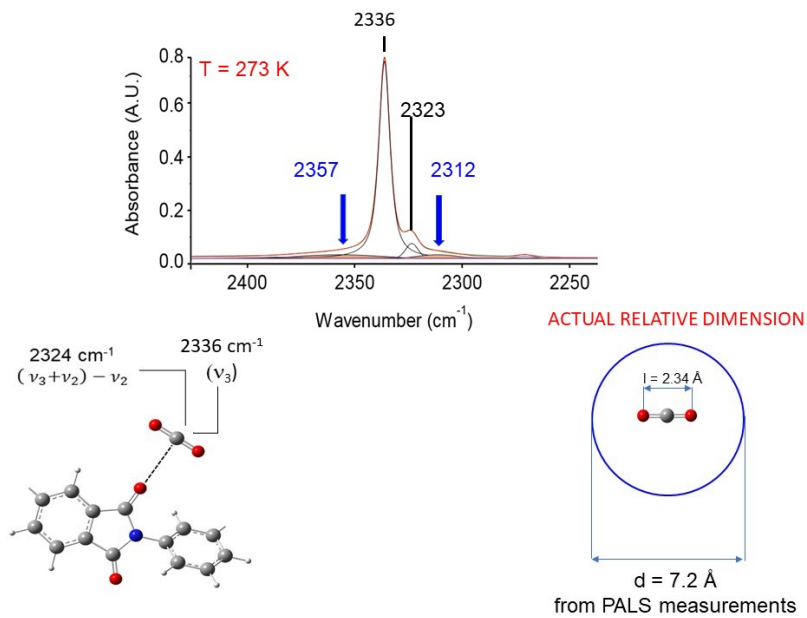


**Figure 2.8:** CO<sub>2</sub> main peak curve fitting

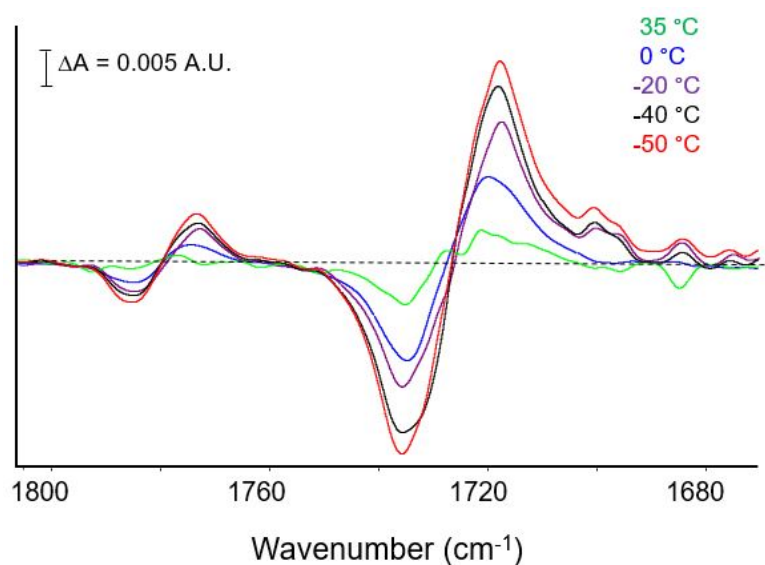


**Figure 2.9:** PEI carbonyl group difference spectra as a function of temperature

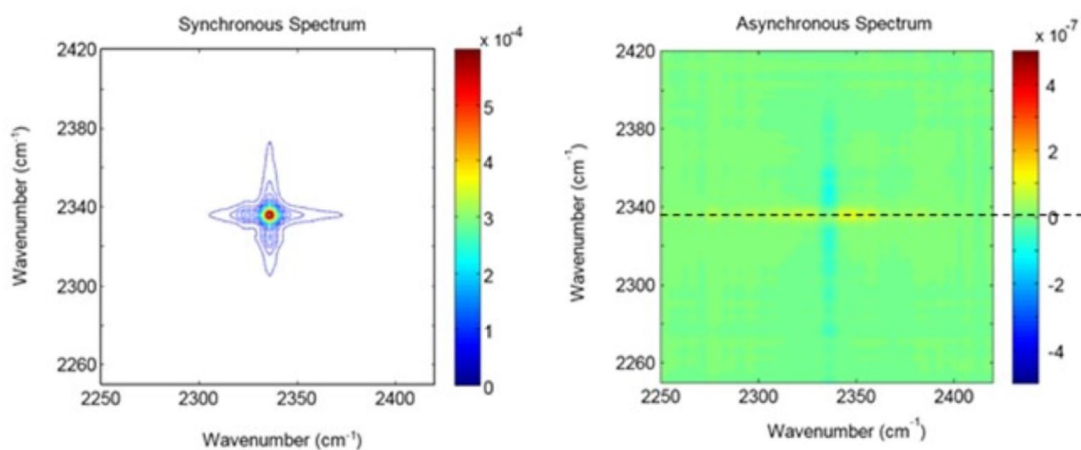


**Figure 2.10:** PEI—CO<sub>2</sub>, 2D-COS analysis at 35 °C

The shoulder at 2324 cm<sup>-1</sup> appears from the Fermi resonance effect acting on the combination plus difference transition (hot band) of the bending and stretching signals at 2336 and 653 cm<sup>-1</sup> [65]. No split of the main peak is observed during sorption as would appear when two different species of the same adsorbate are interacting with the polymer. The two broader bands at 2360 and 2314 cm<sup>-1</sup> are assigned to the P-R rotovibrational branches of the spectrum of non-interacting CO<sub>2</sub> molecules in a gas-like state, possibly residing into excess free-volume elements frozen in the glassy structure. However the absorbance signal is too weak to confirm the presence of this additional species. Summarizing, from the FTIR analysis, a unique CO<sub>2</sub> species is recognised within the matrix,

i.e. the one which is interacting with the carbonyl group. The interaction strength depends on the concentration and on the kinetic energy of the penetrant sorbed within the matrix and, consequently, on the temperature chosen.

2D-COS analysis confirms that at 35°C the dynamic absorbance components evolve synchronously: the synchronous spectrum displays a highly characteristic cross-shape [66]. A single autopeak is detected at 2336 cm<sup>-1</sup>, corresponding to the main component in the frequency spectrum. The off-diagonal wings extend by about 30 cm<sup>-1</sup> and reflect the presence of two weak components increasing in sorption or decreasing in desorption with the same rate of the main peak. The elongated shape of the off-diagonal features indicates that these two components are significantly broader than the main peak. The asynchronous spectrum is featureless at 35°C. Only noise is present, despite the significant intensity of the analytical band and its complex, multicomponent structure. This demonstrates that all the components evolve synchronously. In other words, the species they originate from have a comparable molecular mobility thus indicating the presence of a unique penetrant species at 35°C. The latter weakly interacts with the carbonyl groups: its kinetic energy is sufficiently high at this temperature to overcome the interaction and the species is thought to experience both gas and interacting states. On the other hand, at 0°C the kinetic energy is depleted, the interaction with the polymer gets stronger. Moreover, the concentration of carbon dioxide increases when the temperature lowers at a fixed outer gas phase pressure and the probability of having more interactions increases as well. Difference spectroscopy confirms this result. 2D-COS also confirms that the shoulder at 2324 cm<sup>-1</sup> is not a signal characterizing a separate interacting species.

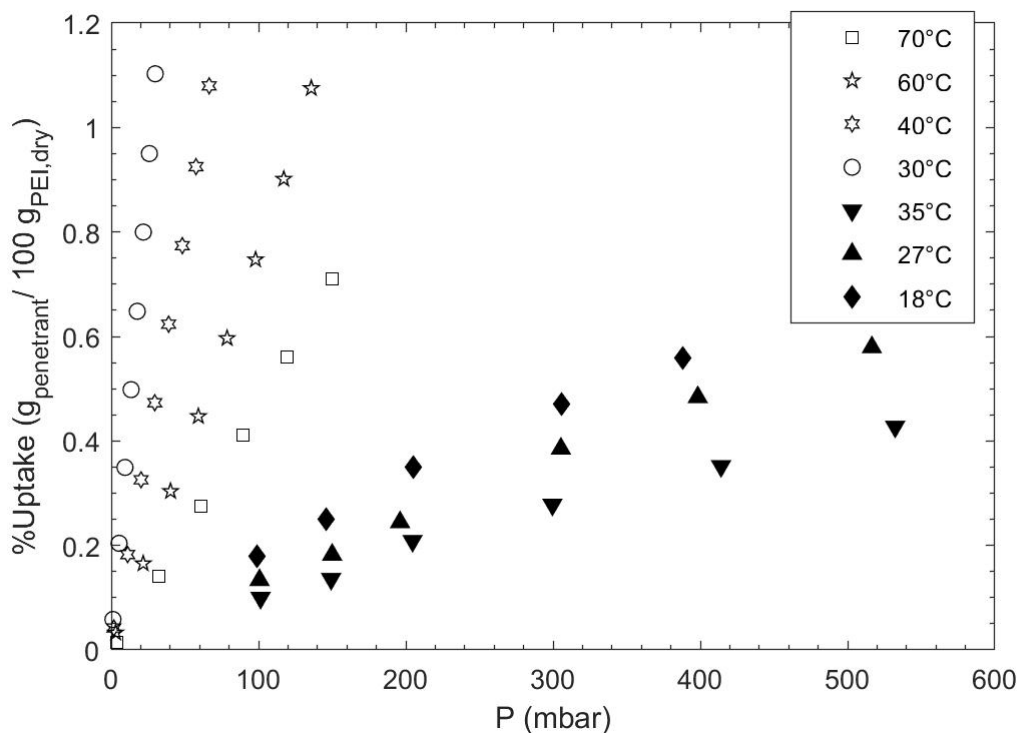


**Figure 2.11:** Comparison of gravimetric sorption data for the PEI—H<sub>2</sub>O and PEI—CO<sub>2</sub> systems. Open markers: PEI—H<sub>2</sub>O; Full markers: PEI—CO<sub>2</sub> [56]

Three models are applied to describe the behaviour of the system under investigation: the dual sorption theory; the NELF-SL and the NETGP-NRHB frameworks. It is observed experimentally that CO<sub>2</sub> is a low sorbing gas with respect to water vapour in the chosen thermodynamic conditions. Indeed, figure 2.11 reports the comparison with the sorption isotherms for the system PEI—H<sub>2</sub>O [56]. These data were obtained with the same apparatus used in this work. The difference between the two penetrants are evident although the pressures at which the tests were conducted are different. Strong HB interactions favors sorption of water in PEI: the authors discovered that two water layers build up on the polymer chain. The former is tied to the carbonyl oxygens of the two imide groups constituting each repeating unit through HB bonds whereas the latter is connected to the first layer through HB bonds which are expected to be energetically and quantitatively lower than the former.

The results of the dual sorption fitting are shown in figure 2.13: seven parameters are introduced by the model to describe the mixture as shown in table 2.1 (see equations 1.96 and 1.101). The Henry's contribution is on the order of 2E-10 g<sub>CO<sub>2</sub></sub>/100 g<sub>PEI,dry</sub> whereas the Langmuir's is on the order of 1E-1 g<sub>CO<sub>2</sub></sub>/100 g<sub>PEI,dry</sub> so that the former can be ignored.

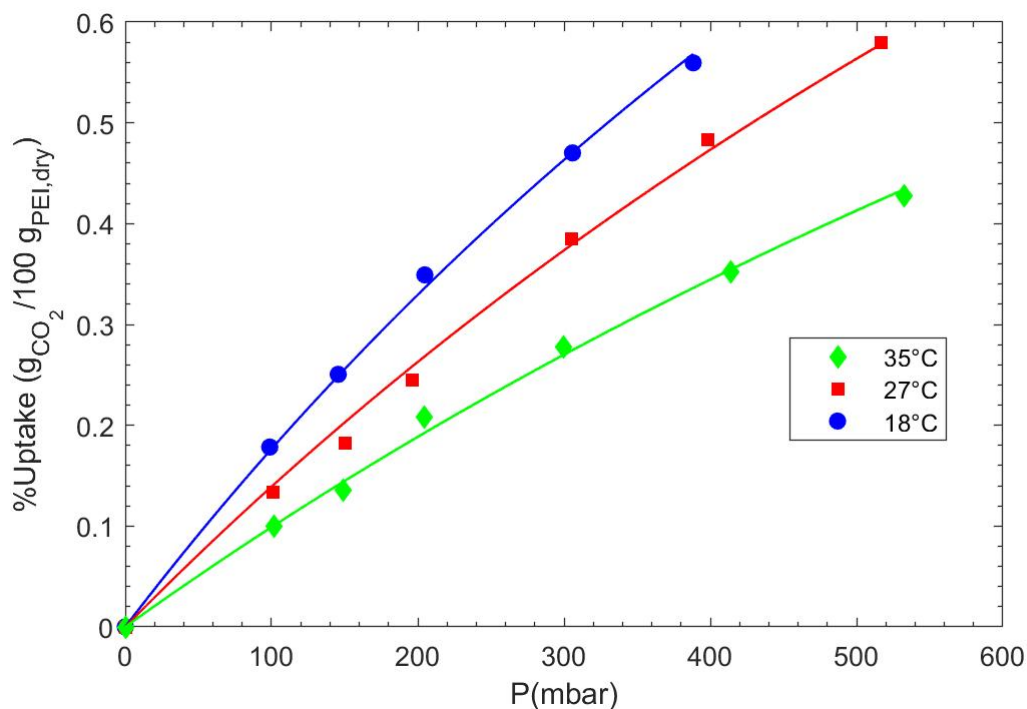
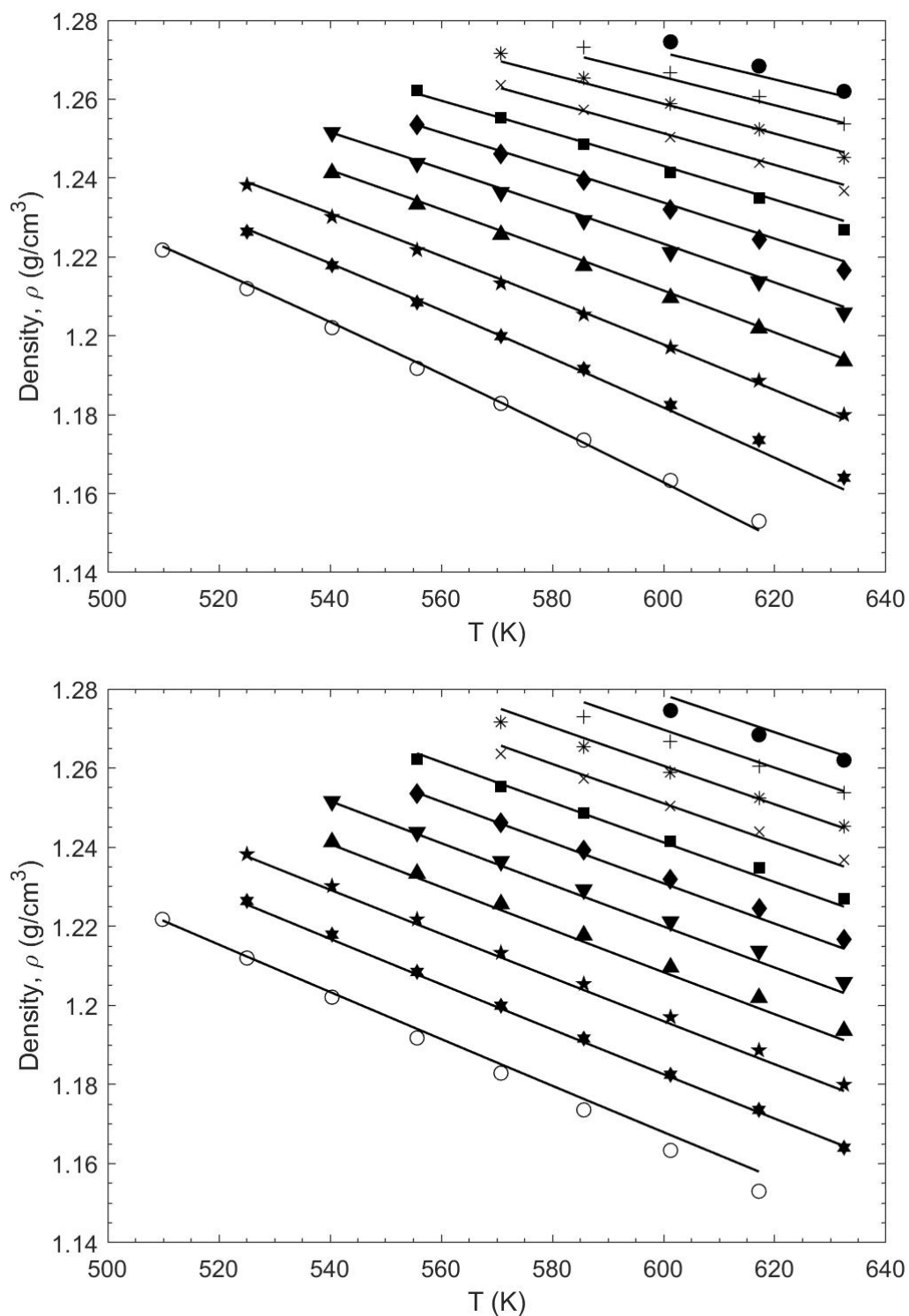


**Figure 2.12:** Dual mode fitting of the PEI-CO<sub>2</sub> mixture

T(K)	$K_{d,0}$ ( $\text{g}_{\text{CO}_2}/100 \text{ g}_{\text{PEI,dry}} \text{ mbar}$ )	$Ch'$ ( $\text{g}_{\text{CO}_2}/100 \text{ g}_{\text{PEI,dry}}$ )	$b_0$ ( $\text{mbar}^{-1}$ )	$\Delta H_k$ (J/mol)	$\Delta H_b$ (J/mol)
291.15		2.469			
300.15	5.34E-14	2.378	6.06E-07	-9.29E+03	-1.73E+04
308.15		2.004			

**Table 2.1:** Dual Sorption parameters of pure PEI and CO<sub>2</sub>

The Langmuir's saturation concentrations,  $C_i$ , are not trustworthy since saturation is only attained at high pressures where also the Henry's contribution must be taken into account. Consequently, the affinity parameters cannot be interpreted quantitatively too. The model only returns a qualitative picture of the problem, i.e. sorption of CO<sub>2</sub> is only taking place in the Langmuir's sites, i.e. in the excess free volume available in the polymer matrix. Within the framework of the dual mode theory, the penetrant is thought to act as a free volume filler. This process is exothermic as suggested by the sign of  $\Delta H_b$  which describes the penetrant enthalpy difference in the gas state and in the condensed Langmuir sites.

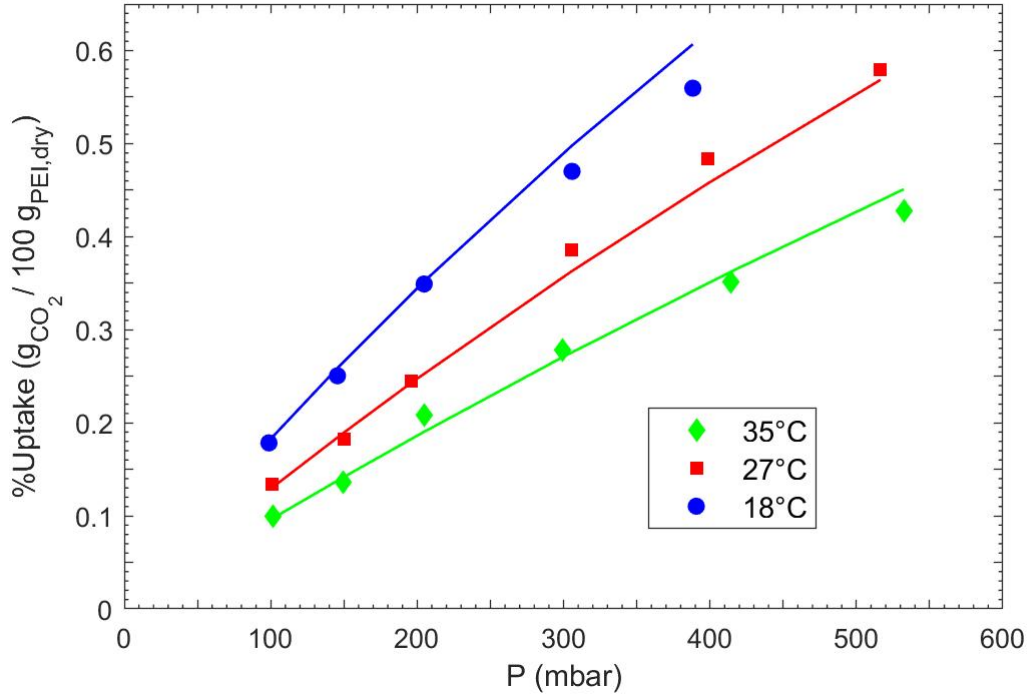


**Figure 2.13:** PVT data of PEI: (up) SL fitting; (down) NRHB fitting. ●: 200; +: 180; \*:160; ×: 140; ■: 120; ◆: 100; ▼: 100; ▲: 80; ★: 60; ★•: 40; ○: 20 in MPa [57]

Substance	$T^*$ (K)	$P^*$ (MPa)	$\rho^*$ (g/cm <sup>3</sup> )	Reference
PEI	893	545	1.354	This work
CO <sub>2</sub>	300	630	1.515	[46]

**Table 2.2:** SL parameters of pure PEI and CO<sub>2</sub>

Substance	$\epsilon_s^*$ (J/mol)	$\epsilon_h^*$ (J/mol K)	$v_{sp,0}^*$ (cm <sup>3</sup> /g)	s	Reference
PEI	5.503	6775.2	0.7228	0.743	[56]
CO <sub>2</sub>	-4.3	3096.3	0.9545	0.909	This work

**Table 2.3:** NRHB parameters of pure PEI and CO<sub>2</sub>**Figure 2.14:** NELF-SL fitting of PEI—CO<sub>2</sub> sorption data

Next, the NELF-SL and NELF-NRHB approaches are followed and compared. First, the parameters of pure CO<sub>2</sub> and PEI are derived based on vapour—liquid equilibrium data and PVT data respectively. All of them can be found in the literature and, particularly, the former from the Perry's chemical engineer's handbook and the latter from the work done by Scherillo *et al.* [67, 57]. The SL and NRHB statistical lattice

fluid models are applied (figures 2.13 and ??) and the parameter values are reported in table 2.2 and 2.3. The NELF-SL model is fit to the experimental sorption data already provided in figure 2.4. The results are presented in figure 2.14 and the value of the binary interaction parameter  $\zeta_{12}$  is 0.96872. The parameter value is slightly lower than one indicating the affinity is also slightly low between the two compounds. No swelling is occurring so that  $k_{sw}$  is zero. No specific directional interactions are predicted to occur by the model at the thermodynamic conditions chosen. The result of the NETGP-NRHB model fitting is given in figure 2.15. Particularly, it is assumed that the penetrant could interact with the matrix through a weak acid—base Lewis reaction: the oxygen of the carbonyl groups belonging to the imide ring attracts the carbon atom of the solute so that the bond could be related to a HB interaction both energetically and entropically. The CO<sub>2</sub> carbon with its excess positive charge is the acidic species and the carbonyl oxygen is the base (in the Lewis sense). The new physical description is more exhaustive than the one provided by the NELF-SL framework where only *mean field interactions* are considered. The model parameters are given in table 2.4. The nomenclature is chosen as follows

- 1- the penetrant is substance #1 and its donor group (-C-) is assigned a value of #1
- 2- the polymer under investigation is substance #2 and its acceptor group (O=) is assigned a value of #1

It is clear that the NELF-SL model fits the data better than the NETGP-NRHB model. More parameters are not needed to describe the sorption process and specific interactions are not to be taken into account at the thermodynamic conditions investigated. The theoretical analysis confirms only mean field type interactions are taking place during sorption. Presumably, the PEI carbonyl groups are uniformly distributed and highly concentrated so that the interactions observed from the FTIR experiments are weak and uniformly distributed too.

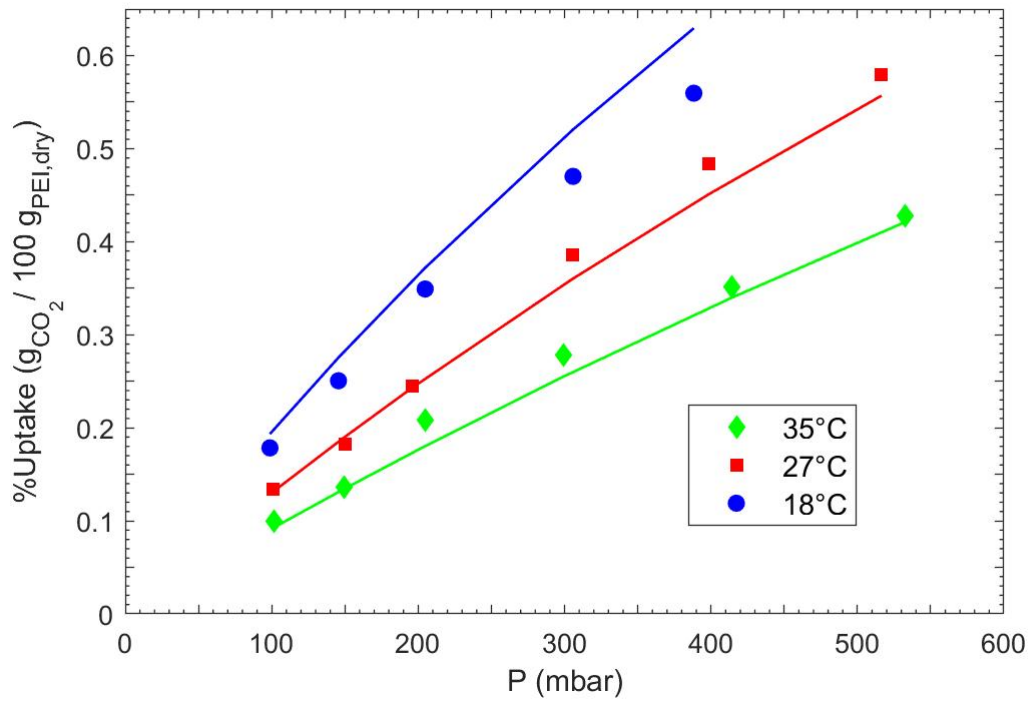


**Figure 2.15:** NETGP-NRHB fitting of PEI—CO<sub>2</sub> sorption data

$\zeta_{12}$	$E_{12}^{hb}$ (J/mol)	$S_{12}^{hb}$ (J/mol K)	Reference
$0.9407 \pm 0.0002$	-25.41	-2.74E-08	This Work

**Table 2.4:** NRHB parameters for the PEI—CO<sub>2</sub> mixture based on the NETGP framework

## Chapter 3

# PS—Toluene System

In the III chapter mass transport of Toluene vapour in atactic Polystyrene (A-PS) is investigated. Toluene is a good solvent for A-PS and it is capable of plasticizing it. Toluene and A-PS (unit chain) structures are outlined in figure 3.1.

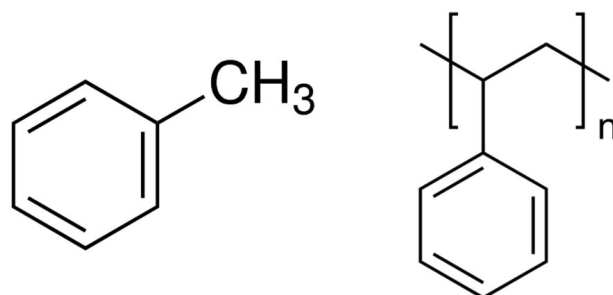


**Figure 3.1:** Toluene (left) and PS unit chain (right) chemical formulas

The research work has been focused on the A-PS plasticization due to sorption-desorption of the penetrant. A large variety of *dynamic* and *static* mass transport experiments have been conducted with the aim to understand the mixture behaviour in the glassy and rubbery regions. Arguments supporting the idea that mass transport induces this specific phase transition have already been given in Chapter I. It is shown that thermodynamics controls the phenomenon in the rubbery equilibrium phase whereas the out of equilibrium glassy region is dominated by the specific thermodynamic history of the mixture.

The work of Doumenc *et al.* was continued in this sense by investigating more profoundly the mixture behaviour in the glassy and rubbery states [68, 69, 70, 71]: indeed either temperature or pressure or both of them simultaneously are controlled in the vapour phase to reach this goal. Polymer density relaxation and mass transport are affecting each other in the glassy region. Usually, the effective order of mass sorption kinetics,  $n$  over time,  $\Delta m \propto t^n$ , at fixed temperature, where an initially glassy dry polymer is swollen up to a rubbery state, is typically higher than the 0.5 value predicted by Fick's law. Several types of sorption kinetics have been actually named after data from integral sorption experiments of this kind, according to the effective order: *anomalous kinetics* ( $0.5 < n < 1$ ), *Case II* ( $n = 1$ ) and *Super Case II* ( $n > 1$ ) sorption kinetics [72, 73, 74]. Usually stepwise sorption/desorption experiments (static experiments) are conducted to measure the characteristic relaxation times spectra of the mixture (see *PEI—CO<sub>2</sub>* in chapter I). Indeed, this work aims to the definition of alternative and faster experimental protocols to retrieve unambiguous data useful to the evaluation of relaxation rate in polymer–solute systems. The experimental data and comments are reported in this chapter by following the scheme used in the paper published in the literature [75]. At the end of the chapter, a comprehensive modeling of the experimental data is presented through the NRHB approach [76].

### 3.1 Materials

Samples in the form of self-standing thick films, or supported thin layers, are prepared from the same source of A-PS (weight average molecular weight  $M_w = 270,000$  g/mol; polydispersity index  $M_w/M_n = 1.1$ ) kindly supplied by Versalis S.p.A., Mantua, Italy. Toluene, used either for sample preparation or for sorption/desorption tests, is employed as provided by the supplier (HPLC grade, Sigma-Aldrich). Self-standing thick films (around 90  $\mu\text{m}$ ) are prepared by solvent casting a toluene-PS solution on a glass petri dish, after a suitable volume of solution is dropped on it. Thin PS coatings (coating thickness lower than 1.0  $\mu\text{m}$ ) deposited on top of aluminum foils (thickness 17  $\mu\text{m}$ , Italchim S.r.l., Bologna, Italy) are obtained by a spin coating process, starting from a PS—Toluene solution (PS 7% by weight). By modifying the spinning rate, it is possible to obtain thin films with different thickness. Two series of coating films, 430 and 750 nm thick, are actually prepared and used for the sorption experiments. Disks with a diameter of 13 mm are cut from the PS spin coated aluminum foils, using a sharp cutting die. For all kind of samples, removal of residual traces of toluene is pursued by treating them at 120°C under vacuum for few hours followed by overnight cooling. Thickness of free standing PS film is measured by means of a mechanical micrometer, while the estimate of the average thickness of PS coating films is obtained after the evaluation of the coating mass. For the latter procedure, the weight of the coating film

is calculated after the difference between the weight of coated disk and corresponding bare aluminum disk, as obtained after cleaning it by means of a solvent.

## 3.2 Apparatuses and Methods

A Mettler Toledo (Mettler-Toledo S.p.A., Via Vialba 42, 20026 Novate Milanese MI, Italy) analytical balance (resolution 1E-05 g) is used for the evaluation of apparent weight of both coated and cleaned disks. The average thickness of the coating is finally estimated from its mass, based on the total area of the disk and on estimated room conditions value for mass density of polystyrene ( $1.04\text{g}/\text{cm}^3$ ). A MDSC Discovery (TA Instruments 159 Lukens Drive, New Castle, DE 19720 USA) is used to determine the glass transition temperature of pure A-PS. Two different homemade apparatuses are used to evaluate sorption/desorption of Toluene into/from A-PS. The following two subsections describe each of them.

### 3.2.1 Pressure Decay

A two-chambers pressure decay rig is used to perform pure component sorption steps from a vapour phase into free standing thick polymer films. The pressure of the vapour phase is monitored during the process and the number of moles of vapour absorbed into the polymer sample are calculated at any time during the process based on the pressure value in gaseous phase (figure 3.2). The pressure decay apparatus for vapour sorption tests consists of vacuum solvent-resistant fittings, tubes, valves and vessels; all the closed measuring volumes (from V2 to T3) are accurately calibrated with helium to have a good control over the experimental procedure and to obtain suitable sorption results. Degassed liquid toluene is charged in the T1 penetrant reservoir; then air is evacuated from the system by the rotary vane vacuum pump P1, installed ahead of a properly designed liquid nitrogen trap to prevent both vapour solvent release and oil pump backstreaming into the system. Well known weight of polystyrene thin film samples (weighted by a Mettler-Toledo analytical balance, sensitivity 1E-05 g, after overnight vacuum treatment) are placed in the sample holder T3. All the system is then evacuated at high vacuum and set to the experimental temperature, controlled by an air oven with a PID controller. A vapour solvent pre-charge is done for each sorption step, between V2 and V3 valves.

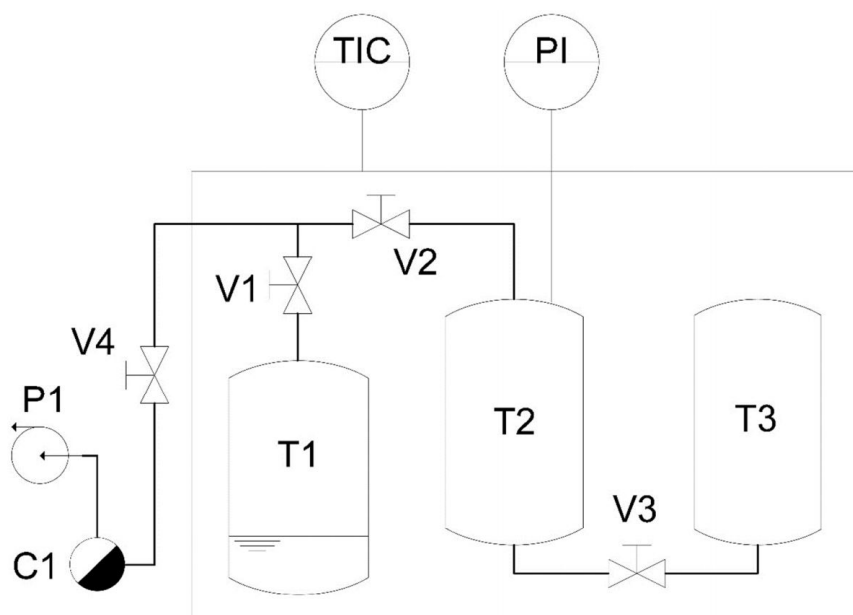


**Figure 3.2:** Pressure decay apparatus process diagram for *static* measurements: TIC, Temperature Indicator and PID Controller; PI: Pressure Indicator (Edwards Barocel<sup>®</sup> pressure/vacuum transducer, 0-100 mbar ranged); V1,V2,V3 and V4 are the manually operated valves; P1: two stages rotary vane vacuum pump (Edwards); C1, liquid nitrogen trap; T1, degassed liquid toluene reservoir; T2, vapour pre-charge chamber; T3, sample holder

In order to provide a reference for the equilibrium solubility of toluene in the investigated polystyrene, conventional *static* sorption tests of toluene vapour in A-PS are performed with the pressure decay apparatus shown in figure 3.2. The term *static* stands for the step pressure change at the beginning of each experiment. In a typical procedure, free-standing thick PS films are placed in a sample holder and treated under high vacuum to remove any trace of volatiles from the polymer, then the samples are exposed to toluene vapour. The toluene vapour is first introduced in a pre-chamber, of known volume, where the temperature is set to a constant value. After the attainment of the equilibrium value of pressure, the gas is expanded into the sample chamber through a valve and the pressure decrease, due to toluene sorption within the samples, is monitored and acquired over time. Each sorption step for this type of experiment is performed until a constant value of pressure (within the experimental accuracy) is recorded in the sample chamber for at least 24 hours. The corresponding (apparent) equilibrium amount of moles of toluene absorbed in PS is then evaluated through the toluene mole balance applied to the whole system. The calculation is based on the knowledge of: the calibrated volumes of both the pre- and the sample chambers; the volume occupied by the A-PS samples; the value of pressure in the chambers before/after the sorption test, making use of a volumetric equation of state for the gaseous phase. Sorption stepwise tests are then performed to characterize PS behaviour at higher pressures.

### 3.2.2 Dynamic Gravimetry

A gravimetric apparatus for *Dynamic* tests has been set up to monitor mass of toluene absorbed into samples of PS coated aluminum disks from pure component vapour phase. A controlled environment, gold plated, CAHN-D200 electronic microbalance (B1 in figure 3.3) with a resolution of  $1\text{E-}07$  g and an accuracy of  $\pm 3\text{E-}07$  g is used to perform the experiments. The sample, consisting in an assembly of several hundreds PS-coated aluminum disks, piled up and hold together by a titanium wire passing through their central points, is hanged to the measuring arm of the balance. The sample and the hanging wire are located in a glass water jacketed compartment (B2) kept at a controlled temperature. The balance is connected, by service lines, to a flask dead volume (T2), to a liquid toluene reservoir (T1), to a combined pumping station incorporating turbopump and membrane backing pump (Pfeiffer HiCUBE 80, ultimate pressure  $1\text{E-}07$  mbar, pumping speed 35 l/s; P1 in figure 3.3), to a pressure transducer (a MKS Baratron 121 A, absolute capacitance gauge with a full range of 100 Torr, a resolution of 0.01 Torr and an accuracy equal to  $\pm 0.5\%$  of the reading) and to an electronically controlled throttle valve (MKS 653B; V5 in figure 3.3). Pressure of the toluene vapour within the equipment and in the sample compartment is controlled by a MKS 651C controller (PIC), that receives the pressure value from the MKS Baratron 121 A transducer and drives the throttle valve to obtain the desired set point value of pressure. Pressure is maintained at the desired value by a dynamical balance between the toluene vapour outflow through the throttle valve (separating the equipment from the vacuum pump) and the toluene vapour inflow from a solvent reservoir with a manually controlled needle valve (V1). The set point for the pressure controller is provided by a LabVIEW<sup>®</sup> code that supplies to the controller the desired value of pressure at each time. Here, follows a lists of the experiments conducted with this apparatus:

- a) isobaric tests where the sample temperature changes linearly at a specific rate (*dynamic* test);
- b) isothermal tests where the pressure changes linearly at a specific rate (*dynamic* test) or stepwise (*integral static* test);
- c) isoactivity tests performed by concurrent control of the sample temperature and pressure as function of time (*dynamic* test).

A LabVIEW<sup>®</sup> code has been also designed to acquire and record the balance reading, the throttle valve status, the pressure reading and the temperature value of the sample, with a maximum acquisition frequency of 20 points per second. The temperature of the sample compartment is controlled by a programmable liquid fluid temperature bath (Julabo CF41) with an accuracy of  $\pm 0.01^\circ\text{C}$ . Balance head, pressure transducer, solvent reservoir, dead volume flask and service lines are contained in a case where a constant temperature value of  $35^\circ\text{C}$  is assured by an air flow at controlled temperature (accuracy  $\pm 0.1^\circ\text{C}$ ). The liquid toluene contained in the solvent reservoir are first

degassed by several freezing-thawing cycles. During the drying stage which precedes the tests, high vacuum is attained by activating both the turbomolecular pump and the membrane backing pump. Conversely, during the tests, only the membrane backing pump is activated for pressure control purposes. Correction for the effect of buoyancy on the measured values of weight change is quantified by first determining the apparent volume of balance system, including hanging wires, sample and counterweights. This volume is evaluated by introducing within the balance volume pure helium at several pressures, thus promoting a lift (and, in turn, a change in weight), proportional to the density of the gas, that is related to the buoyancy effect on both arms of the balance. Using a reliable equation of state for helium gas it is possible to determine the apparent volume of the balance, assuming that the sample and the components of the apparatus do not absorb any helium. This apparent volume is used to quantify the buoyancy effect due to toluene vapour during the test, that is needed to correct raw gravimetric results for toluene sorption in A-PS. It is important to note that, in the calculation of the buoyancy effect due to toluene, the variation of volume of PS as a consequence of sorption has always been considered negligible.

*integral static* sorption tests and *dynamic* sorption/desorption experiments have been performed in the *dynamic* gravimetric sorption/desorption apparatus. For the sake of clarity, *integral* stands for the initial pressure of each step experiment which is zero. Conversely, a *dynamic* desorption/sorption experiment is any experiment during which a low m.w. compound in the vapour state is adsorbed into/desorbed from a polymer sample as its chemical potential in the surrounding pure component gaseous phase is continuously modified at a controlled rate over time. PS coated aluminum disks are chosen instead of free-standing thick PS films. The goal is to bring the polymer-penetrant mixture in an equilibrium rubbery state before a *dynamic* sorption experiment starts. The obtained raw data in terms of sample weight change were elaborated to evaluate the ratio of toluene absorbed mass over that of neat “dry” A-PS, referred to in the following figures as *mass ratio*, or the toluene *mass fraction*,  $\Omega$ . Experimental conditions (in terms of rate of change of pressure and/or temperature) and sample thickness are properly selected as described in the following sections.

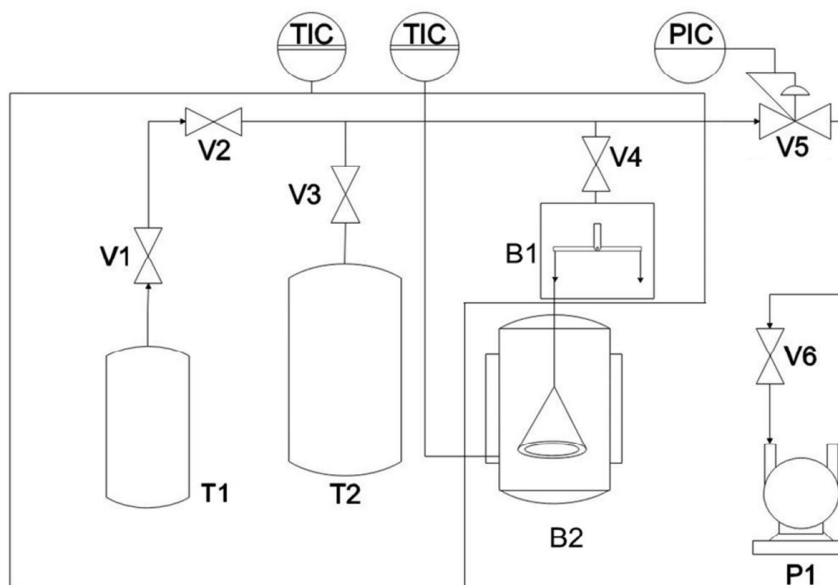


**Figure 3.3:** Gravimetric apparatus process diagram for *dynamic* measurements: TIC, Temperature Indicator and Controller; PIC, Pressure Indicator and Controller (pressure transducer MKS 121 A and pressure controller MKS 651C); V1, V2, V3, V4 and V6 are the manually operated valves; V5 electronically controlled throttle valve (MKS 653B); P1 turbomolecular pump (Pfeiffer I-cube module) with membrane pump stage; T1, degassed liquid toluene reservoir; T2, dead volume flask; B1, Cahn D-200 microbalance head case; B2, water jacketed sample compartment

### 3.3 Results and Discussion

In this section the experimental results are presented and discussed in the order that follows:

- a) the  $T_g$  of pure A-PS is evaluated by a MDSC experiment;
- b) the outcomes of *static* isothermal tests performed at 40°C in the pressure decay apparatus are reported;
- c) the results of a typical *integral static* isothermal test performed in the gravimetric apparatus for *dynamic* tests are highlighted;
- d) *dynamic* tests needed to evaluate the hypotheses of instantaneous mass transport kinetics are provided;
- e) the results of isothermal, isobaric and isoactivity *dynamic* tests are shown.

### 3.3.1 MDSC experiments on A-PS

Two MDSC experiments have been conducted at 5°C/min and 2.5°C/min respectively. Before the run, the device heat capacity and reversing heat capacity have been calibrated by heating a sapphire standard sample in the temperature range of [0, 200] °C at the two heating rate of interest as follows:

- a) Heating ramp 2.5°C/min
  - a.1) Range of temperature tested [0; 200] °C
  - a.2) Modulation frequency 30 s;
  - a.3) Modulation Amplitude  $\pm 0.199^\circ\text{C}$ ;
  - a.4) Sample Mass 25.07 mg;
  - a.5) Method heat-only;
- b) Heating ramp 5°C/min
  - b.1) Range of temperature tested [0; 200] °C
  - b.2) Modulation frequency 30 s;
  - b.3) Modulation Amplitude  $\pm 0.398^\circ\text{C}$ ;
  - b.4) Sample Mass 25.07 mg;
  - b.5) Method heat-only;

The device cell constant and temperature sensors have also been calibrated with an Indium sample. The purge gas used is pure N<sub>2</sub>. The modulation amplitudes are given by the software and are a good compromise between the signal to noise ratio of the device and the heating rate chosen. Based on the features already mentioned, the following thermal measurements have been conducted (sample mass 6.91 mg):

- a) Range of temperature tested [25; 150] °C;
- b) Heating ramp 2.5°C/min;
- c) Cooling ramp at 2.5°C/min;
- d) points b) and c) are repeated once again;
- e) Heating ramp 5°C/min;
- f) Cooling ramp at 5°C/min;

Specimen disks fitting the Al pan and whose thickness is of the order of  $\sim 100 \mu\text{m}$  are prepared. The process used is a hot-stage with a ramp of 5°C/min up to 150°C. The specific heat capacity signals (total, reversing and non-reversing) measured during heating are given in figure 3.4up whereas the same signals during cooling are presented in figure 3.4down. The measurement is repeatable as shown during cooling by comparing the total heat capacity signals for the three consecutive scans. However, a quantitative analysis of the heat capacity is only possible for the heating scans due to the followed calibration procedure. On the contrary, the cooling experiments are analysed only in

terms of the  $T_g$  measured. During the heating scan, a lower heating rate induces a lower enthalpic relaxation peak (compare with figure 1.6) [22, 77]. Usually, the glass transition temperature is identified by studying the evolution of the reversing or the total heat capacity signal during heating. The inflection point of the heat capacity step change is identified as the transition point. During heating, the step change of the total heat capacity is affected by the glassy enthalpic relaxation history (*non-reversing* signal) whereas the *reversing* signal is well separated from the total signal and does not depend on the chosen heating rate. During heating, the *reversing* signal returns a glass transition temperature of  $\sim 106$  °C. On the other hand, during cooling, the specimen is subject to a rubbery—glassy transition: no enthalpic relaxation affects the total signal and a clear step change is observed. Heating and cooling experiments are inherently different since, at the beginning, the specimen is in a glassy non equilibrium state or in a rubbery equilibrium state respectively. The true glass transition value is usually ascribed to a specimen cooled at an infinite low rate .

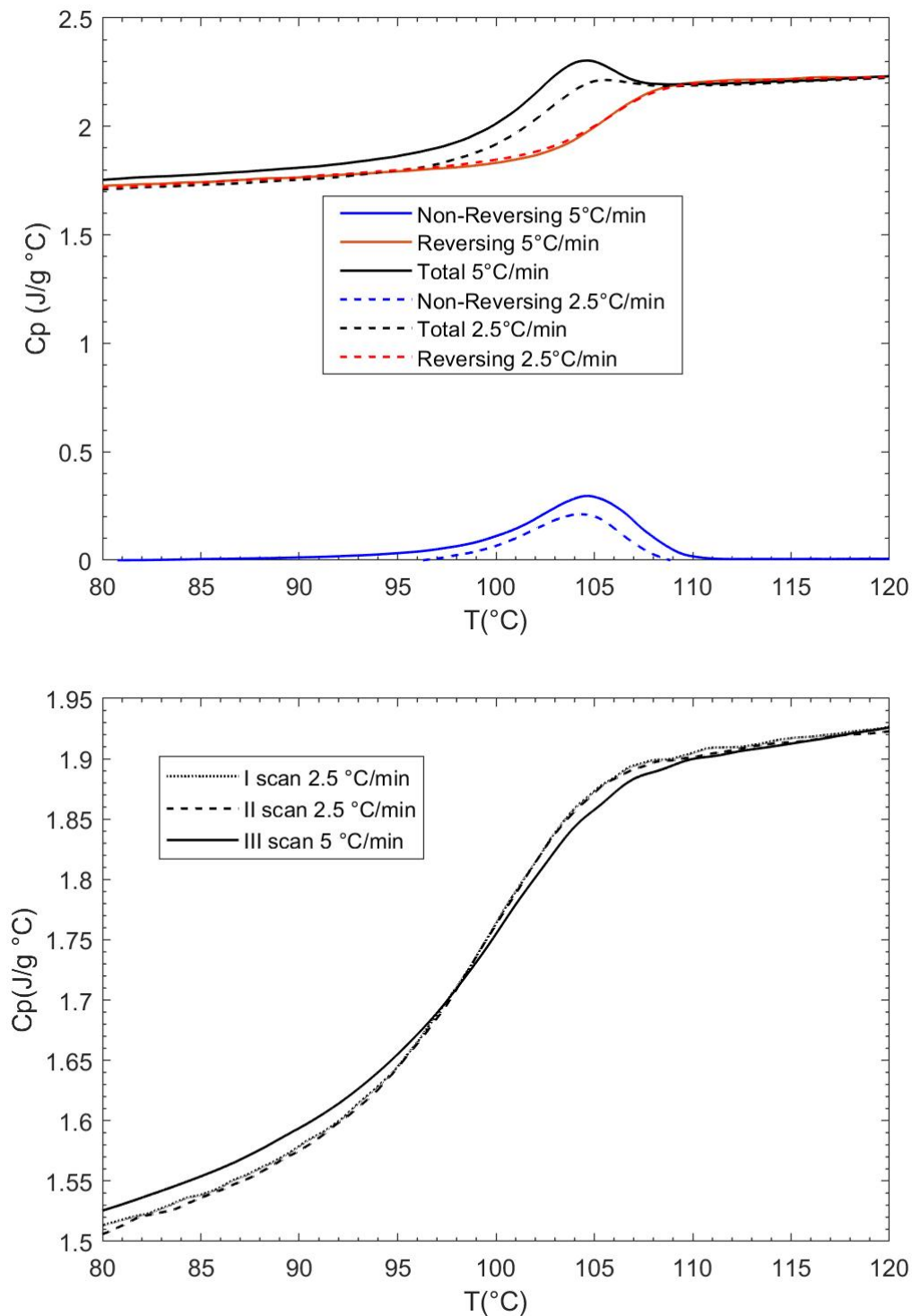


**Figure 3.4:** MDSC experiments on A-PS. Up: comparison between heating scan rates. Down: comparison between cooling scan rate

As shown in figure 1.6 down, the signal does not change by lowering the cooling rate from 5 to 2.5 °C/min: although the calibration does not enable a correct separation of the *reversing* and *non-reversing* signals, the glass transition temperature is clearly identified from the step change in the total signal and it is equal to  $\sim 100$  °C.

### 3.3.2 Static sorption tests

Stepwise sorption tests at 40°C on 90  $\mu\text{m}$  thick free standing PS-films were performed in a pressure decay apparatus. Some relevant examples are reported in figure 3.5 where three different kinds of behaviour have been detected. A pseudo-Fickian sorption kinetics (figure 3.5a) resulted from the first step of the sequence of differential experiments (in the concentration range up to 0.03 toluene mass ratio), displaying an estimated average mutual diffusion coefficient of the order of  $1\text{E-}11$   $\text{cm}^2/\text{s}$ . Conversely, high concentration (in the range 0.11 to 0.13 of toluene mass ratio) sorption steps (figure 3.5c) exhibit a typical Fickian sorption behaviour, characterized by an average mutual diffusion coefficient for toluene in PS of the order of  $1\text{E-}08$   $\text{cm}^2/\text{s}$ . In the intermediate toluene concentration range, a two-stage sorption kinetics was detected (figure 3.5b), with a characteristic time of the diffusion stage that is intermediate between those recorded at lower and higher concentrations. In this pressure range, diffusion rate for PS—Toluene mixture estimated for the initial diffusive stage, is consistent with the values retrieved by Krueger and Sadowski for the same system (and at the same temperature) near glass transition [78]. The long term stage of the sorption process, which can be typically associated with relaxation phenomena in PS, is accompanied by a significant increase in toluene mass uptake in the polymer sample. The order parameters  $n$ , evaluated from the obtained sorption kinetics in differential sorption steps, indicated the toluene pressure at which glass-to-rubber transition occurs at 40°C is approximately 28 mbar, as it is clearly marked by onset of clear Fickian type kinetics (order of kinetics  $n = 0.5$ ) for sorption steps performed at a pressure of toluene vapour above this value. The isotherm sorption curve obtained with these tests is shown in figure 3.6: the kink associated with the glass transition is highlighted.

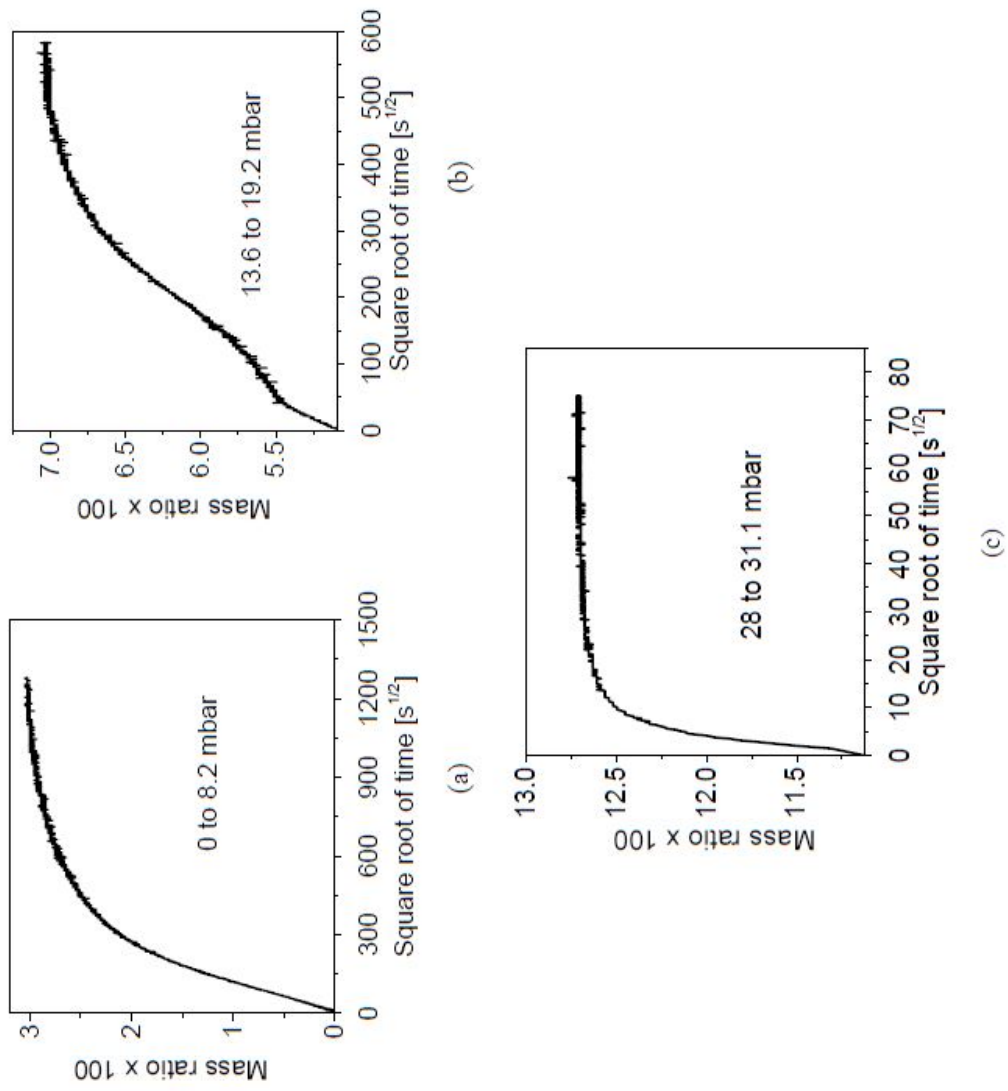


**Figure 3.5:** Pressure decay *static* sorption experiments of Toluene in A-PS at 40°C [75].

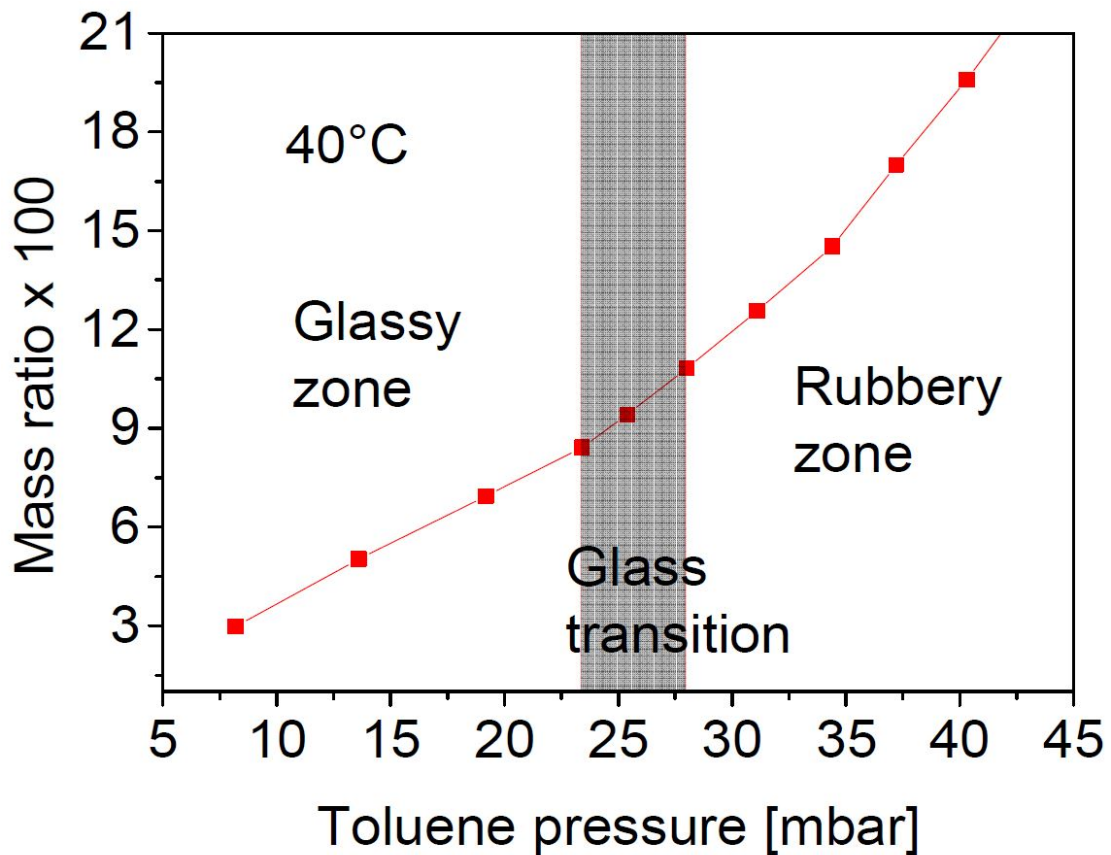


**Figure 3.6:** Pressure decay sorption isotherm of Toluene in A-PS at 40°C [75].

As discussed in section 3.2.2, static sorption tests have been also performed on aluminum disks coated with thin PS films, prior to each dynamic sorption/desorption experiment, to bring the PS—Toluene mixture to a rubbery state, thus erasing any memory effect related to previous treatments. Figures 3.7a and 3.7b report the results at 40°C—40 mbar and 20°C—33 mbar of pressure of toluene vapour, respectively. Thin PS coating films (750 nm thick) have been tested. In view of the small value of volume-to-surface ratio of the sample, the characteristic time of the diffusion process is very small, and it can be roughly estimated to be shorter than 1 min. On the other hand, an equilibrium value for the toluene content in PS in the experiment is not reached earlier than one hour after the beginning of the sorption experiment. Opposite to differential sorption steps confined into the glassy region, the relaxation processes involved in integral sorption at time longer than the characteristic time for diffusion lead to a decrease of toluene content in the sample. The overall sorption kinetics indeed show a clear example of overshoot, for which a non-monotonous mass uptake over time is observed in a sorption process at constant boundary conditions. Due to its relevance to the interpretation of non-Fickian kinetics, the occurrence of overshoot phenomena in sorption

kinetics has been discussed in the literature, with reference to its thermodynamic consistency and to its possible origin. Although this is not the first example of overshoot reported for vapour sorption in thermoplastic material (see, for example, the case of anomalous sorption in PMMA reported by Vrentas *et al.*), it deserves to be noticed in view of clear evidence of the phenomenon given in this case [79]. A deeper investigation of this specific aspect, however, is neglected here; certainly, this topic will be of interest to the future research work.

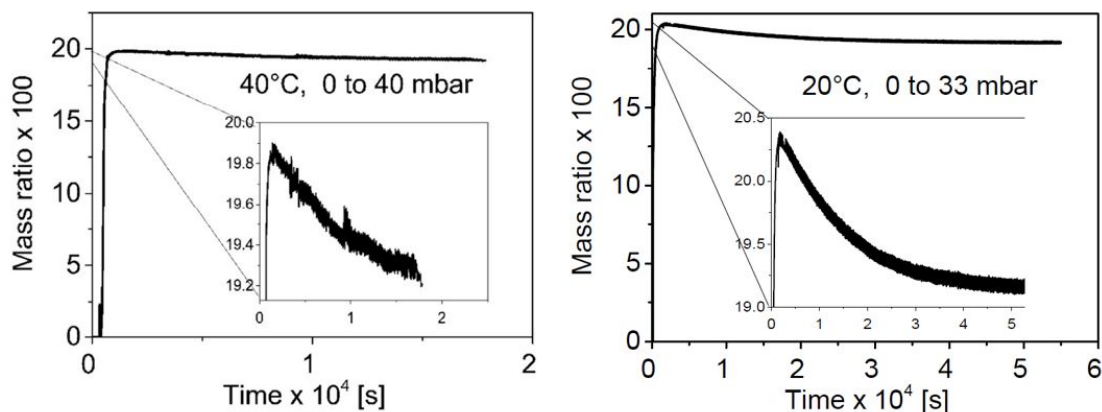


**Figure 3.7:** Gravimetric *static* integral sorption tests of Toluene in A-PS at 40°C and 20°C [75].

*Static* experiments have provided the order of magnitude of the mutual diffusion coefficient for the system at hand. Based on these data, the film thickness of the samples used in *dynamic* experiments is chosen. When an intermediate value of  $D$  ( $1\text{E-}10\text{ cm}^2/\text{s}$ ) is considered, a characteristic time for diffusion process lower than 1 min can be estimated for the case of film thickness lower than  $1\text{ }\mu\text{m}$ . Based on that, the glassy-to-rubbery transition zone at 40°C can be crossed in a dynamic sorption test at a rate as high as 0.16 mbar/min (i.e. the maximum value adopted in this work) keeping as low as few percent the relative variation of apparent equilibrium solubility within the characteristic time for diffusion. Diffusion of low MW compounds in organic thermoplastic polymers is simultaneously affected by the chemistry of the polymeric material, the out of equilibrium relaxation phenomena encountered because of its glassy state and the rate of change of boundary conditions. Thus, in order to study the relaxation behaviour of the polymer-penetrant mixture due to the change of thermodynamic boundary conditions of the vapour external phase, thin PS coating films have been prepared for dynamic sorption tests based on the previous line of reasoning. The thickness is chosen to accelerate toluene transport to such an extent that the diffusion process is infinitely fast with respect to the boundary condition rate of change; indeed the diffusion process must be only ruled by the relaxation phenomena associated with the polymer matrix. According to the above consideration, the difference between minimum and maximum solute concentration in the polymer sample due to diffusion kinetics is limited to at the most

1% of the average value, even within the glassy region, for the rate of pressure variation mentioned above. In order to verify the reliability of these estimates for the cases of both rubbery and glassy states of the polymeric mixture, preliminary tests have been performed to ensure the diffusion resistance in a dynamic sorption test is actually negligible for the rate of pressure change of interest to this work. A first test was run on PS coating film 750 nm thick, performing isothermal dynamic sorption experiments at 40°C in which toluene pressure is changed in a cyclic fashion, confined into the rubbery region at very high pressure of toluene vapour. Under those conditions, it is reasonable to assume that the relaxation time is low enough to allow for the phenomenon to be ignored, and differences observed for the mass ratio measured at the same toluene pressure between sorption/desorption branches are only attributed to diffusion resistance in the solid. Results from this kind of experiments are reported in figure 3.8 for the case of two different values of the rate of change for toluene pressure. As one can see, the uncertainty in solute content due to diffusion resistance is lower than 1%, even for the case of the highest rate used (0.16 mbar/min).

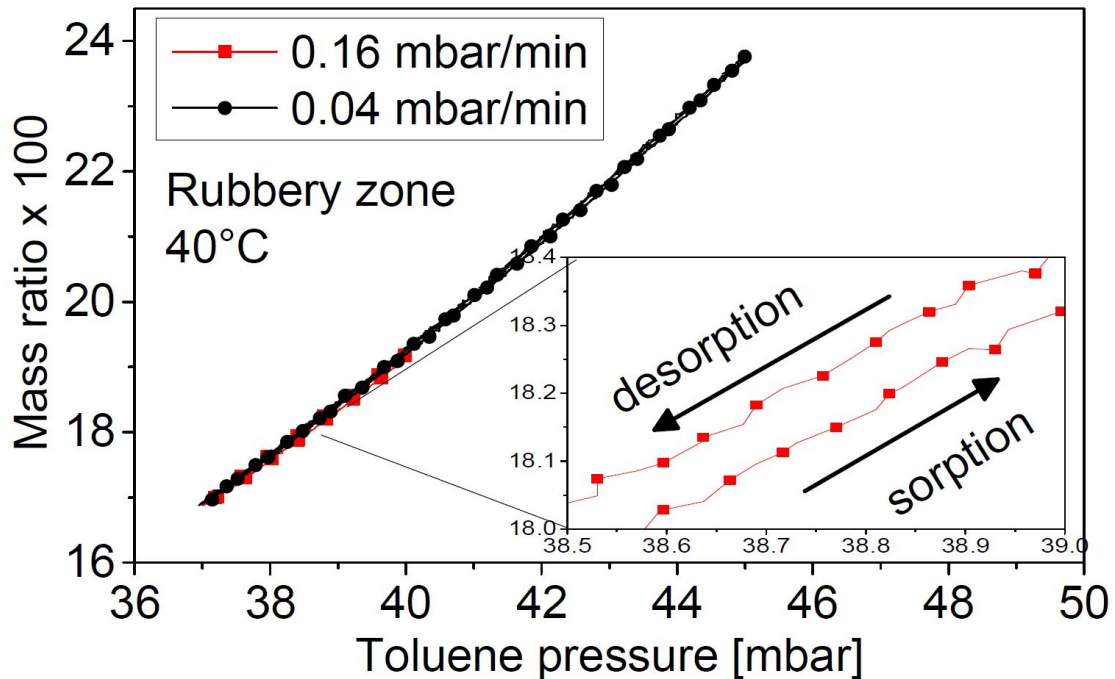


**Figure 3.8:** Gravimetric dynamic desorption/sorption experiment of Toluene in A-PS at 40°C in the rubbery zone [75].

The same kind of test cannot be considered to verify that diffusive resistance is negligible in the glassy polymer mixture, as the significant effect of the slow relaxation phenomena would invariably affect the result of a cyclic process, performed below the glass transition. A different test has been thus designed, simply comparing the result for

toluene mass ratio as a function of toluene pressure in the gaseous phase for dynamic desorption test run at the same pressure change rate in PS samples of different thickness. Experimental data have been obtained at 40°C with the same isothermal dynamic desorption test performed on 750 nm and 430 nm thick PS coating films, bringing both samples from rubbery conditions down below the glass transition zone, as identified from static sorption experiments. No significant difference has been observed between the data retrieved for both samples (figure 3.9), thus confirming that the diffusion resistance does not affect appreciably the dynamic desorption tests considered in this work even when the polymer mixture is in the glassy state. Indeed, the *dynamic* experiments which are presented in the following sections have been only conducted on the sample of 750 nm thickness.

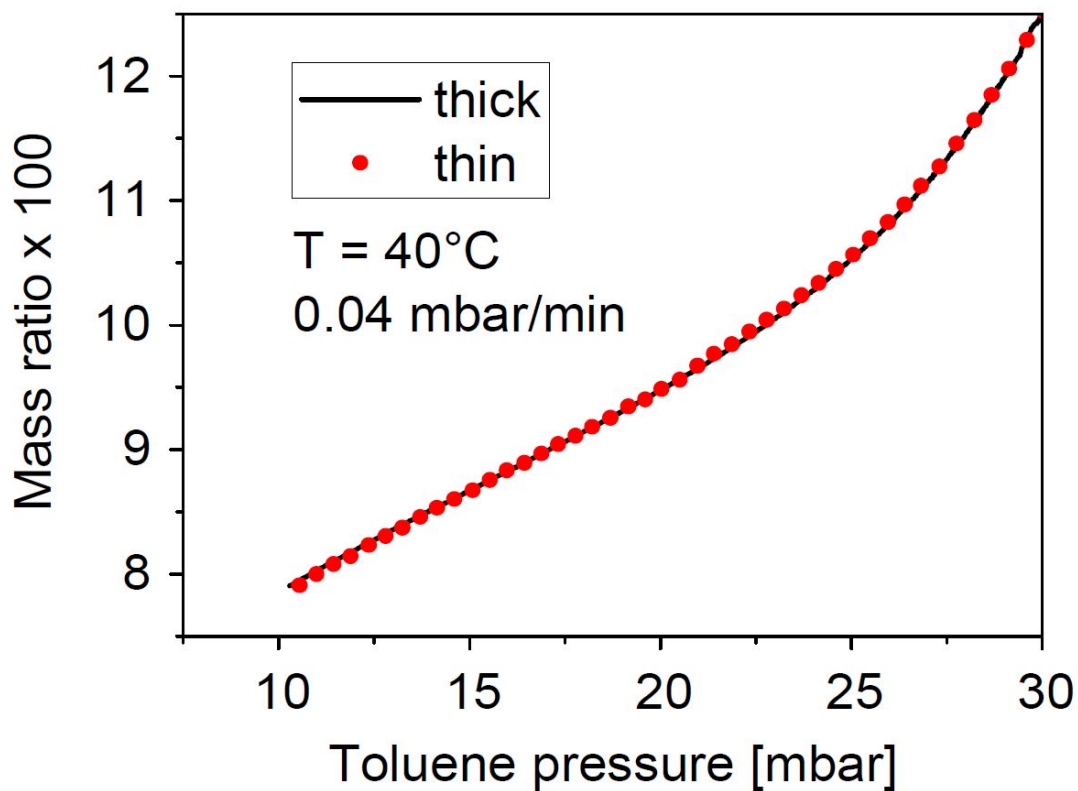


**Figure 3.9:** Gravimetric dynamic desorption experiments: comparison between specimens of different thickness [75].

### 3.3.3 Dynamic Experiments

Different kinds of toluene sorption/desorption tests in thin PS coating films were performed in this work according to the *dynamic* protocol already described. Results for a 40°C isothermal sorption-desorption cycle, spanning both above and below the glass transition zone (identified in figure 3.6), are reported in figure 3.10. Following a preliminary integral sorption experiment at a toluene pressure of 40 mbar, solute desorption was allowed by decreasing linearly the pressure of toluene vapour at a constant controlled rate of 0.16 mbar/min down to 10 mbar. After completing the pressure decrease stage, pressure of toluene vapour is increased up to 40 mbar again, at the same rate of 0.16 mbar/min. A hysteretic behaviour is monitored (figure 3.7), more evidently at low pressures.

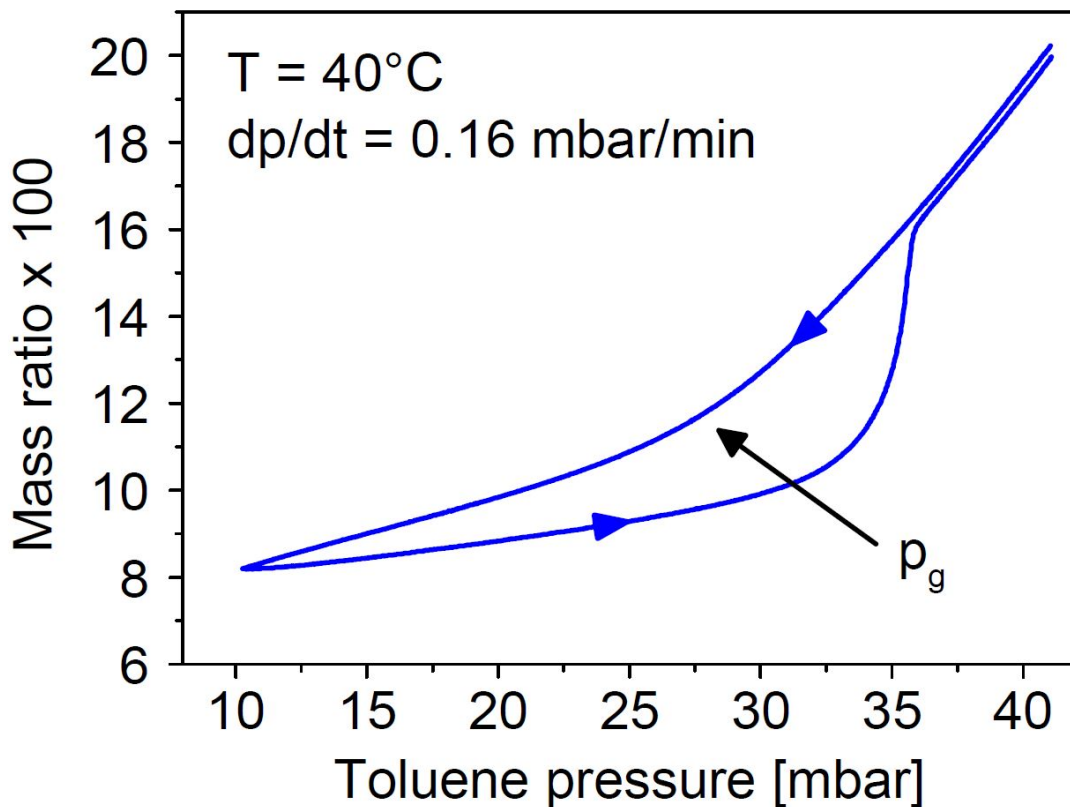


**Figure 3.10:** Gravimetric dynamic desorption/sorption cyclic experiment of Toluene in A-PS in the rubbery/glassy zones [75].

At high pressures, desorption/sorption branches do not overlap. Several relevant features of solute mass ratio,  $\Omega$ , obtained from the desorption/sorption cycle in figure 3.10 deserve to be highlighted, as they are evidenced in all similar tests performed at different

temperatures or rates of change for pressure:

- a) a step discontinuity of the isothermal solubility coefficient (i.e. the slope of toluene mass ratio as a function of pressure) is observed during the desorption stage. This coefficient is higher at toluene pressure values above the kink. The latter is thought to be the transition point from the rubbery to the glassy phases and the set of three thermodynamic variables  $\{T, P, \Omega\}$  is referred to as  $\{T_g, P_g, \Omega_g\}$ ;
- b) in the low pressure range of the cycle, the solubility coefficient is higher along the desorption branch (decreasing pressure) as compared to the sorption branch (increasing pressure);
- c) the sorption branch recovers the mass ratio values of the desorption branch at pressure values significantly higher than the kink where the transition should occur;
- d) a small, although not negligible, difference is measured at values of pressure close to the starting point between the desorption/sorption curves.

It is worth noting that a similar behaviour was also observed by Doumenc *et al.* for toluene in PMMA [69]. While all features in the above list could be the subject of specific analysis relevant to the study of relaxation behaviour in polymer-solute system, in the present context the attention is only focused on the features displayed by the desorption branch. In what follows, the observed transition from rubber-like to glassy-like state in *dynamic* desorption tests is analyzed in detail, evaluating the variation of  $P_g$  with temperature and pressure rate. First, a sensitivity study of the rate of pressure decrease has been conducted at 40°C, from 40 mbar down to 10 mbar. The whole set of results is presented in a log-log plot in figure 3.11 along with the *static* sorption tests carried out with the pressure decay apparatus. It is evident that the results obtained from *dynamic* tests are quite different from those of *static* tests. In fact, at pressure values above the transition region, the results from *static* sorption and *dynamic* desorption tests are almost equal. Indeed, an equilibrium rubbery state for the PS—Toluene mixture in contact with the toluene vapour phase is expected to be attained in both cases. Actually, a small difference in the solubility coefficient (which is higher in the case of calculated *static* sorption tests) is appreciated in the rubbery region: the approximation of infinitely fast desorption kinetics is maintained although it is expected to be truly valid only at very high pressures. Moreover, the amount of absorbed toluene is higher in the case of *dynamic* desorption tests and, most likely, these features can be attributed to residual relaxation processes in the rubbery state that occurs during the faster desorption tests. The mechanical constraint experienced by supported film used in desorption runs, as opposed to the case of free standing films used in *static* sorption tests, could have also played a role in the difference between the solubilities. It should be finally kept in mind that two different types of measurements of mass uptake (manometric and gravimetric respectively) have been employed and, consequently, different small systematic errors characterize the two distinct measurement techniques.

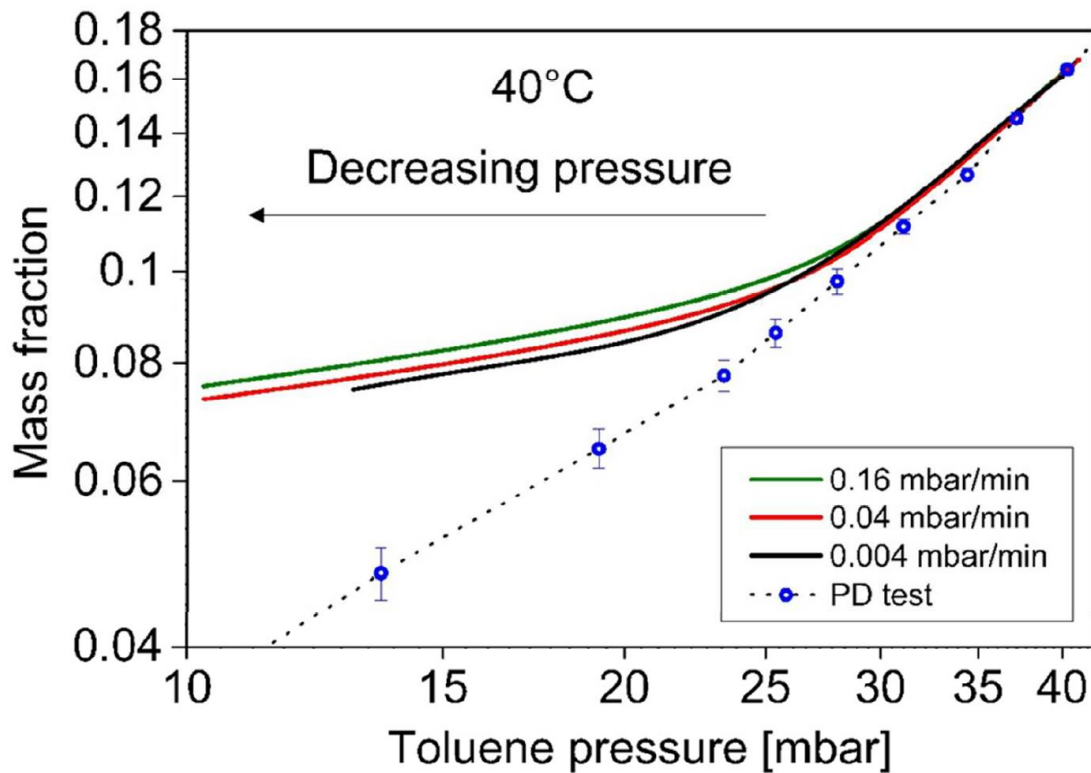


**Figure 3.11:** Gravimetric dynamic desorption isothermal experiments: effect of depressurization rate on desorption of Toluene from A-PS [75].

Conversely, at pressure values lower than  $P_g$ , data collected for *dynamic* desorption tests markedly depart from *static* sorption experiments results. In view of the non-equilibrium nature of the glassy state and of its history dependent behaviour, this feature is attributed to the different history of the sample in a *dynamic* desorption test with respect to *static* sorption conditions. The effect of both the sample history and the non-equilibrium nature of polymer-penetrant mixture is also recognized from the apparent solubilities measured in the glassy region for desorption runs conducted at different depressurisation rates. By ruling out the effect of diffusive resistance on apparent solubility measured in *dynamic* desorption test, the results in figure 3.11 are now only discussed in terms of both the variation of vapour boundary conditions and the characteristic time for relaxation phenomena in the polymer phase. Indeed, the characteristic time describing the change of boundary conditions is kept constant in each *dynamic* desorption test and it is inversely proportional to the depressurisation rate. On the other hand, the characteristic time of polymer relaxation can be assumed to be roughly independent from the rate of pressure decrease, but it dramatically increases as the toluene concentration decreases in the system. At relatively high pressure of toluene vapour the relaxation time is much smaller than the characteristic time of variation of boundary

conditions and the apparent solubility measured at an assigned toluene pressure in a *dynamic* desorption test is ultimately very close to the thermodynamic equilibrium value, independently of the rate of decrease of pressure. On the other hand, the apparent solubility departs from the equilibrium value when the relaxation time increases above the characteristic time of variation in boundary conditions, which occurs across the transition zone. More specifically, departure from equilibrium conditions occurs at lower toluene concentration for the case of slower depressurisation rate experiments because lower toluene concentrations need to be reached for the characteristic relaxation time to match the corresponding time for variation of boundary conditions in these cases. Consequently, the location of the rubber-to-glass transition occurs at lower values of  $P_g$  the lower is the rate of pressure decrease. This behaviour has remarkable analogies with the case of a pure polymer submitted to a temperature decrease at constant pressure where, as pointed out in Chapter I, the higher the cooling rate, the higher the experimentally observed glass transition temperature. In such a case, the glass transition temperature,  $T_g$ , is marked by a clear step discontinuity of the slope of the specific volume vs. temperature. If one considers the glass transition as a II order thermodynamic transition, the  $T_g$  value should be independent from the rate of temperature decrease. However, the experimental evidence of the underlying thermodynamic transition is affected by kinetic factors: i.e. the experimentally accessible glass transition occurs at temperatures located above the purely thermodynamic glass transition. At the  $T_g$ , the reduction of the macromolecular mobility prevents the polymer structure from attaining an equilibrium rubbery state. In summary, the apparent solubility isotherm retrieved from a single isothermal dynamic desorption test displays a step discontinuity of the apparent solubility coefficient by comparing equilibrium and non-equilibrium branches. Linear dependences of solute content from the pressure of vapour solute can be distinctly recognized above and below the transition region, with clearly higher sensitivity for the upper branch with respect to the lower one. Different values of glass transition pressure,  $P_g$ , retrieved at different values of the rate of pressure decrease, are reported in table 3.1 along with the values of  $\Omega_g$  at which the transition occurs at 40°C.

P-Rate (mbar/min)	$P_g$ (mbar)	$\Omega_g$
0.16	28.7	0.113
0.04	28.3	0.101
0.01	27.7	0.099
0.004	26.5	0.099

**Table 3.1:** Gravimetric dynamic isotherml at 40°C:  $P_g - \Omega_g$  couples as a function of P rate [75].

The procedure adopted to locate the discontinuity in a plot of mass fraction of toluene as a function of pressure is reported here. The attention is focused here on the specific case of the isothermal experiments, the procedure being the same for the isoactivity

tests. The procedure is based on the determination of the pressure at which the second derivative of the plot of toluene mass fraction vs pressure shows a maximum. In detail, the function representing the second derivative of a smoothed function built by fitting sorption data was calculated. The value of the transition pressure,  $P_g$ , was assumed as being the abscissa of the maximum in the second derivative. In figure 3.12 (left) is reported, as an example, the case of an isothermal test conducted at 30°C and at pressure decrease rate of 0.16 mbar/min. In some cases, the behaviour of the mass fraction vs pressure plot is linear both above and below the transition. In such cases, a simpler procedure is possible that provides the same results as the one described above. In fact, the intersection of the two linear fittings enables the extrapolation of the glass transition pressure (in figure 3.13 (right) is illustrated the case of an isothermal experiment performed at 70°C at a pressure decrease rate of 0.16 mbar/min). The transition pressure value corresponds to the abscissa of the intersection point. Characteristic times for relaxation not only depend on the solute concentration but also on the temperature so that the departure from equilibrium of the apparent solubility during dynamic desorption experiments are expected to change considerably when tests are run at different temperatures. The driving force is of course the chemical potential of toluene in the two phases. The best way to define it experimentally in the vapour phase is by calculating its activity as the ratio of the vapour pressure over the saturation pressure at the temperature investigated. Then, when comparing dynamic desorption results at different temperatures, it is useful to refer to plots for apparent solubility as function of solute activity, as illustrated in figure 3.13. Data have been recorded in the temperature range 20 to 92°C, at a fixed depressurization rate of 0.16 mbar/min. At high toluene activity, very similar solute contents are observed at different temperatures whereas different apparent solubilities are evidenced in desorption runs in the low activity region.

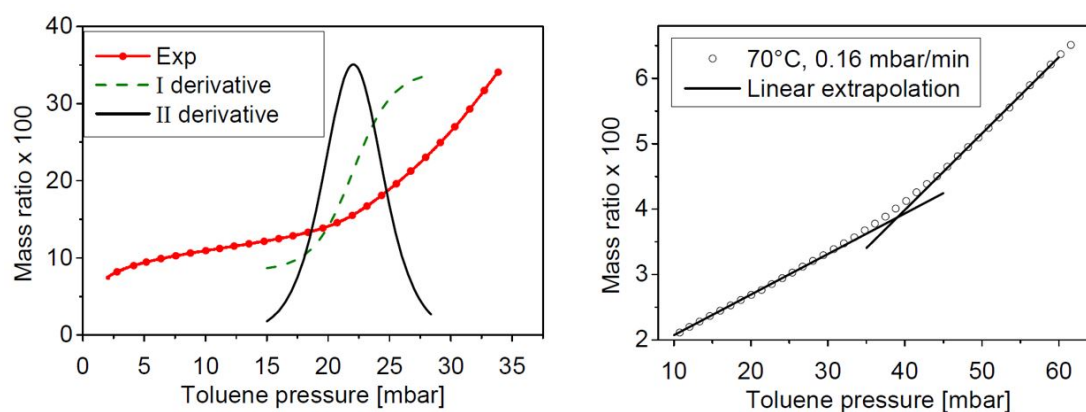


**Figure 3.12:** Evaluation of the glass transition pressure from a gravimetric dynamic isothermal desorption test [75].

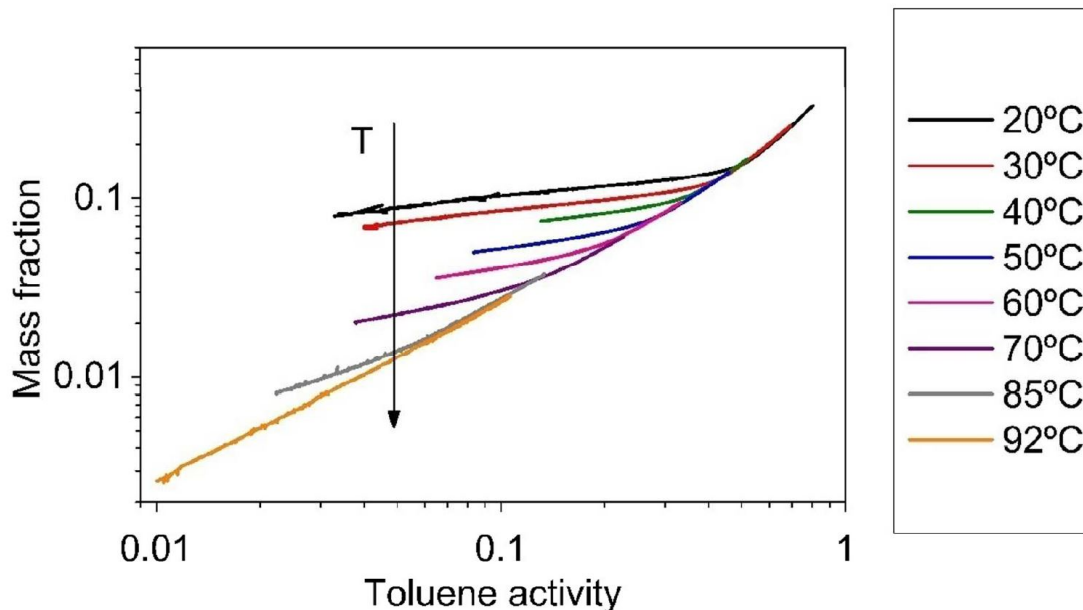


**Figure 3.13:** Gravimetric dynamic isothermal desorption experiments: effect of temperature on desorption of Toluene from A-PS [75].

More specifically, the positive departure of apparent solubility from common equilibrium solubility trends is limited to lower activity ranges for the case of higher temperature experiments. This feature is easily explained by considering the time associated with changing the boundary conditions is the same for all the experiments whereas the characteristic time for relaxation as a function of toluene content significantly depends on the temperature. Moreover, the latter is reached at lower solute contents for the case of higher temperatures, i.e. both the temperature and the penetrant have the power to increase the polymer chain mobility. These data were analyzed to determine the value of  $P_g$  at each temperature, by adopting the same mathematical procedure used in the case of isothermal tests performed at 40°C. The values of  $P_g$  determined for each isothermal dynamic desorption test, all at a depressurization rate of 0.16 mbar/min, are reported in table 3.2 along with the corresponding toluene mass fraction,  $\Omega_g$ . Data in table 3.2 show that the  $P_g$  in PS—Toluene system changes with temperature in a non-monotonous way, contrary to the solute concentration dependence, and particularly a maximum is observed around 60°C. This behaviour is the result of the combined effects of temperature and pressure on sorption and on the subsequent associated plasticization phenomenon. Based on the above evidence, it can be anticipated that at toluene pressures below the above mentioned maximum value, a finite temperature range exists in which the system is in a glassy state, while rubbery conditions are recognized both below a lower limit temperature or above an upper one. This also means that, by exposing a PS sample to a fixed toluene pressure, a rubbery to glassy transition could occur either

by lowering the temperature below the upper limit or raising it above the lower limit of the corresponding temperature range within which the glassy state is observed. The latter phenomenon is called *retrograde vitrification* in the literature and it results from the reduction in solute concentration/plasticization effect occurring when the temperature is increased at constant solute pressure [80, 81, 82]. Opposite to what happens in the high temperature/low concentration range, solute induced plasticization prevails on the opposite temperature effect in the low temperature/high concentration range. A confirmation of this behaviour has been looked for in this work by performing isobaric dynamic sorption/desorption experiments.

$T_g$ (K)	$P_g$ (mbar)	$\Omega_g$
293.15	15.0±2.0	0.159
303.15	22.0±2.0	0.135
313.15	30.1±2.0	0.113
323.15	35.7±2.0	0.081
333.15	40.2±2.0	0.060
343.15	39.1±2.0	0.039
358.15	30.55±2.0	0.018

**Table 3.2:** PS—Toluene glass transition triples  $T_g - P_g - \Omega_g$  [75].

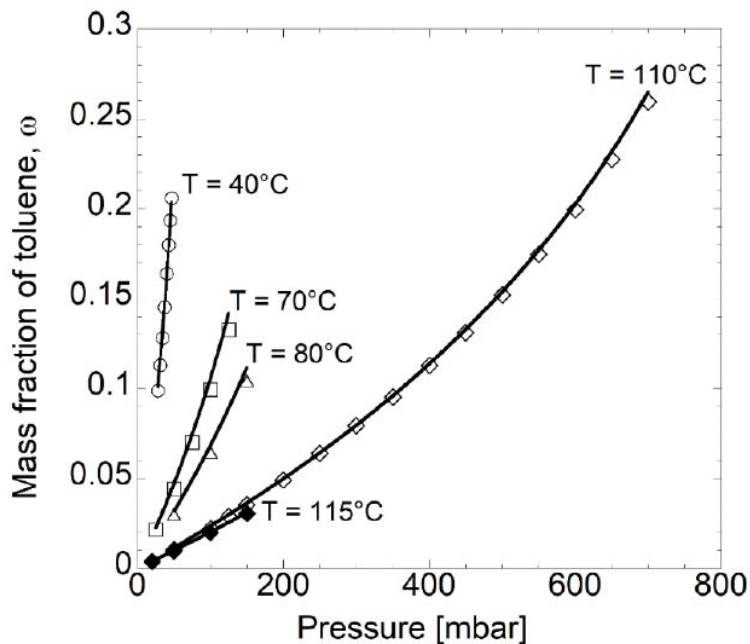


**Figure 3.14:** NETGP-NRHB fitting of PS—Toluene sorption isotherms [76, 78, 75]

$\zeta_{12}$	$E_{12}^{hb}$ (J/mol)	$S_{12}^{hb}$ (J/mol K)	Reference
$1.0015 \pm 0.0002$	0	0	This Work

**Table 3.3:** NRHB parameters for the PS—Toluene mixture based on the NETGP framework

One dynamic isobaric test was performed by maintaining a constant pressure of 36 mbar: first, the temperature is linearly increased from 30°C to 92°C at a constant rate of temperature change of 2°C/hour.; then, it is linearly decreased back to 30°C at the same rate. The apparent solubility data obtained are reported in figure 3.15. With regard to the experimental data at lower and higher temperatures in the range explored, sorption and desorption runs show similar solubility coefficients, which is consistent with the interpretation that the measured solute contents in those regions represent different parts of the same equilibrium solubility isobaric curve. At intermediate temperatures, on the other hand, higher solute contents are shown for the case of desorption (heating) runs with respect to that of sorption (cooling), thus confirming the existence of a non-equilibrium region at the assigned toluene pressure. The observed behaviour is interpreted as follows: at the starting conditions (low temperature), the PS—Toluene mixture is in a rubbery state; then, as the temperature is increased a rubber-to-glass transition occurs, promoted by the decrease in solubility related to the heating of the system. Further increase of T promotes a glass-to-rubber transition again. When the temperature is decreased again, the mixture displays a rubber-to-glass transition and further cooling promotes a glass-to-rubber transition too. Different from the case of isothermal paths, the non-equilibrium glassy region along isobaric lines is confined and its limited extension does not allow for a characteristic value of glassy solubility coefficient to be retrieved. Under these circumstances, the procedure used to identify glass transition point after experimental data from isothermal experiments cannot be directly extended to the case of isobaric test. To circumvent this difficulty, a different approach has been adopted in this case to estimate the two rubber-to-glass transition points (one along the heating path, the other along the cooling path), as detailed in what follows. The thermodynamic approach based on a non-random compressible lattice fluid theory (Non Random Hydrogen Bonding, NRHB) has been used to model the phase equilibrium between the polymer-penetrant mixture in the rubbery state and the toluene vapour phase. It is important to note here that, since the system at hand is not endowed with specific self- and cross- hydrogen bonding (HB) interactions, the terms of NRHB model associated with formation of HBs have been consistently set equal to zero. In order to predict the mixture behaviour during the isobaric experiment it is first necessary to determine the *binary interaction parameter*  $\zeta_{12}$  from the equilibrium sorption isotherms taken from the literature. Interestingly, its value is independent of temperature as shown in the fitting from figure 3.14.

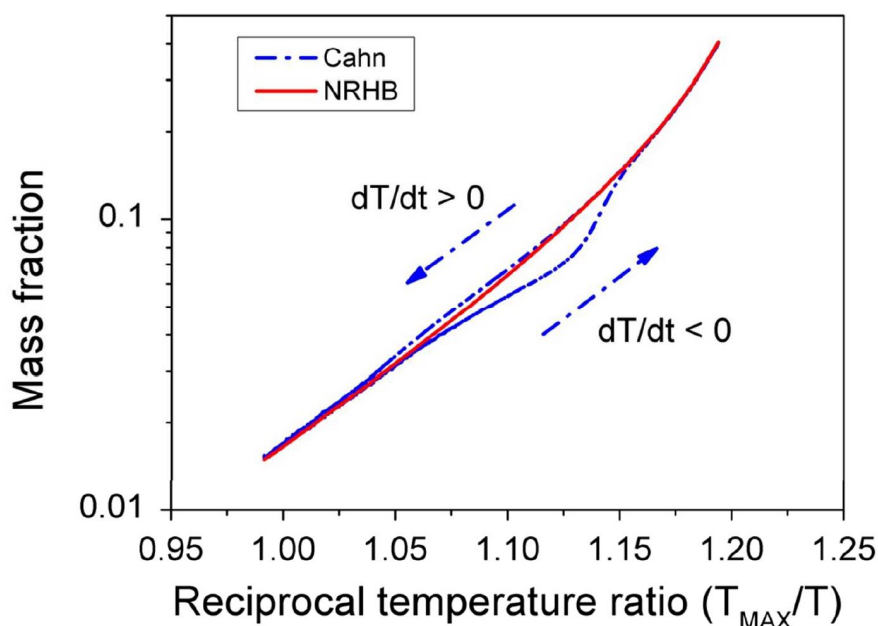


**Figure 3.15:** Gravimetric dynamic desorption/sorption isobaric cyclic experiment on the PS—Toluene system [75].

An excellent prediction of the sorption (desorption) data in the lowest and highest temperature regions, where the polymer mixture is expected to be in a rubbery state (see continuous red line in figure 3.15), is obtained. Small but significant deviations are instead observed for experimental data from model prediction in the intermediate temperature region, where the system is expected to be in the glassy state. Indeed, the NRHB model has been developed for equilibrium rubbery systems and it is not expected to properly describe the thermodynamics of a system in a glassy state. The rubber-to-glass transition has been then assumed to occur at that point in isobaric curve for solute content where the difference between experimental data and equilibrium results obtained by using the NRHB model becomes significant. The exact point transition point is located where the departure becomes higher than 1% of the value of the experimental mass ratio. Obviously, this procedure is affected by a higher error when compared to the case of the procedure adopted for isothermal tests. In table 3.4, values of  $T_g$  and  $\Omega_g$  are reported as evaluated from the isobaric test ( $P = 36$  mbar). As anticipated, two different rubber-to-glass transition points have been identified, along cooling and heating paths of the experiment, corresponding to higher and lower temperature limits for the glassy region at the assigned toluene pressure. Interestingly, the recovery of rubbery condition from the glassy state (glass-to-rubber transitions) for both cooling and heating runs in isobaric experiments (figure 3.15) occurs at temperatures well beyond the transition points indicated in table 3.4, parallel to what shown for the same kind of recovery by isothermal experiments in sorption runs with respect to transition point retrieved after

data from desorption runs

	$T_g$ (K)	$\Omega_g$
Heating Path	$319 \pm 8$	0.105
Cooling Path	$343 \pm 8$	0.036

**Table 3.4:** Isobaric experiment at 36 mbar:  $T_g - \Omega_g$  couples as a function of the heating history [75].

A third kind of dynamic experiment has been performed in this work for the PS—Toluene system, during which the temperature is decreased linearly at a prescribed rate, while toluene activity,  $a_T$ , is kept at an approximately constant value. This is accomplished by properly changing the toluene pressure in the vapour phase. Toluene activity is again defined as the following ratio:

$$a_T = \frac{P}{P_s(T)}$$

Particularly, after the system is brought into a rubbery state, the system temperature is always decreased at a rate of  $2^\circ\text{C}/\text{hour}$ . Figure 3.16 shows that the condition of constant activity is met as planned. Results for three different isoactivity tests corresponding to the case  $a_T = \{0.11; 0.20; 0.30\}$  have been collected in this work.

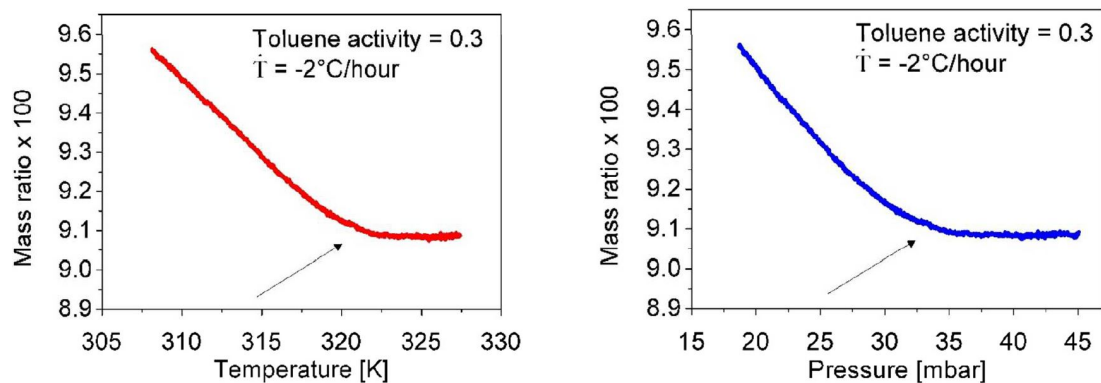


**Figure 3.16:** Gravimetric dynamic isoactivity sorption experiments of Toluene in A-PS [75].

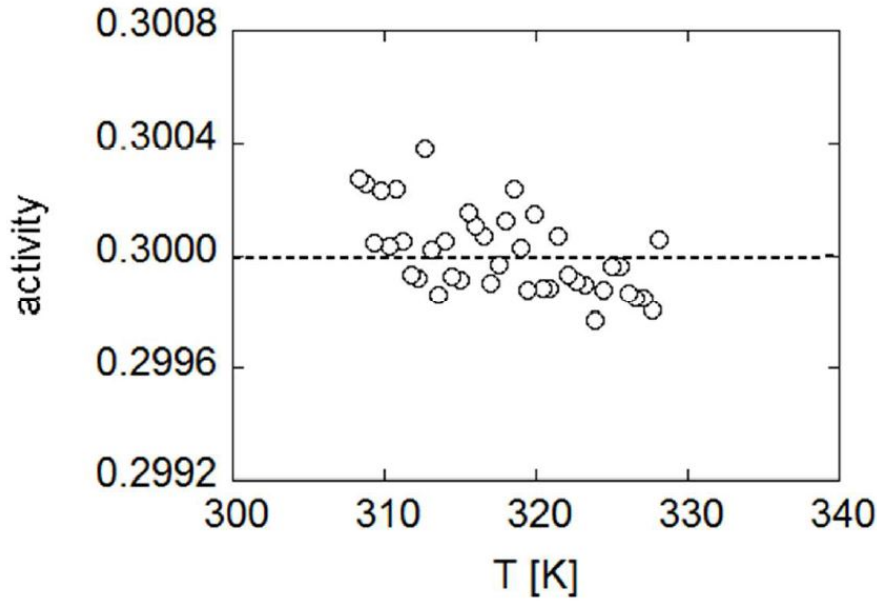


**Figure 3.17:** Activity values measured during the 0.3 gravimetric dynamic isoactivity experiment (Peng Robinson EOS) [75].

$a_T$	$T_g(\text{K})$	$P_g(\text{mbar})$	$\Omega_g$
0.11	$349.0 \pm 4$	$37.1 \pm 2$	0.029
0.20	$337.9 \pm 4$	$40.1 \pm 2$	0.054
0.30	$319.0 \pm 4$	$33.1 \pm 2$	0.083

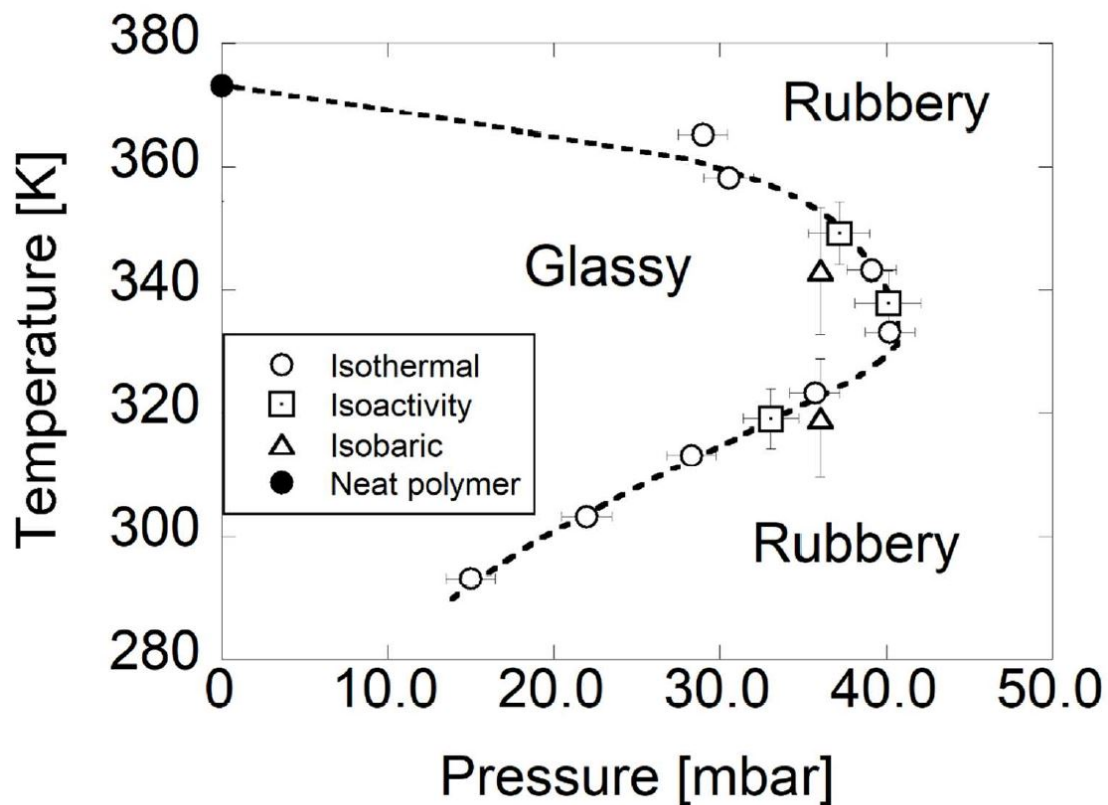
**Table 3.5:** Isoactivity experiments:  $T_g - P_g - \Omega_g$  triples [75].

Figure 3.16 reports the results obtained in the case of toluene activity equal to 0.30. Similarly to the case of isothermal tests, during isoactivity experiments there is evidence of a clear change for the sensitivity of apparent solubility to the potential variable modulated in the test, as the latter is moved from higher to lower values. Indeed, the solubility coefficient in this case,  $d\Omega/dT$ , increases as temperature decreases in a relatively narrow temperature interval (see arrows in figure 3.15) from a negligible value registered at high temperature to a maximum value that appears to be substantially constant in the lower temperature range. The results are consistent with the assumption of a unique rubber-to-glass transition in the temperature range explored within the isoactivity experiment performed. In view of the features exhibited, the tests results are elaborated similarly to the case of isothermal experiments to identify the set of three thermodynamic variables  $\{T, P, \Omega\}$  which identifies the glass transition. Results from the mentioned analysis after data retrieved in isoactivity experiments are reported in

table 3.5, in terms of temperature, pressure, and toluene mass fraction at which rubber-to-glass transition occurs. Figure 3.17 gives an example which confirms the activity is maintained constant during the experiment.

### 3.4 Theoretical interpretation

The entire set of data of rubber-to-glass transition points for manipulated process variables (T and P), as derived from the analysis of isothermal, isobaric and isoactivity tests, is shown in the state diagram pictured in figure 3.18. Figure 3.19 summarizes a scheme of the PS—Toluene transition envelop investigated. It is important to stress here that points represented in the plot have been identified based only on desorption (isothermal tests and isobaric heating test) and sorption (isobaric cooling test and isoactivity tests) processes whose continuous variation of specific process variables is imposed in order to induce a state change from equilibrium (rubbery) to non-equilibrium (glassy) conditions.



**Figure 3.18:** Total set of glass transition points retrieved from the gravimetric dynamic experiments [75].

The evident changes in the solubility coefficient (i.e. the sensitivity of the solute mass ratio against the process variable) for each experiment define the transition point. Mentioned discontinuities of the solubility are indeed consistent with the interpretation of a thermodynamic second order phase transition, according to the definition given by Ehrenfest [31]. In Chapter I, a detailed thermodynamic theory for the II order phase transition behaviour in liquid binary mixtures is provided. The line of reasoning follows the theory of De Bruyn Ouboter and Beenakker: the case of a polymer-penetrant mixture in contact with the penetrant vapour phase is analysed. The hypotheses of zero polymer composition within the vapour phase and of equal T and P within both phases are assumed. It is worth discussing in some details here, why we have ruled out the possibility that the observed transition is to be ascribed to a first order transition of the polymer-toluene phase. As a matter of fact, it is reasonable that, in the case of a first order transition, a discontinuity should occur in the toluene concentration within the two condensate phases. This should result in the experimental evidence of an abrupt change in the value of toluene mass ratio at the transition itself that, instead, has never been observed at the detected transition points. Moreover, if the observed transition were of the first order type, we would expect a reduction of the value of pressure at the transition as the pressure decrease rate is increased in an isothermal experiment, contrary to what is observed in the case of our experiments. In fact, in the case of a first order transition we can attain metastable phases (like supercooled vapour or superheated liquid) while in the case of a true second order thermodynamic transition this would not be allowed. Finally, it is worth noting that the trend of transition points obtained for polymer-toluene mixture is consistent with the location of glass transition of pure polystyrene. In the case of the system under investigation, the liquid mixture displaying the II order transition corresponds to the polymer mixture phase in equilibrium with the external vapour phase. It has been shown in the previous sections that the exact location of the transition point slightly depends on the rate at which the process variable is changed in the test, so it is better to refer to a transition rather than a boundary region. It is explicitly noted here that the transitions observed experimentally need to be interpreted as the experimentally accessible, kinetically affected, manifestations of the underlying II order thermodynamic transitions. Data for low-pressure glass transition temperature of dry polystyrene (neat polymer), corresponding to the case of null value of toluene pressure, has been added too in figure 3.18. Its value is obtained from the total specific heat capacity signal related to the MDSC experiment. It is noted that results from isobaric and isoactivity experiments are qualitatively consistent with those retrieved from isothermal experiments, although a non-negligible quantitative discrepancy is evident, that is likely due to the different procedure used to retrieve the transition points. Most notably, figure 3.18 confirms that the PS—Toluene system is characterized by the so-called *type IV* behaviour, otherwise called *retrograde vitrification* at pressures and temperatures lower than 40 mbar and 60°C, respectively. The diagram defines in detail the transition region

into the glassy state and the interval of toluene pressure for retrograde vitrification extends below 15 mbar. Furthermore, the state diagram illustrates number and nature of transitions the system experiences in different kind of experiments. Typical paths for isothermal, isobaric and isoactivity dynamic experiments performed are schematized in figure 3.19 for the specific case of a system displaying *type IV* behaviour.

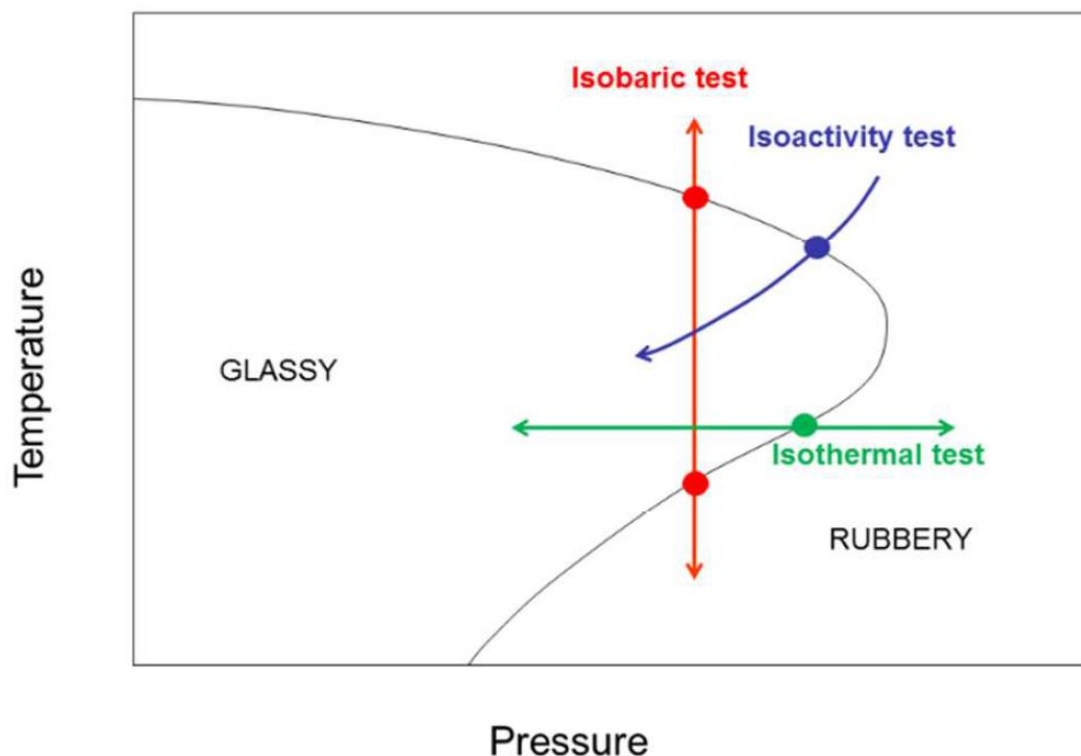


**Figure 3.19:** *Dynamic* desorption or sorption tests scheme: measuring the *retrograde vitrification* phenomenon

Onwards, the modelling of *retrograde vitrification*, i.e. the phase diagram for the PS—Toluene system, is presented. The experiments show that the plasticizing action depends in a complex fashion upon the combined effects of fluid pressure and of temperature on fluid sorption within the polymer. In Chapter I, a profound analysis of how this problem is treated in the literature is given along with thermodynamic proofs of the  $T_g$  depression. In this work, the NRHB compressible lattice fluid model is used to describe the thermodynamics of the PS—Toluene mixture at equilibrium: the sorption isotherms of toluene in PS are fit by the model by the binary interaction parameter and the entropy of the mixture is evaluated. Then, the prediction of the glass transition as a function of pressure and temperature of the system and of composition of toluene within the polymer follows: according to the Gibbs-Di Marzio criterion, the configurational entropy

of the mixture vanishes when transition from the rubbery to the glassy state is accomplished. In the present context, in view of the absence of hydrogen bonding and other specific interactions, the contribution to the model equations from hydrogen bonding is omitted. The NRHB parameters of pure A-PS and toluene are listed in table 3.6.

Substance	$\epsilon_s^*$ (J/mol)	$\epsilon_h^*$ (J/mol K)	$v_{sp,0}^*$ (cm <sup>3</sup> /g)	s	Reference
A-PS	4.5361	5341.5	0.9027	0.667	[38]
Toluene	0.0768	5097.2	1.06205	0.757	[40]

**Table 3.6:** NRHB parameters of pure A-PS and Toluene

The procedure used to solve the problem at hand is described next in detail:

- a) the *flex energy* parameter of the pure polymer chain is derived by letting the entropy of pure A-PS vanish at the  $T_g$  chosen from the MDSC experiment;
- b) the NRHB binary interaction parameter ( $\zeta_{12}$ ) of the PS—Toluene system is evaluated by fitting simultaneously multiple sorption isotherms of toluene in A-PS taken from the literature [75, 78];
- c) after fixing the pressure of the vapour phase, the set of values  $\{T_g; \Omega_g; \rho^\beta; \rho^\alpha; \Gamma_{ij}\}$  that simultaneously solves the set of equations describing equilibrium between the vapour and the mixture phases and the vanishing of the mixture configurational entropy (equation 1.63a) are derived. Here follows a description of the equations used in this work:
  - c.1) equilibrium between the two separate phases is identified by the validity of both the EOSs of the vapour and the mixture phases (equations 1.50 and 1.62a);
  - c.2) the equality of the toluene chemical potentials between the two phases (equations 1.51 and 1.62b)
  - c.3) the vanishing of the mixture configurational entropy (equation 1.63a)

Of course, the value of  $P$  chosen is the  $P_g$  of the polymer—penetrant mixture. Moreover,  $\rho^\beta$  and  $\rho^\alpha$  represent the equilibrium densities of the vapour phase and of the mixture phase respectively. Worthnoting, the flex energy of the polymer is derived from an experimental  $T_g$  which is theoretically different from the ideal glass transition temperature  $T_2$ . Consequently, it is here interpreted as an *apparent flex energy*: calorimetric analysis has been performed by cooling PS at a rate of 5 °C/min, while the dynamic sorption experimental data for the mixture refer to a rate of change of pressure of 0.16 mbar/min and a rate of change of temperature of 2°C/h, respectively for isothermal tests and for isobaric and isoactivity tests. It is impossible to confirm whether the conditions at which the calorimetric and dynamic sorption experiments have been actually performed at similar conditions in terms of molecular mobility. In fact, the kinetic effects

affecting the accessible transition could be different for different experiments, thus possibly resulting in some inconsistency in assuming a unique value of the *apparent flex energy* for all the experimental conditions analyzed. Moreover, in the case of the low M.W. component (toluene in the present context), it is assumed that the *flex energy* is zero, following again Condo *et al.*. This is equivalent to assume the penetrant to be fully flexible. It is worth noting that  $Z_i$ , the bond coordination number (bond conformations) for bond of type  $i$ , is, in general, different from the coordination number of the lattice (indicated by  $z$  in Chapter 1). here it is assumed  $Z = 4$  as already pointed out in Chapter 1. A specific Matlab<sup>®</sup> code based on the trust-region reflective algorithm is applied to solve the non-linear set of equations (point c). The contribution of configurational entropy given by hydrogen bond (equation 1.63c) is of course absent in the system studied. The value of the *apparent flex energy*,  $\Delta\varepsilon_2$ , is 3418.63 J mol<sup>-1</sup>. Following this procedure the  $T_g$  vs pressure envelop is predicted. As reported in figure 3.20, theoretically determined values are in good agreement with experimental data, displaying all the relevant features highlighted by the experimental analysis, including the retrograde vitrification phenomenon. In the same plot, it is also reported, in red, the phase equilibrium values calculated by NRHB for vapor pressure of toluene as a function of pressure (these results are virtually coincident with experimental ones), thus showing that, in the range of interest, the toluene phase is always in the vapour state. Location of transition depends upon the rate of change of boundary conditions imposed during dynamic sorption experiments (figure 3.11). In figure 3.21, it is highlighted how the sensitivity study of depressurisation rate affect the value of  $P_g$  with respect to the theoretical predicted value. As the value of pressure rate is decreased, the values of  $P_g$  predicted theoretically are approached. In light of the previous discussion, this result likely indicates that the cooling rate of calorimetric experiments are consistent with values of rate of change of pressure lower than those actually adopted in the performed experiments for the purpose of determining the correct value of the apparent flex energy.

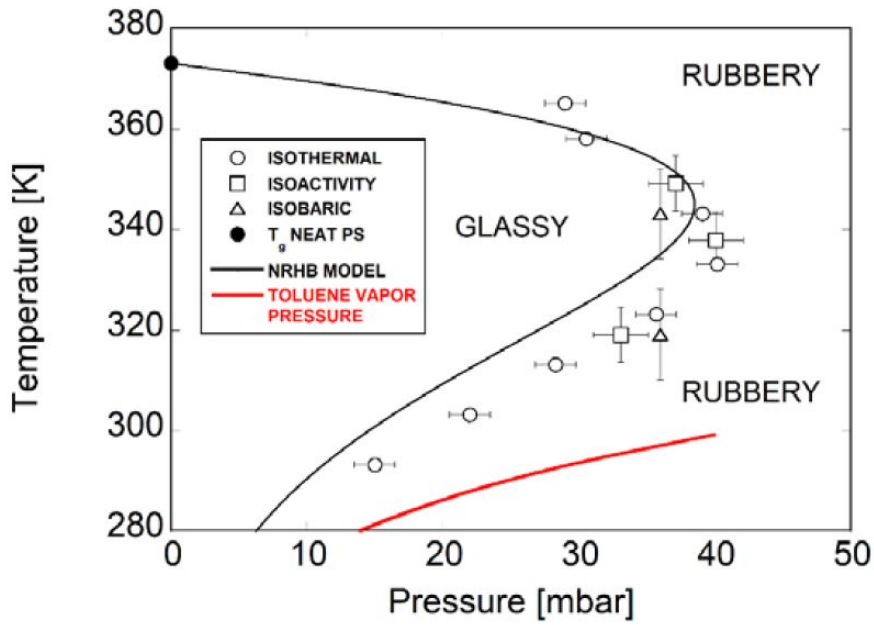


Figure 3.20: GD—NRHB prediction of retrograde vitrification for the PS—Toluene system [76]

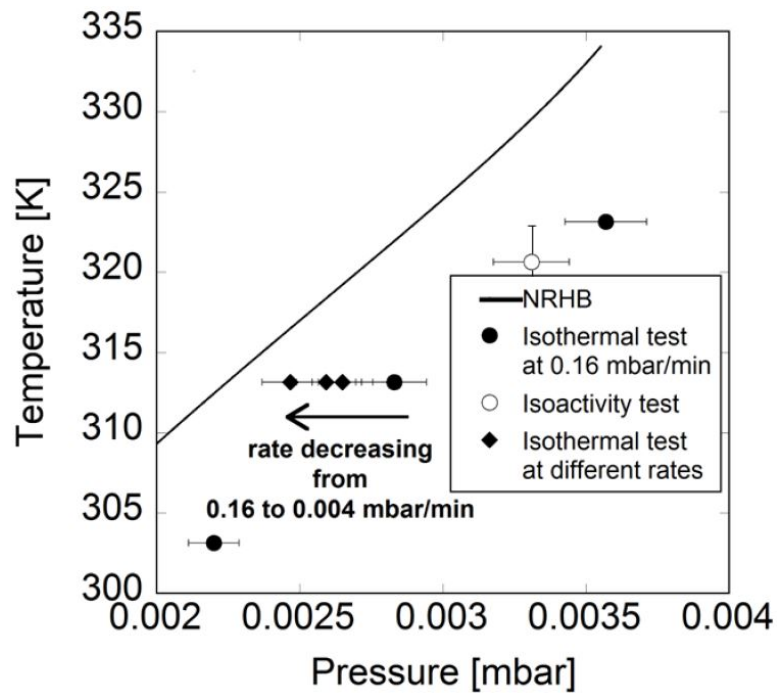


Figure 3.21: Dependence of  $P_g$  on the depressurization rate: comparison with the GD—NRHB approach

# Chapter 4

## PPO—Benzene System

The last part of this PhD research work focuses on the system PPO—Benzene. With respect to the systems already presented, the behaviour of this mixture is much more complex: although PPO is a semicrystalline polymer by nature, the sorption of solvent from the vapour phase can induce as well crystallization provided the neat polymer structure is forced to be amorphous after quenching. The Poly(2,6-dimethyl-1,4-phenylene)oxide (or PPO<sup>®</sup> resin) was first commercialized in 1964: it is obtained from the free-radical, step-growth, oxidative-coupling polymerization of 2,6-xyleneol (figure 4.1) together with a small amount of diphenoquinone [83, 84]. Indeed, it is an aromatic thermoplastic polymer showing very high values of glass transition temperature ( $\sim 487\text{K}$ ): its properties make it suitable for use as a membrane for gas separations. Particularly, although its structure is rigid, the good transport properties are a consequence of the high degree of free volume estimated in the literature around 18%. Other properties are: high impact strength, chemical stability to mineral and organic acids and low water absorption. A limitation that had restricted its commercialization is its high  $T_g$  in relation to the susceptibility of its methyl groups to thermal oxidation which poses problems for melt processing. In this work, induced crystallisation of amorphous PPO by sorption of benzene from the pure penetrant vapour phase is studied. This phenomenon has been experimentally investigated in the literature for a few organic polymers. For instance, Kampou *et al.* studied crystallization of polycarbonate induced by acetone [85]. Overbergh *et al.* studied sorption of acetone and dichloromethane in isotactic and amorphous polystyrene (IPS and APS respectively) [86]. Chiou *et al.* investigated the solvent induced crystallization phenomenon of miscible blends of poly(vinylidene fluoride) and poly(methyl methacrylate) and to a lesser extent in polyethylene terephthalate through sorption of  $\text{CO}_2$  [87]. The increase of free volume within the polymeric matrix due to vapour sorption is thought to increase chain mobility and to activate crystallisation. Sorption kinetics depends on several factors: diffusion through the matrix, relaxation of the polymeric chains and their crystallisation. The specimen geometry

also plays an important role: the diffusion time increases the greater the thickness so that a relaxation and/or crystallisation front may appear. The time needed by the system to reach equilibrium in a static sorption experiment can be very long (order of magnitude months) which justifies the lack of scientific contributions to this topic in the literature. However, the relevance of understanding and controlling polymer phase transitions is huge. Tailoring the molecular structure of polymeric membranes is the ultimate goal engineers pursue to improve separation performances. For instance, Guerra *et al.* discovered that inducing crystallisation of syndiotactic PPO through sorption of benzene causes the crystallites structure to become nanoporous [88]. The crystallites are thought to originate around the penetrant molecules. This phenomenon improves separation properties of low molecular weight compounds such as methane and carbon dioxide because the solubility of the crystalline phase becomes higher than the amorphous glassy phase unexpectedly [89]. Here, a thermodynamic approach is followed to study PPO crystallisation induced by sorption of benzene. Gravimetric experiments are combined with the EOS thermodynamic theory based on the statistical framework NRHB. In order to study the possible glass transition taking place before crystallisation occurs (i.e. at lower benzene activities) the Gibbs—Di Marzio theory is applied.

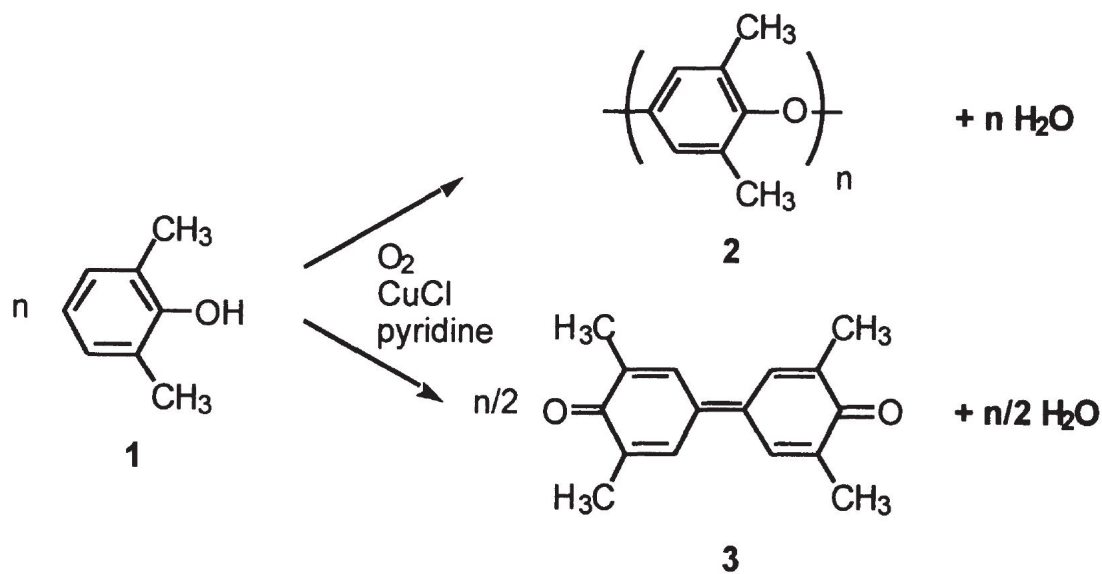


**Figure 4.1:** Polymerization reaction of PPO: (1) 2,6-xyleneol; (2) PPO unit chain; (3) diphenoquinone

## 4.1 Materials

Semicrystalline PPO (sPPO) was purchased by Sigma-Aldrich and it has weight-averaged and number-averaged molecular masses equal to 59,000 Mw and 17,000 Mn respectively. Benzene was purchased from Aldrich ( $P_s = 243.59$  mbar at 40°C) and

used without further purification. PPO amorphous (in the following aPPO) films were obtained by compression molding after melting at 290 °C.

## 4.2 Apparatuses and Methods

PPO's physical properties of interest are easily found in the literature [89].  $T_g$  was measured by using a DSC Q1000 from TA Instruments (New Castle, DE) and it is equal to 211°C approximately. The measurement was performed at a heating rate of 5°C/min in the temperature range 25—400 °C. PVT measurements were conducted by using a PVT GNOMIX (Boulder, CO.) apparatus through isothermal pressure scan. The density at 1 atm and 25°C was measured by flotation and it is equal to  $1.016 \pm 0.0004$  g cm<sup>-3</sup>. In this work, gravimetric sorption experiments were conducted with the same apparatus used for the PEI—CO<sub>2</sub> system. Sorption kinetics of Benzene into PPO were measured at 40°C. From these data, the corresponding sorption isotherm was derived along with the  $P_g$  at 40°C. Time resolved *in situ* FTIR spectra were obtained through an apparatus similar to the gravimetric one. A scheme is presented in figure 4.2. A vacuum tight FTIR cell has been appropriately designed to monitor the FTIR transmission spectrum of the PPO<sup>®</sup> film exposed to a controlled benzene environment. The cell is made of stainless steel and it is equipped with a water jacket for temperature control. KBr windows have been used and sealing between cell and windows is warranted by o-rings. A VCR<sup>®</sup> fitting enables a leak tight removable closure of the system. The apparatus temperature is kept at the same temperature of the test cell through heating tapes. Pressure is monitored by means of a MKS Baratron 121 pressure transducer with a full scale of 1000 Torr, a sensitivity of 0.01 torr and an accuracy of  $\pm 0.5\%$  of the reading. The instrument used is a Perkin-Elmer System 2000 interferometer equipped with a Germanium/KBr beam splitter and a wide band DTGS detector. Instrumental parameters are as follows: resolution 4 cm<sup>-1</sup>; optical path difference (OPD) velocity 0.2 cm s<sup>-1</sup>; spectral range 4000-400 cm<sup>-1</sup>. The set of three thermodynamic glass transition values  $\{T_g; P_g; \omega_g\}$  was modelled by combining the Gibbs—Di Marzio (GD) approach and the NRHB lattice fluid statistical framework. The latter provides a description of the fluid mixture equilibrium properties.

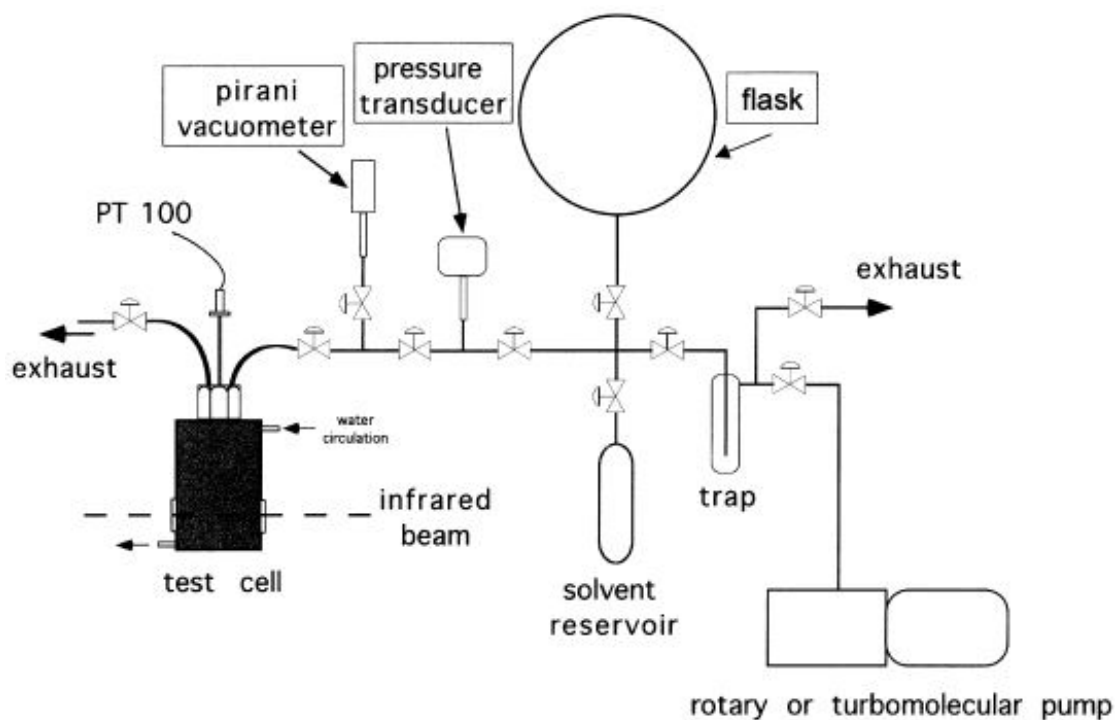


**Figure 4.2:** FTIR *in situ* vapour sorption apparatus [60]

### 4.3 Results and Discussion

aPPO films of average thickness  $\sim 128.6 \mu\text{m}$  are first tested. The registered sorption kinetics is given in figure 4.3(up): after high vacuum is attained, an integral sorption experiment is performed by fixing the benzene activity at 0.786 approximately. PPO is amorphous at the beginning of the experiment but it partially crystallizes during sorption. This phenomenon is observed from a peak during the kinetics, indicating that part of the polymer matrix is forcing the penetrant to be desorbed [86]. Indeed, the crystalline domains which have a lower sorption capacity than the amorphous phase force the penetrant to be desorbed. As a matter of fact, the penetrant acts as a solvent at such a high activity and plasticizes the matrix: the consequence is a reduction of both the  $T_g$  and the  $T_m$ . The experiment is repeated once again on the partially crystallised sample and the activity attained is equal to 0.76. No peak is observed because PPO has already crystallised during the previous experiment and, as expected, the measured equilibrium value is only slightly lower than the equilibrium value at 0.78 activity. Figure 4.3(down) reports the measured kinetics of the II sorption experiment.

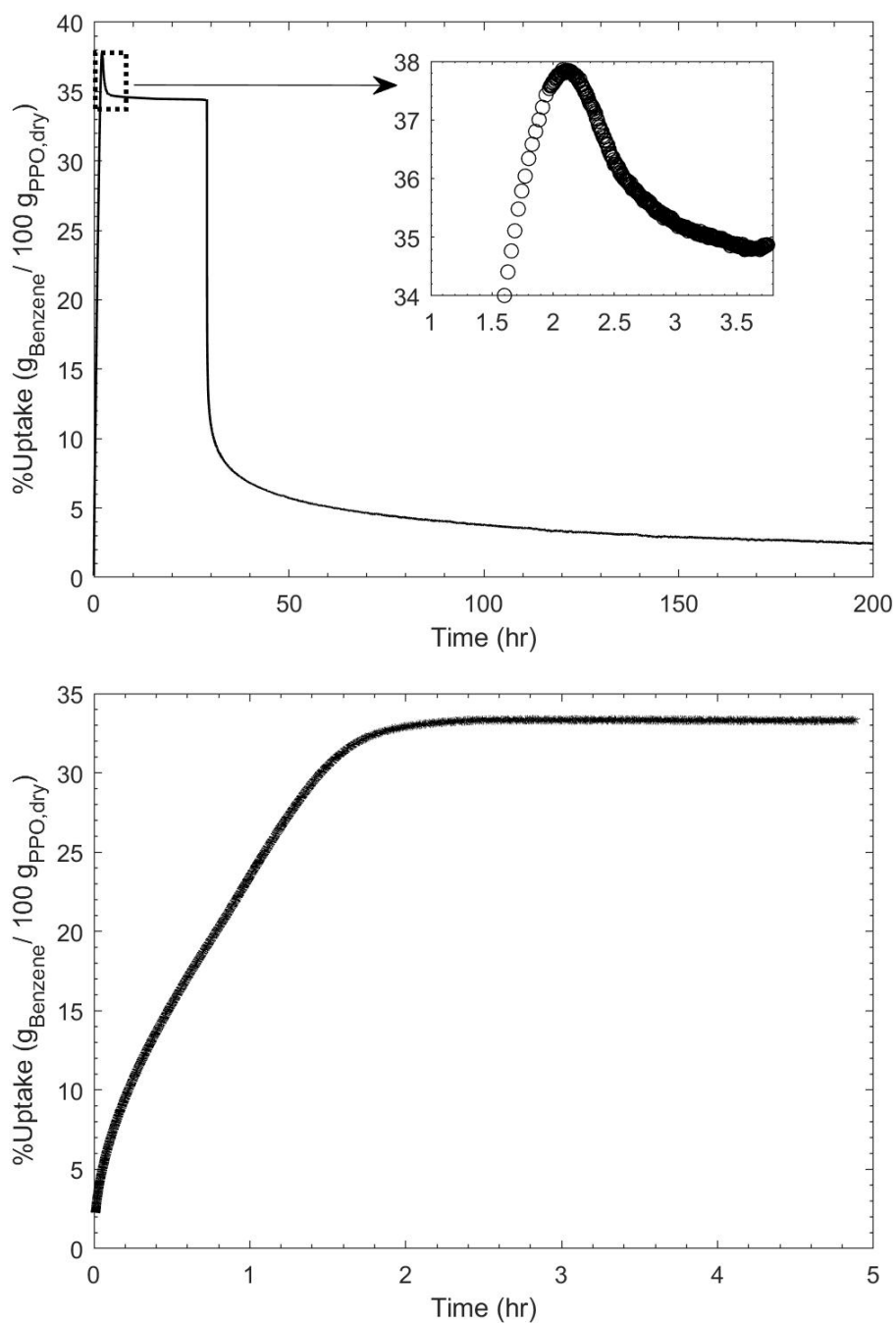


**Figure 4.3:** Up: gravimetric sorption kinetics of Benzene in aPPO (first experiment). Down: gravimetric sorption kinetics of Benzene in sPPO (second experiment following the first one).

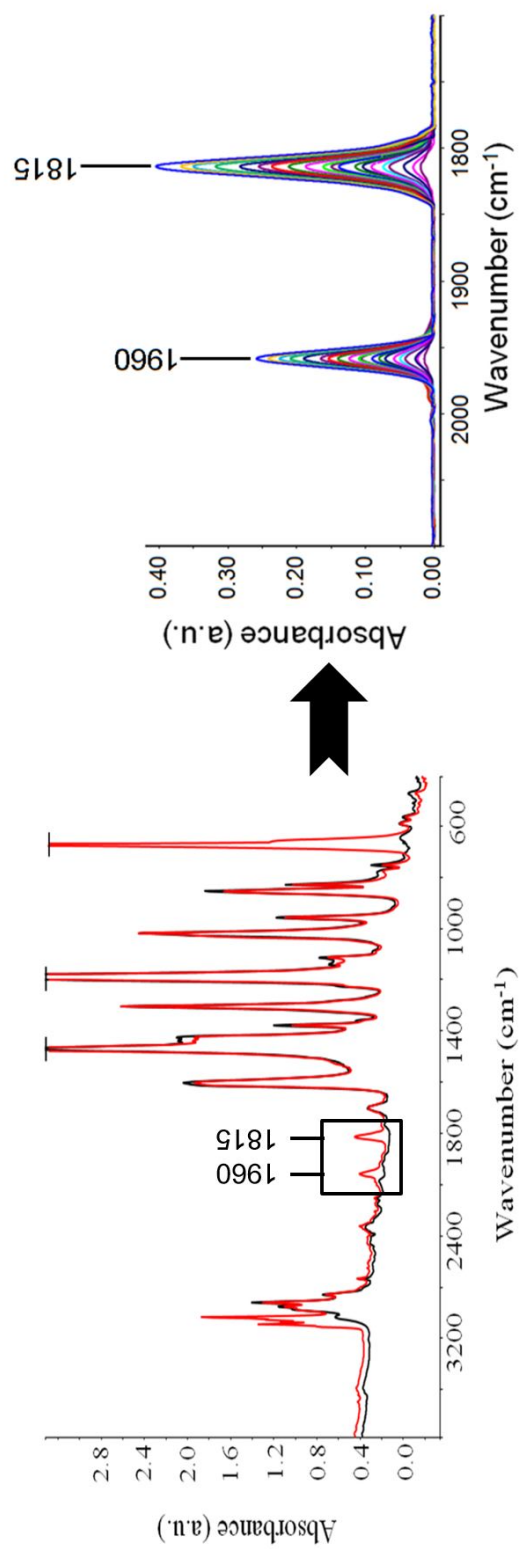


**Figure 4.4:** *In situ* time resolved FTIR spectra: sorption of Benzene in PPO. Left: Spectra recorded at  $t = 0$  (black) and  $t = \infty$  (red). Right: Difference Spectroscopy reveals the peaks of interest

To support the previous considerations, *in situ* FTIR experiments are performed following the same experimental procedure: an aPPO film of average thickness  $\sim 125 \mu\text{m}$  is tested in an integral step at 0.792 activity. Difference spectroscopy is used to retrieve the kinetics from the recorded spectra (figure 4.4). The main peaks evolution at  $1960$  and  $1815 \text{ cm}^{-1}$  is followed since these peaks are well resolved and their intensity is high. The comparison between the gravimetric and the spectroscopic kinetics is presented in figure 4.5. The chosen peaks do not describe fundamental vibrations but, instead, they are combination of fundamentals out-of-plane aromatic C—H bending vibrations in the  $1000\text{--}700 \text{ cm}^{-1}$ . Contrary to the PEI— $\text{CO}_2$  spectra there is no need for a gaussian curve fitting because each one of them is described by one gaussian function.

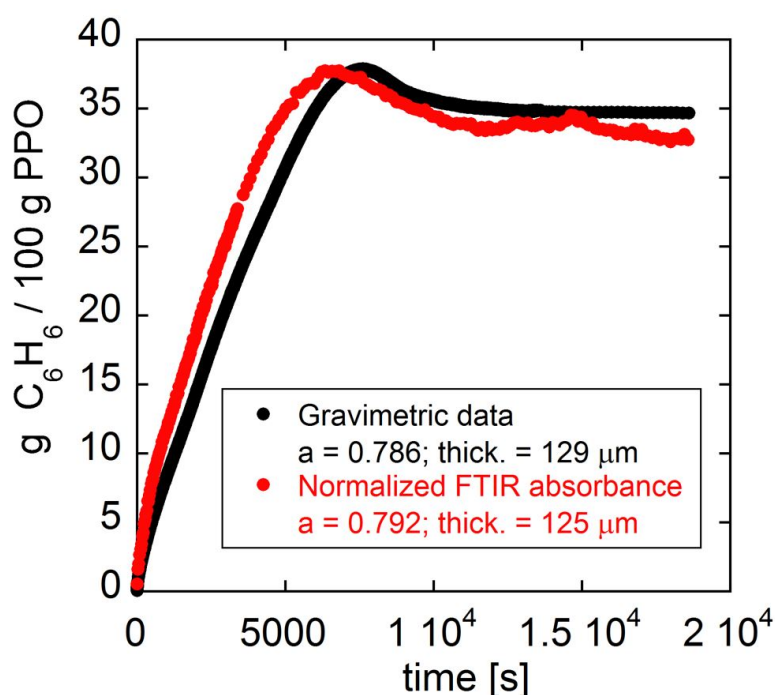


**Figure 4.5:** Gravimetric and FTIR comparison of Benzene in PPO sorption kinetics

Interestingly, *in situ* FTIR also gives information about the structural rearrangement of the membrane during sorption: the crystallization kinetics is easily retrieved from the sharp peaks related to structural order appearing at  $781, 594, 563, 494$  e  $420 \text{ cm}^{-1}$ . In this research work, the bandshape at  $480 \pm 25 \text{ cm}^{-1}$  is analysed: no benzene vibrations are present in this region and, as such, only information regarding crystallisation are retrieved (figure 4.6). The blue spectrum corresponds to the amorphous PPO film. The red spectrum refers to the PPO—Benzene mixture at equilibrium. Particularly, the crystallization kinetics is followed by observing the peak increasing at  $493 \text{ cm}^{-1}$  synchronously followed by the peak lowering at  $470 \text{ cm}^{-1}$ . The former corresponds to the new crystalline phase whereas the latter to the old amorphous one. The

data show crystallization induced by benzene is a two step process mainly activated when the sorption peak is attained i.e. when the concentration of penetrant is the highest within the matrix. The sample FTIR spectra colours associated with the kinetics are inverted. Moreover, the wide angle X-ray scattering technique is used to confirm the sample structural change (figure 4.7): at the beginning one sharp peak describes the free volume distribution of the amorphous phase is unimodal; at the end of the experiment several peaks demonstrates the completion of crystallisation.

A second set of stepwise sorption gravimetric experiments are conducted on a new sample of aPPO. The PPO film thickness is about  $\sim 145\mu\text{m}$ . The goal is to obtain the sorption isotherm for the amorphous sample at  $40^\circ\text{C}$  in order to investigate the thermodynamic variables couple  $\{P_g; \omega_g\}$  at which vitrification occurs.  $T_g$  is of course equal to  $40^\circ\text{C}$ . Moreover, when comparing these data with the ones obtained in the first measurement campaign, a clear picture of the crystallisation effect on the final solvent uptake arises. Figure 4.8 shows the sorption isotherm at  $40^\circ\text{C}$ . The possible plasticisation elbow is found at  $40 \pm 0.1^\circ\text{C}$  in the domain

$$\begin{cases} P_g > 112 \text{ mbar} \\ \Omega_g > 15 \text{ g/100g} \end{cases} \quad (4.1)$$

The uptake difference between the equilibrium values of aPPO and sPPO at 0.786 is approximately 25% of the predicted aPPO uptake. The errorbars were evaluated based on the spring displacement calibration error with the correction for the buoyancy effect and on the random error during the measurement. The order of magnitude is lower than 2.5% of the measured mean value.

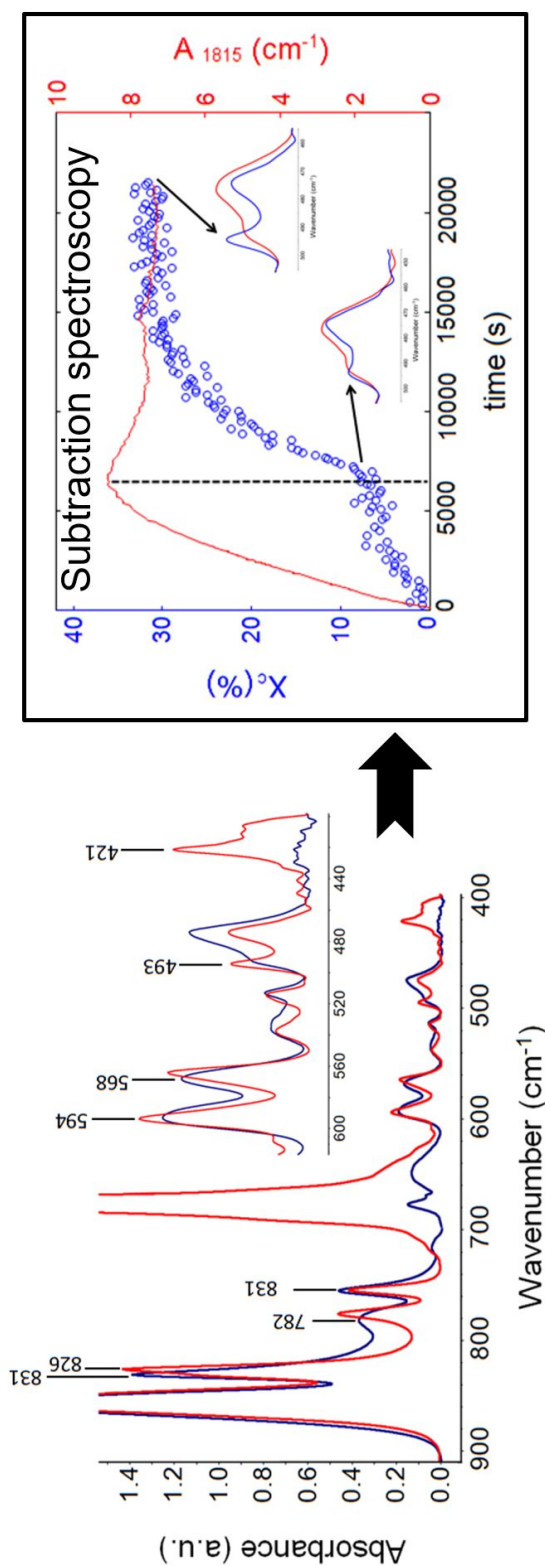


**Figure 4.6:** *In situ* time resolved FTIR spectra: analysis of the solvent induced crystallisation

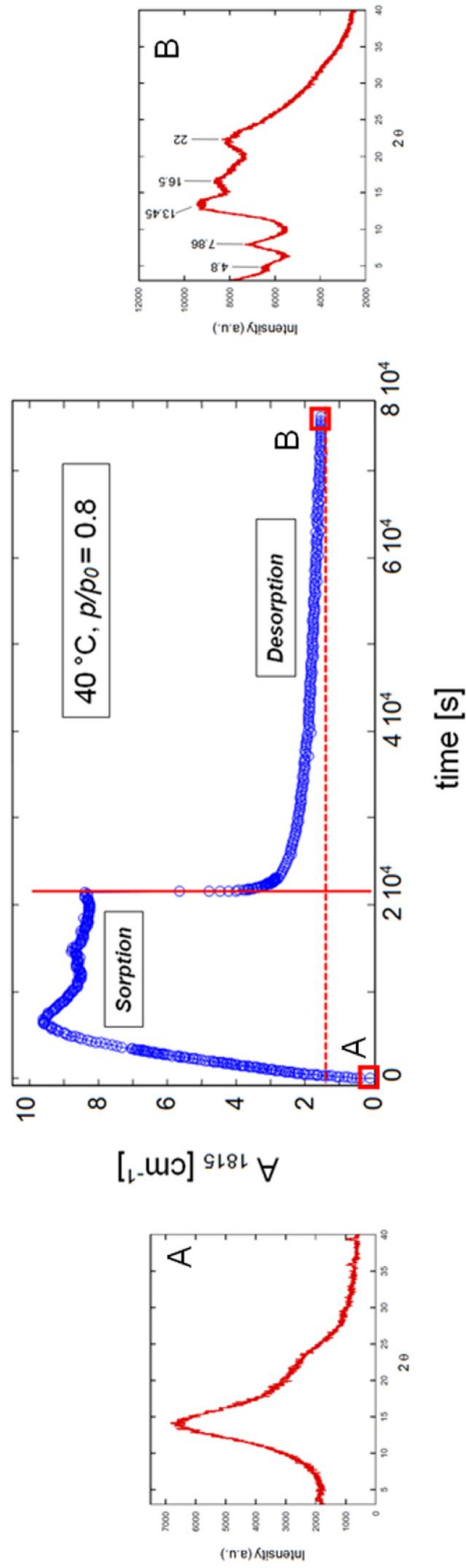


**Figure 4.7:** Evidence of solvent induced crystallisation from WAXS experiments

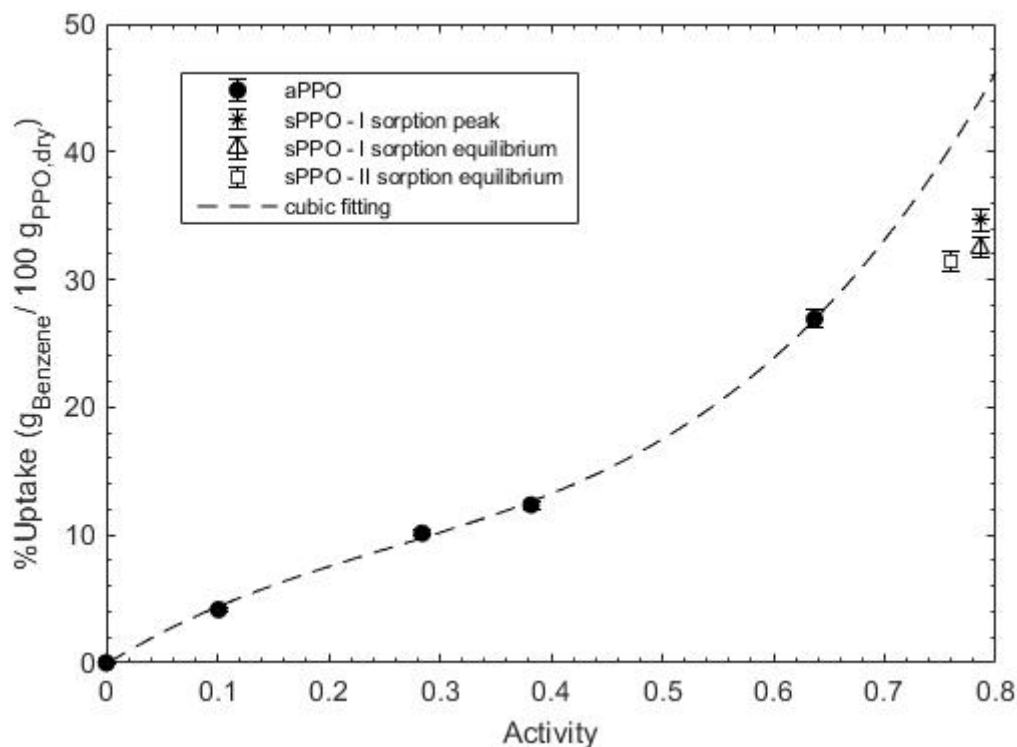


**Figure 4.8:** Sorption isotherm of Benzene in aPPO at 40°C

In order to predict the PPO—Benzene system phase diagram in the region of vapour benzene, the thermodynamic Gibbs and Di Marzio approach combined with the NRHB statistical lattice fluid model was implemented [45, 39]. The full description of the model is given in chapter I. Here, the results are presented and discussed. The locus of points which describes the decrease of the glass transition temperature due to sorption of benzene is defined by the surface in 3D relating the thermodynamic variables temperature, pressure and composition. The chemistry of benzene and PPO's unit chain is alike so that their affinity is high; consequently, the former acts as a good solvent for the glassy polymer and the solubility is very high too. Applying the line of thought of Ouboter and following the same approach used for the PS—Toluene system, it is here described an easy and straightforward thermodynamic procedure to predict the phase diagram of such simple polymer penetrant binary mixtures. The hypothesis which is here assumed is that PPO plasticizes at 40°C when immersed in the pure benzene vapour at an activity higher than 0.45. This also implies the system attains equilibrium with the vapour phase in this thermodynamic range.

First, the NRHB parameters of the pure polymer and penetrant compounds are derived from PVT and liquid-vapour equilibrium data respectively. In figure 4.9, the NRHB model is fit to PPO PVT data found in the literature [89]. Conversely, benzene parameter values are already found in the literature *et al.* [40]. The whole set of

parameters is given in table 4.1.

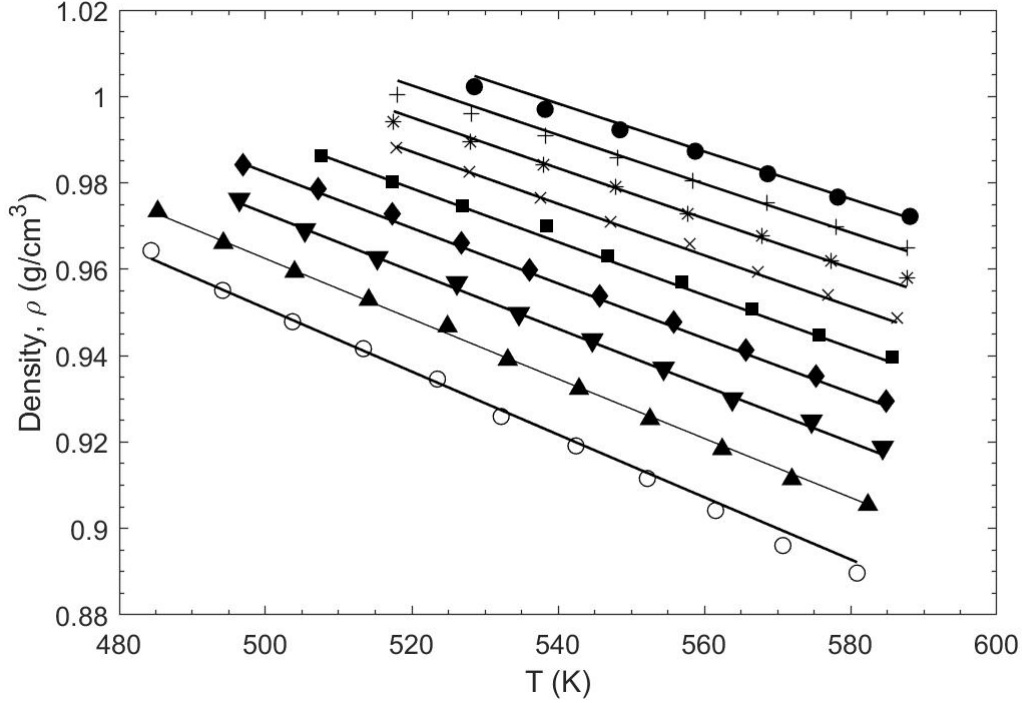


**Figure 4.9:** Fitting of the NRHB model on PPO PVT data

Substance	$\epsilon_s^*$ (J/mol)	$\epsilon_h^*$ (J/mol K)	$v_{sp,0}^*$ (cm <sup>3</sup> /g)	s	Reference
PPO	3.439	5317.3	0.862	0.7481	This work
Benzene	-0.2889	5148.5	1.06697	0.753	[40]

**Table 4.1:** NRHB parameters of pure PPO and Benzene

Second, the NRHB statistical lattice fluid framework is applied to describe equilibrium of the PPO—benzene mixture. All the hypotheses stated in Chapter I are here assumed. At equilibrium, the equality of benzene chemical potentials between the two phases and the validity of the mixture EOS must hold true simultaneously. Their solution returns the density and the composition of the mixture at equilibrium as a function of the binary parameter  $\zeta_{ij}$ . The latter must be fit to the equilibrium sorption data obtained when the mixture is in a rubbery state. In this case, because only one sorption data point is measured in the rubbery state, it is not possible to determine accurately the value of the mean field interaction parameter  $\zeta_{12}$ . Consequently, by assuming the high affinity between the two compounds, a value of zero is assigned to it.

Next, the *flex energy* of the polymer is calculated [30]. The same procedure applied to the PS—Toluene system is used: that is, the configurational entropy of the pure polymer vanishes at its glass transition temperature (equation 1.63a). No HB contributions are to be considered in this problem as well. The *flex energy* of PPO,  $\Delta\varepsilon_2$ , is 4209.9 J mol<sup>-1</sup>. It is reminded here the *flex energy* is assumed to be not dependent on the composition and the temperature of the mixture, i.e. it is a specific property of the polymer.  $\Delta\varepsilon_{PPO}$  is greater than  $\Delta\varepsilon_{PS}$  because PPOs chains are more rigid as confirmed by its higher  $T_g$  and, consequently, more energy is required by a single bond to move to the high energy state.

Last, the same algorithm implemented in Matlab® for the PS—Toluene system is used to calculate the  $\{T_g; P_g; \omega_g\}$  phase diagram for the PPO—Benzene system. By fixing the system glass transition pressure ( $P_g$ ), the unknown variables at the transition are:  $T_g$ ; benzene uptake  $\omega_{1,g}$ ; the mixture density. Figure 4.10 shows the phase diagram of the PPO—Benzene system obtained from the GD-NRHB model. As already explained in chapter I, the main argument of the theory is that the configurational entropy vanishes at the thermodynamic  $T_g$ . So the vitrification curve is obtained by deriving the set of three thermodynamic glass transition values  $\{T_g; P_g; \omega_g\}$  that simultaneously validates:

- 1- the equilibrium between the mixture and the vapour phase, i.e. equality of the penetrant chemical potentials in both phases as well as verification of the EOS in the two phases (no gradients of pressure and temperature are assumed in each and both phases);
- 2- the vanishing of the mixture phase entropy.

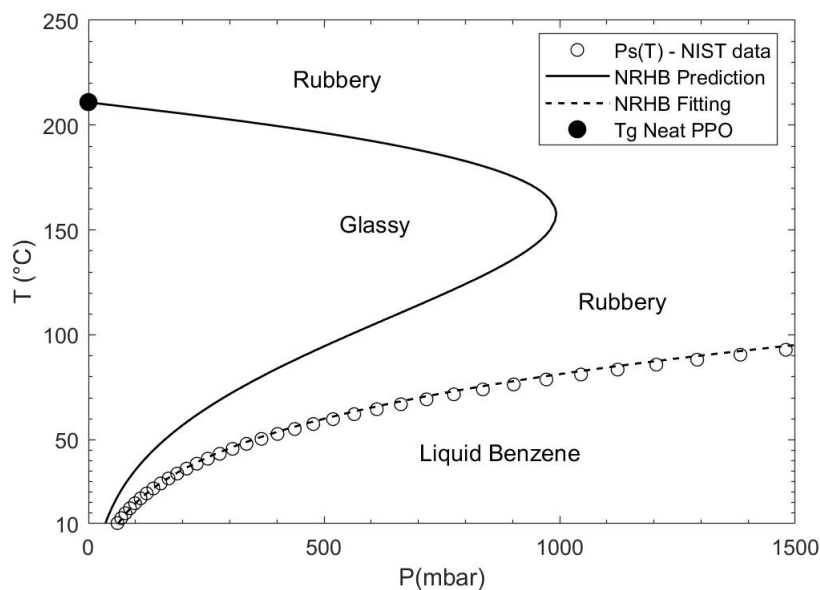


**Figure 4.10:** Prediction of PPO—Benzene P vs. T phase diagram

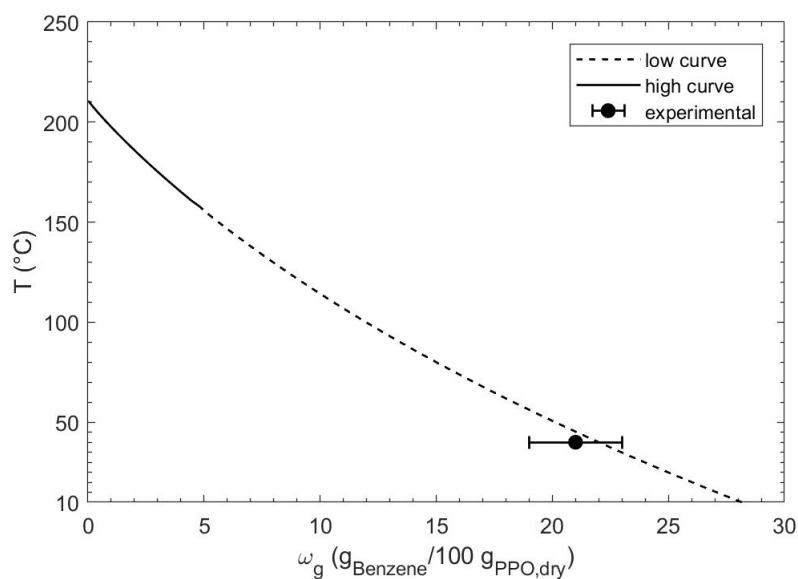


**Figure 4.11:** Prediction of PPO—Benzene Tg depression

The solubility of the penetrant increases by lowering the temperature during an isobaric experiment because the chemical potential of the penetrant in the gas phase increases as well. Generally, the latter is well approximated by the activity of the vapour phase defined as the ratio of  $P$  over the saturation pressure. The competition between the

cooling process and the solubility increase triggers plasticization of the matrix although vitrification has already occurred. In figure 4.11,  $T_g$  depression due to the increase of the penetrant % uptake is highlighted. The model predicts very well the expected value of benzene concentration inducing plasticization at 40°C. The latter is taken from the maximum of the cubic fitting second derivative curve (cf. Chapter III). The concentration error bar includes the range where the knee would be expected. Worthnoting, the model needs only two parameters to describe the system: the binary interaction parameter  $\zeta_{12}$  and the *flex energy* of the polymer. The former can be derived from several isotherm sorption curves at thermodynamic conditions inducing plasticization of the membrane. The latter is evaluated with a separate calorimetric experiment. This is still a controversial argument: the approach from Gibbs and Di Marzio aims to find the II order thermodynamic glass transition of the mixture whereas the calorimetric transition is affected by the rate of the cooling process and, as such, it provides a kinetic  $T_g$ . It is assumed here that a thermodynamic transition is underlying the kinetic glass transition observed during the calorimetric experiment [75]. Moreover, the model returns the set of three  $\{T_g; P_g; \omega_g\}$  values corresponding to a desorption kinetics from the equilibrium rubbery state. By analogy, the hypothetical desorption rate can be correlated to the cooling rate chosen for the calorimetric process.

# Conclusions

Three polymer—penetrant systems have been investigated during this PhD program. The problem consisted in the characterization of the mixture when a pure light gas or a pure solvent in the vapour state is absorbed by the polymeric matrix. The techniques implemented to achieve this goal are widely presented in this thesis. Particularly, the combination of gravimetry and FTIR spectroscopy is very useful to understand how the penetrant influences the polymer structure and, consequently, whether specific interactions between the two compounds are taking place. Thermodynamics of internal state variables describes the sorption phenomena very well when combined with statistical lattice fluid models such as the theories from the Sanchez and Lacombe or Panayiotou *et al.* [36, 39].

The system Ultem<sup>®</sup> PEI—CO<sub>2</sub> was tested at subatmospheric pressures and several temperatures. The results show the presence of a unique adsorbate species interacting with the matrix carbonyl groups through acid—base Lewis interactions. Possibly, at 35°C the bond strength may not overcome the probe kinetic energy and enables the adsorbate species to move freely within the free volume. By lowering the temperature, the probe kinetic energy is depleted and, the adsorbate only experiences the interaction with the matrix. A 2D-COS analysis confirms the presence of the interacting adsorbate species. Anyway, polymer—penetrant interactions are weak at the thermodynamic conditions tested and no structural variation is observed. This is also confirmed by the NELF-SL modeling approach.

Sorption of Toluene in atactic Polystyrene induces plasticization of the matrix at temperatures lower than the pure polymer  $T_g$ . In the case of a mixture, the glass transition phenomenon must be described by the set of three thermodynamic variables  $\{T_g, P_g, \omega_g\}$ . Desorption of the penetrant from the rubbery mixture during either an isothermal, an isobaric or an isoactivity dynamic experiment deviates from equilibrium: the observed kink of the penetrant concentration vs. pressure or temperature is proof of a II order thermodynamic transition following the line of reasoning of classical equilibrium thermodynamics. The kink is attributed to the mixture rubbery to glassy transition. The transition point is also affected by the perturbation time and kinetics cannot be ruled out as well as calorimetry and dilatometry in the case of pure polymers. The  $T_g$ — $P_g$  phase diagram clearly highlights the *retrograde vitrification* phenomenon:

under specific thermodynamic circumstances, the rubbery mixture vitrifies again when heated. Indeed the penetrant is desorbed and the chain mobility is arrested inducing vitrification of the polymeric matrix. The NRHB statistical lattice fluid model accurately describes the mixture at equilibrium. By applying the Gibbs—Di Marzio approach, the model is capable of predicting the mixture transition phase diagram.

Sorption of benzene within Poly(2,6-dimethyl-1,4-phenylene)oxide (or PPO<sup>®</sup> resin) depletes both the glass transition temperature and the melting temperature of the semicrystalline polymer. Particularly, the solvent has proved to both plasticize the amorphous glassy matrix at an activity of  $\sim 0.45$  and induce crystallization at an activity of  $\sim 0.65$  at 40°C. Gravimetric experiments have been supported by FTIR *in situ* tests: crystallization of the amorphous matrix is observed by an overshoot during sorption indicating desorption of the penetrant from the newly formed crystallites. Spectroscopy enables the evaluation of the crystallization kinetics. The new crystalline phase is described in detail by X-Ray diffractive measurement. Again NRHB greatly predicts at 40°C the thermodynamic couple of variables  $\{P_g, \omega_g\}$  by zeroing the configurational entropy.

# Future Directions

The future research activity will consist in:

- 1- modeling the dynamic experiments conducted on the A-PS—Toluene system;
- 2- modeling the melting temperature depletion due to sorption of a penetrant;
- 3- starting sorption experiments of a mixture of gases into the polymer matrix.

Particularly, the first goal is being pursued by using a kinetic equation for the polymer specific volume during the sorption/desorption processes. Indeed, the specific volume is the internal state variable of the implemented model and the assumption of pseudoequilibrium generally stated at temperatures much lower than  $T_g$  cannot be made here. Empirical equations have been provided in the literature (e.g. the KAHR model) [26]. They describe the behaviour of the specific volume of a pure thermoplastic polymer during cooling from the equilibrium rubbery state.

To reach the second goal, a theory capable of describing crystallisation of a mixture must be implemented. Moreover, in order to perform experiments in which a mixture of gases is absorbed by the polymer matrix, a new apparatus is being built up. These experiments are necessary because real applications involve a multicomponent gas phase, not a pure one. Indeed, a competition between the species usually takes place during sorption and the outcome can be very different [55]. Ideality is obtained when the sorption process of a gas mixture into the polymer phase is analogous to the sorption process of pure gases happening separately.

# References

- [1] Licari, J.J. *Coating Materials for Electronic Applications*, Noyes Publications: Totnes, Devon UK, 2004
- [2] Kirian, E.; Hassler, J.C. High-Pressure Torsional Braid Analysis (HP-TBA): A new technique for assessment of thermal transitions and changes in moduli of polymers exposed to supercritical or compressed fluids, *J. Supercrit. Fluids* **2019**, 143, 223
- [3] Baker, R.W. *Membrane Technology and Applications*, John Wiley & Sons, Ltd: Chichester, West Sussex, England, 2004
- [4] Noble, R.D.; Stern, S.A. Membrane Separations Technology Principles and Applications, in *Membrane Science and Technology Series*, 2 Elsevier Science B.V.: Amsterdam, The Netherlands, 1995
- [5] Debenedetti, P. G. *Metastable Liquids: Concepts and Principles*, Princeton University Press: Princeton, New Jersey, 1996.
- [6] Angell, C.A. Structural instability and relaxation in liquid and glassy phases near the fragile liquid limit, *Journal of Non-Crystalline Solids* **1998**, 102, 205
- [7] Badrinarayanan, P.; Zheng, W., Li, Q.; Simon, S.L. The glass transition temperature versus the fictive temperature, *Journal of non-crystalline solids* **2007**, 253, 2603
- [8] Flory, P.; Mandelkern, L.; Hall, H.K. Crystallization in High Polymers. VII. Heat of Fusion of Poly-(N,N'-sebacoylpiperazine) and its Interaction with Diluents, *Journal of the American Chemical Society* **1951**, 73, 2532
- [9] Kovacs, A.J. Transition vitreuse dans les polymères amorphes. Étude phénoménologique, *Fortschr. Hochpolym.-Forsch.* **1963**, Bd. 3, 394
- [10] Spencer, R.S. Volume-Temperature-Time relationships for polystyrene, *Journal of Colloid Science* **1949**, 4, 229
- [11] Saito, S.; Nakajima, T. Glass Transition in Polymers, *J. Appl. Polym. Sci.* **1959**, 4, 93
- [12] McKinney, J.E.; Goldstein, M. PVT relationships for liquid and glassy Poly(vinyl acetate), *Journal of Research of the National Bureau of Standards* **1974**, 78A, 331
- [13] Struik, L.C.E. *Physical ageing in amorphous polymers and other materials*, Elsevier: Amsterdam, 1978.
- [14] Walsh, D.; Zoller, P. *Standard Pressure Volume Temperature Data for Polymers*, CRC press, 1995

- [15] Wittmann, J.C.; Kovacs, A.J. Influence de la stereorégularité des chaînes sur les transitions di polyméthacrylate de méthyle, *Journal of Polymer Science* **1969**, 16, 4443
- [16] Saito, S.; Sasabe, H.; Nakajima, T.; Yada, K. Dielectric Relaxation and Electrical Conduction of Polymers as a Function of Pressure and Temperature *Journal of Polymer Science* **1968**, 6, 1297
- [17] Muzeau, E.; Perez, J.; Johari, G.P. Mechanical Spectrometry of the  $\alpha$ -Relaxation in Poly(methylmethacrylate) *Macromolecules* **1991**, 24, 4113
- [18] Muzeau, E.; Vigier, G.; Vassoille, R. Physical aging phenomena in an amorphous polymer at temperatures far below the glass transition, *Journal of Non-Crystalline Solids* **1994**, 172, 575
- [19] Höhne, G.W.H.; Hemminger, W.F.; Flammersheim, H.J. *Differential Scanning Calorimetry*; Springer: Verlag Berlin Heidelberg, 2003
- [20] Shick, C. Temperature modulated differential scanning calorimetry (TMDSC)—basics and applications to polymers. In *Applications to Polymers and Plastics*; Handbook of Thermal Analysis and Calorimetry 3; Elsevier: 2002
- [21] Lacey, A.A.; Price, D.M.; Reading, M. Theory and Practice of MTDSC. In *Modulated Temperature Differential Scanning Calorimetry: Theoretical and Practical Applications in Polymer Characterisation*; Hot Topics in Thermal Analysis and Calorimetry 6; Springer: AA Dordrecht, 2006; pp 1—80
- [22] Hourston, D.J.; Song, M.; Hammiche, A.; Pollock, H.M.; Reading, M. Modulated differential scanning calorimetry: 2. Studies of physical ageing in polystyrene, *Polymer*, 1996, 37, 243
- [23] Hill, A.J.; Tant, M.R. The Structure and Properties of Glassy Polymers, An Overview. In *Structure and Properties of Glassy Polymers*; ACS Symposium Series 710; American Chemical Society: Washington, DC, 1998, pp 1—20
- [24] Turnbull, D.; Cohen, M.H. Free Volume Model of the Amorphous Phase: Glass Transition, *The Journal of Chemical Physics* **1961**, 34, 120
- [25] Saito, N.; Okano, K.; Iwayanagi, S.; Hideshima, T. Molecular Motion in Solid State Polymers. In *Advances in research and Applications*; Solid State Physics; Academic Press: New York, USA, 1963; pp 343—502
- [26] Kovacs, A.J.; Aklonis, J.J., Hutchinson, J.M.; Ramos, A.R. Isobaric volume and enthalpy recovery of glasses. II. A transparent multiparameter theory, *Journal of Polymer Science: Polymer Physics* **1979**, 17, 1097
- [27] Vrentas, J.S.; Vrentas, C.M.; Duda, J.L. Comparison of Free-Volume Theories *Polymer Journal* **1993**, 25, 99
- [28] Fujita, H. Notes on Free Volume theories, *Polymer Journal* **1991**, 23, 1499
- [29] Di Marzio, E.; Gibbs, J.H. Chain Stiffness and the lattice theory of polymer phases, *The Journal of Chemical Physics* **1958**, 28, 807
- [30] Gibbs, J.H.; Di Marzio, E. Nature of the glass transition and the glassy state, *The*

- Journal of Chemical Physics* **1958**, 28, 373
- [31] Astarita, G. *Thermodynamics: An Advanced Textbook for Chemical Engineers*, Plenum Press, 1989
- [32] Landau, L.D.; Lifshitz, E.M. *Statistical Physics part I*. In *Course of Theoretical Physics* vol. 5 Pergamon Press, 1980, pp 446—511
- [33] Flory, P.J. *Principles of Polymer Chemistry*, Cornell University Press, New York, USA, 1953, pp 495—539
- [34] Sanchez, I.C.; Lacombe, R.H. An Elementary Molecular Theory of Classical Fluids. Pure Fluids, *The Journal of Physical Chemistry* **1976**, 80 (21), 2352
- [35] Sanchez, I.C.; Lacombe, R.H. Statistical Thermodynamics of Fluid Mixtures, *The Journal of Physical Chemistry* **1976**, 80 (23), 2568
- [36] Sanchez, I.C.; Lacombe, R.H. Statistical Thermodynamics of Polymer Solutions, *Macromolecules* **1978**, 11 (6), 1145
- [37] Condo, P.D.; Sanchez, I.C.; Panayiotou, C.G.; Johnston, K.P. Glass Transition Behavior Including Retrograde Vitrification, *Macromolecules* **1992**, 25, 6119
- [38] Panayiotou, C.; Pantoula, M.; Stefanis, E.; Tsvintzelis, I.; Economou, I.G. Non-random Hydrogen-Bonding Model of Fluids and Their Mixtures. 1. Pure Fluids, *Ind. Eng. Chem. Res.* **2004**, 43, 6592
- [39] Panayiotou, C.; Stefanis, E.; Tsvintzelis, I.; Economou, I.G. Nonrandom Hydrogen-Bonding Model of Fluids and Their Mixtures. 2. Multicomponent Mixtures, *Ind. Eng. Chem. Res.* **2007**, 46, 2628
- [40] Tsvintzelis, I.; Spyriouni, T.; Economou, I.G. Modeling of fluid phase equilibria with two thermodynamic theories: Non-random hydrogen bonding (NRHB) and statistical associating fluid theory (SAFT), *Fluid Phase Equilibria* **2007**, 253, 19
- [40] Tsvintzelis, I.; Kontogeorgis, G.M. Modeling the vapor–liquid equilibria of polymer–solvent mixtures: Systems with complex hydrogen bonding behavior, *Fluid Phase Equilibria* **2009**, 280, 100
- [41] Veytsman, B.A. Are Lattice Models Valid for Fluids with Hydrogen Bonds?, *J. Phys. Chem.* **1990**, 94, 8499
- [42] Fredenslund, A.; Jones, R.L.; Prausnitz, J.M. Group-Contribution Estimation of Activity Coefficients in Nonideal Liquid Mixtures, *AIChE Journal* **1975**, 21 (6), 1086
- [43] Nicolais, L.; Borzachiello, A.; Lee, S.M. Environmental Resistance of High Performance Polymeric Matrices and Composites. In *Wiley Encyclopedia of Composites* part 2, Wiley, 2012
- [44] Prinos, J.; Panayiotou, C. Glass transition temperature in hydrogen-bonded polymer mixtures, *Polymer* **1995**, 36 (6), 1223
- [45] Di Marzio, E.; Gibbs, J.H. Molecular Interpretation of Glass Temperature Depression by Plasticizers, *J. Polymer Sci.A* **1963**, 1, 1417
- [46] Doghieri, F.; Sarti, G.C. Nonequilibrium Lattice Fluids: A Predictive Model for

- the Solubility in Glassy Polymers, *Macromolecules* **1996**, 29 (24), 7885
- [47] Sarti, G.C.; Doghieri, F. Predictions of the solubility of gases in glassy polymers based on the NELF model, *Chem. Eng. Sci.* **1998**, 53 (19), 3435
- [48] Freeman, B.; Pinnau, I. Solubility of Gaseous Mixtures in Glassy Polymers: NELF Predictions. In *Polymer Membranes for Gas and Vapor Separation* Ch. 13, ACS Symposium Series; American Chemical Society: Washington, DC, 1999
- [49] Scherillo, G.; Sanguigno L.; Galizia, M.; Lavorgna, M.; Musto, P.; Mensitieri, G. Non-equilibrium compressible lattice theories accounting for hydrogen bonding interactions: Modeling water sorption thermodynamics in fluorinated polyimides, *Fluid Phase Equilibria* **2012**, 334, 166
- [50] Wypych, G. Handbook of Plasticizers, ChemTec Publishing, 2012, Toronto, Canada
- [51] Platzer, N.A.J. Plasticization and Plasticizer Processes. In *Advances in Chemistry Series* vol 48, ACS Publications, 1965
- [52] De Bruyn Ouboter, R.; Beenakker, J. J. M. First and second order transitions in liquid binary mixtures *Physica* **1961**, 27, 1074
- [53] Myers, A.L. Thermodynamics of Adsorption in porous materials, *AIChE Journal* **2002**, 48 (1), 145
- [54] Koros, W. J.; Paul, O. R.; Huvard, G. S. Energetics of gas sorption in glassy polymers, *Polymer*, **1979**, 20, 956
- [55] Yampolskii, Y.; Pinnau, I.; Freeman, B. Materials Science of Membranes for Gas and Vapor Separation, John Wiley & sons Ltd., Chichester, England 2006
- [56] De Nicola, A.; Correa, A.; Milano, G.; La Manna, P.; Musto, P.; Mensitieri, G.; Scherillo, G. Local Structure and Dynamics of Water Absorbed in Poly(ether imide): A Hydrogen Bonding Anatomy, *J. Phys. Chem.B* **2017**, 121 (14), 3162
- [57] Scherillo, G.; Petretta, M.; Galizia, M.; La Manna, P.; Musto, P.; Mensitieri, G. Thermodynamics of water sorption in high performance glassy thermoplastic polymers, *Frontiers in Chemistry* **2014**, 2, 25
- [58] Seymour, R.B.; Kirshenbaum, G.S. Discovery and development of polyetherimides. In *High Performance Polymers: Their Origin and Development*, Proceedings of the Symposium on the History of High Performance Polymers at the American Chemical Society Meeting, Elsevier, New York, USA, 1986
- [59] White, D. M. Polyetherimides Via Nitro-Displacement Polymerization: Monomer Synthesis and <sup>13</sup>C-NMR Analysis of Monomers and Polymers, *J. Polymer Sci.* **1981**, 19, 1635
- [60] Cotugno, S.; Larobina, D.; Mensitieri, G.; Musto, P.; Ragosta, G. A novel spectroscopic approach to investigate transport processes in polymers: the case of water-epoxy system, *Polymer* **2001**, 42, 6431
- [61] Musto, P.; La Manna, P.; Pannico, M.; Mensitieri, G.; Gargiulo, N.; Caputo, D. Molecular interactions of CO<sub>2</sub> with the CuBTC metal organic framework: an FTIR

- study based on two-dimensional correlation spectroscopy, *J. Molecular Structure* **2018**, 1166, 326
- [62] Crank, J. *The Mathematics of Diffusion*, Clarendon Press, Oxford, UK, 1975
- [63] Colthup, N. B.; Daly, L.H.; Wiberley, S.E. *Introduction to Infrared and Raman Spectroscopy*, Academic Press Inc. San Diego, CA, USA
- [64] Carbon Dioxide IR Spectrum, NIST Standard Reference Database 35 - NIST/EPA Gas Phase Infrared Library Copyright by the U.S. Department of Commerce on behalf of the United States
- [65] Stull, V.R.; Wyatt, P.J.; Plass, G.N. The Infrared Transmittance of Carbon Dioxide, *Applied Optics* **1964**, 3, 243
- [66] Noda, I.; Dowrey, A.E.; Marcott, C.; Story, G.M.; Ozaki, Y. Generalized Two-Dimensional Correlation Spectroscopy, *Appl. Spectrosc. A* **2000**, 54 (7), 236
- [67] Green, D.; Perry, R.H. Physical and Chemical Data, In *Perry's Chemical Engineers Handbook* section 2, The McGraw-Hill Companies Inc., USA, 2008
- [68] Doumenc, F.; Guerrier, B.; Allain, C. Solvent sorption in glassy polymer films coupling between solvent diffusion and viscoelastic relaxation, *Proceedings of 4<sup>th</sup> ICCHMT* **2005**, 473
- [69] Bodiguel, H.; Doumenc, F.; Guerrier, B. Aging in PMMA/Toluene films, *AIP conference proceedings* **2008**
- [70] Doumenc, F.; Bodiguel, H.; Guerrier, B. Physical aging of glassy PMMA/Toluene films: Influence of drying/swelling history, *Eur. Phys. J.* **2008**, 27, 3
- [71] de Mezquia, D.A.; Doumenc, F.; Bou-Ali, M.M. Sorption isotherm, glass transition, and diffusion coefficient of Polyacrylamide/Water solutions, *J. Chem. Eng. Data* **2012**, 57, 776
- [72] Hopfenberg, H. B. Permeability of plastic films and coatings to gases, vapors, and liquids. In *Polymer Science and Technology* vol. 6, Plenum Press, New York, 1974, pp 73-86
- [73] Sanopoulou, M.; Roussis, P.P.; Petropoulos, J.H. A detailed study of the viscoelastic nature of vapor sorption and transport in a cellulosic polymer. I. Origin and physical implications of deviations from fickian sorption kinetics, *J. Pol. Sci. B* **1995**, 33, 993
- [74] Sanopoulou, M.; Roussis, P.P.; Petropoulos, J.H. A detailed study of the viscoelastic nature of vapor sorption and transport in a cellulosic polymer. II. Sorption and longitudinal swelling kinetic correlations, *J. Pol. Sci. B* **1995**, 33, 2125
- [75] Pierleoni, D.; Minelli, M.; Scherillo, G.; Mensitieri, G.; Loianno, V.; Bonavolontà, F.; Doghieri Analysis of a Polystyrene—Toluene system through “dynamic” sorption tests: glass transitions and retrograde vitrification, *J. Phys. Chem. B* **2017**, 121 (42), 9969
- [76] Scherillo, G.; Loianno, V.; Pierleoni, D.; Esposito, R.; Brasiello, A.; Minelli, M.; Doghieri, F.; Mensitieri, G. Modeling Retrograde Vitrification in the

- Polystyrene–Toluene System, *J. Phys. Chem. B* **2018**, 122 (11), 3015
- [77] Ichihara, S.; Komatsu, A.; Tsujita, Y.; Nose, T.; Hata, T. Thermodynamic studies on the glass transition and the glassy state of polymers. I. Pressure Dependence of the glass transition temperature and its relation to other thermodynamic properties of polystyrene, *Polymer Journal* **1971**, 2 (4), 530
- [78] Krüger, K. M.; Sadowski, G. Fickian and non-Fickian sorption kinetics of toluene in glassy polystyrene, *Macromolecules* **2005**, 38, 8408
- [79] Vrentas, J.S.; Duda, J.L.; Hou, A.C. Anomalous sorption in poly(ethyl methacrylate), *J. Appl. Polym. Sci.* **1984**, 29, 399
- [80] Condo, P.D.; Johnston, K.P. Retrograde vitrification of polymers with compressed fluid diluents: experimental confirmation, *Macromolecules* **1992**, 25, 6730
- [81] Condo, P.D.; Johnston, K.P. In situ measurement of the glass transition temperature of polymers with compressed fluid diluents, *J. Polym. Sci. B* **1994**, 32, 523
- [82] Pham, J.Q.; Johnston, K.P.; Green, P.F. Retrograde vitrification in CO<sub>2</sub>/Polystyrene thin films, *J. Phys. Chem. B* **2004**, 108, 3457
- [83] Chowdhury, G.; Kruczek, B.; Matsuura, T. Chemical modification of poly(phenylene oxide)s. In *Polyphenylene oxide and modified polyphenylene oxide membranes* Ch. 1, Springer Science & Business Media, New York, 2001
- [84] Hay, A.S. Polymerization by Oxidative Coupling: Discovery and Commercialization of PPO<sup>®</sup> and Noryl<sup>®</sup> Resins
- [85] Kambour, R.P.; Karasz, F.E.; Daane, J.H. Kinetic and Equilibrium Phenomena in the System: Acetone Vapor and Polycarbonate Film, *J. Polym. Sci. A-2* **1966**, 4, 327
- [86] Overbergh, N.; Berghmans, H.; Smets, G. Crystallization of isotactic polystyrene induced by organic vapours, *Polymer* **1975**, 16, 703
- [87] Chiou, J.S.; Barlow, J.W.; Paul, D.R. Polymer Crystallization Induced by Sorption of CO<sub>2</sub> Gas, *J. Appl. Polym. Sci.* **1985**, 30, 3911
- [88] Daniel, C.; Longo, S.; Fasano, G.; Vitillo, J.G.; Guerra, G. Nanoporous Crystalline Phases of Poly(2,6-Dimethyl-1,4-phenylene)oxide, *Chem. Mater.* **2011**, 23, 3195
- [89] Galizia, M.; Daniel, D.; Fasano, G.; Guerra, G.; Mensitieri, G. Gas Sorption and Diffusion in Amorphous and Semicrystalline Nanoporous Poly(2,6-dimethyl-1,4-phenylene)oxide, *Macromolecules* **2012**, 45, 3604
- [90] Sarti, G.C. Sanchez and Lacombe Theory. In *Encyclopedia of Membranes* Ch. S, SpringerReference, Berlin, 2016

# Appendices

# Appendix A

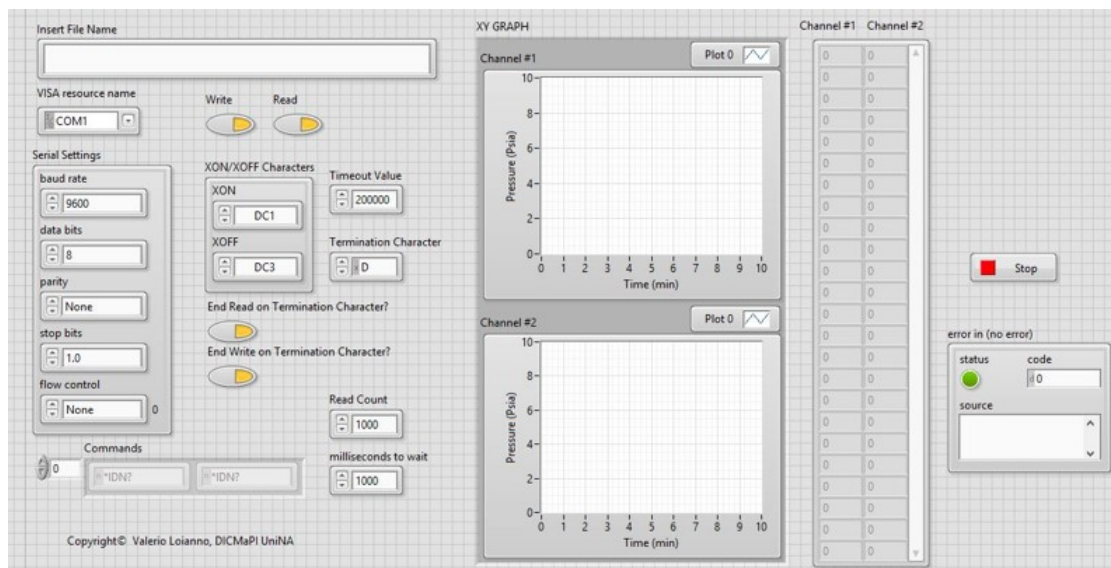


**Figure A.1:** LabVIEW® user interface to acquire two channels pressure data

During my stay at the University of Oklahoma, I had the opportunity to implement a LabVIEW® code to acquire pressure data. Here a picture of the user interface is reported.

	Symbol	Name	Definition/property
Pure component $i$	$\rho_i^*$	Characteristic density of pure component $i$	
	$p_i^*$	Characteristic pressure of pure component $i$	
	$T_i^*$	Characteristic temperature of pure component $i$	
	$r_i^0$	Number of lattice sites occupied by a mole of pure component $i$	$r_i^0 = \frac{M_i}{\rho_i^* v_i^*}$
	$v_i^*$	Volume occupied by a mole of lattice sites of pure substance	$v_i^* = \frac{RT_i^*}{p_i^*}$
	$\varepsilon_i^*$	Characteristic energy of pure component $i$	$\varepsilon_i^* = \frac{T_i^*}{k}$
Mixtures	N	Total number of moles	
	T	Temperature	
	p	Pressure	
	$\rho$	Density	
	$\rho_i$	Density of species $i$	$\rho_i = \omega_i \rho$
	$\omega_i$	Mass fraction, $i=1,2,\dots,N_i$	$\omega_i = \frac{\rho_i}{\rho}$
	$\phi_i$	Volume fraction	$\phi_i = \frac{\omega_i / \rho_i^*}{\sum_i \omega_i / \rho_i^*}$
	$\rho^*$	Characteristic density of the mixture	$\frac{1}{\rho^*} = \sum_i \frac{\omega_i}{\rho_i^*}$
	$p^*$	Characteristic pressure of the mixture	$p^* = \sum_i \phi_i p_i^* - \frac{1}{2} \sum_i \phi_i \sum_{j \neq i} \phi_j \cdot \Delta p_{ij}^*$
	$\Delta p_{ij}^*$	Binary parameter	$\Delta p_{ij}^* = p_i^* + p_j^* - 2(1 - k_{ij}) \sqrt{p_i^* \cdot p_j^*}$
	$k_{ij}, \Psi_{ij}$	Dimensionless binary parameter	$\Psi_{ij} = 1 - k_{ij}$
	$r$	Molar average number of lattice sites occupied by a molecule in the mixture	$r = \sum_i x_i r_i$
	$T^*$	Characteristic temperature of the mixture	$T^* = \frac{v^*}{r} \sum_i x_i v_i^0 \frac{T_i^*}{P_i^*} = \frac{v^* v^*}{R}$
	$\varepsilon^*$	Characteristic energy	$\varepsilon^* = \frac{T^*}{k}$
	$v^*$	Average close-packed molar volume in the mixture	$v^* = \frac{RT^*}{p^*}$
$\tilde{\rho}$	Dimensionless density	$\tilde{\rho} = \frac{\rho}{\rho^*}$	
$\tilde{T}$	Dimensionless temperature	$\tilde{T} = \frac{T}{T^*}$	
$\tilde{p}$	Dimensionless pressure	$\tilde{p} = \frac{p}{p^*}$	
	Volumetric equation of state	$\tilde{\rho}^2 + \tilde{p} + \tilde{T} [\ln(1 - \tilde{\rho}) + (1 - \frac{1}{\tilde{\rho}}) \tilde{\rho}] = 0$	
A	Total Helmholtz free energy	$\frac{A}{NkT^*} = -\tilde{\rho} + \tilde{T} \left[ \left( \frac{1}{\tilde{\rho}} - 1 \right) \ln(1 - \tilde{\rho}) + \frac{1}{\tilde{\rho}} \ln(\tilde{\rho}) + \sum_{i=1}^{N_i} \frac{\phi_i}{r_i} \ln(\phi_i) \right]$	
G	Total Gibbs free energy	$\frac{G}{NkT^*} = -\tilde{\rho} + \frac{\tilde{p}}{\tilde{\rho}} + \tilde{T} \left[ \left( \frac{1}{\tilde{\rho}} - 1 \right) \ln(1 - \tilde{\rho}) + \frac{1}{\tilde{\rho}} \ln(\tilde{\rho}) + \sum_{i=1}^{N_i} \frac{\phi_i}{r_i} \ln(\phi_i) \right]$	

Figure A.2: Sanchez and Lacombe lattice fluid model parameters [90]